Design and Optimization of a Small Reusable Launch Vehicle Using Vertical Landing Techniques

Stephane Contant

Delft University of Technology

TU Delft

Design and Optimization of a Small Reusable Launch Vehicle Using Vertical Landing Techniques

by

Stephane Contant

to obtain the degree of Master of Science
at the Delft University of Technology,
to be defended publicly on Thursday, November 28, 2019 at 13:00.

Student number:	4735676	
Project duration:	March 6, 2019 to November 28, 2019	
Thesis committee:	Ir. B.T.C. Zandbergen,	TU Delft, Supervisor
	Prof.dr. E.K.A Gill,	TU Delft
	Dr.ir. D. Dirkx,	TU Delft

This thesis is confidential and cannot be made public until November 28, 2019.

An electronic version of this thesis is available at `http://repository.tudelft.nl/`.

Cover image: Falcon 9 landing burn, credited to SpaceX.

TU Delft

Abstract

Recent years have seen a drastic increase in the number of small satellites launched per year, as these systems weighing less than 1000 kg have become a less expensive alternative to obtaining scientific data compared to satellites weighing multiple tons. However, one current drawback with these systems is their current price per kilogram to orbit, often reaching over $100k (2018) per kilogram for rideshare and cluster launches. Dedicated small satellite launch vehicles are a third solution to bringing small satellites to orbit that present potential reductions in price per kilogram. In parallel, reusability of the first stage of a launch vehicle using vertical landing techniques also presents the potential for further price per kilogram reductions. A baseline of $20.0k (2018) per kilogram to orbit is deemed as the benchmark for cost-effective solutions, as the current average reported price per kilogram of small launch vehicles totals $29.9k (2018).

With small launch vehicle developers making bold claims about their advertised launch prices, a need for verifying these claims has been established to determine the true potential for price reductions. The combination of reusing the first stage of a small launch vehicle presented the most promising solution to reducing these prices. The scope of this research is to develop a tool capable of costing a small, reusable launch vehicle using a Multidisciplinary Design Analysis approach, before implementing a Multidisciplinary Design Optimization method to optimize such systems for price per flight in the Tudat development environment.

To determine the price per flight and price per kilogram of a small, reusable launch vehicle, the propulsion, geometry and mass of such systems are first modelled, before the trajectory is modelled using a direct ascent for the simulation to the target orbit, and both return-to-launch-site and downrange landing options are considered for the reuse trajectory. Subsequently, a small launch vehicle cost model is integrated into the Multidisciplinary Design Analysis environment and is modified for the inclusion of reusability, before combining these models into the Multidisciplinary Design Optimization tool.

A 100 kg and a 500 kg payload launched to 650 km altitude Sun-synchronous orbit from Plesetsk Cosmodrome are first investigated. Under the design choices made in this study, it is immediately concluded that small, reusable launch vehicles are not a cost-effective solution for the 100 kg payload class, reaching up to five times the benchmark per kilogram. It is also concluded that three-stage launch vehicles are more expensive to launch than two-stage systems. Six different propellant and engine configurations are investigated for both the return-to-launch-site and downrange landing options. While all optimal designs for the former are below the $20.0k (2018) per kilogram assuming 20 launches per annum, 100 total launches and 10 first stage reuses, none of the downrange landing designs meet this target price. Furthermore, only a single design from the previous twelve, namely an RP1-propelled, 9-engine configuration, meets all trajectory path constraints, establishing this design as the optimal case for a small, reusable launch vehicle with a price per kilogram of $18.2k (2018). Nine additional expendable launch vehicles are optimized to compare these to the reusable system, with the configurations ranging in price per kilogram from $20.5k (2018) to $30.4k (2018), further demonstrating the cost-reduction potential of the small, reusable launch vehicle.

The effect of changing the target orbit is observed to have a 9.35% reduction in price per flight while a near-equatorial launch further reduces this value by 3.34%, indicating that it is more important to design the launch vehicle for the target orbit rather than the intended launch site. Over 5 reuses is the minimum number of first stage reuses needed to see an improvement in price per flight compared to an expendable counterpart. Designing for the highest number of total launches and launches per annum is best for cost-reduction of these systems, with 100 total launches and over 10 launches per annum established as minimum values. A sensitivity analysis shows that the errors associated with the cost estimation relationships can reduce the Theoretical First Unit cost of the launch vehicle by 23.9% or increase it by 32.8%, indicating that great caution should be taken when refining future cost estimates. Additionally, the price per flight is not significantly affected by uncertainties in launch vehicle and cost parameters, with greatest sensitivity seen from uncertainty in the inert mass and in the manufacturing cost parameters. Thus, it is concluded that a small, reusable launch vehicle can definitively offer a 30% reduction in price per flight compared to the reported $29.9k per kilogram.

Acknowledgements

The following project is the culmination of my Master's thesis in Aerospace Engineering at the Delft University of Technology. During these last few months of hard work and pushing myself to my limits both physically and mentally, I can definitively stated that this was the most challenging yet rewarding task I have undertaken in my life. There are many people that were essential to my success, and I will forever be grateful for their endless support.

First, I would like to thank my daily supervisor Barry Zandbergen for being a great mentor not only throughout this thesis, but throughout my entire time in Delft. Barry has been an incredible resource in helping me adapt from a non-aerospace background, ceaselessly providing critical feedback that allowed me to become the best engineer I could be. I was given the freedom to explore a topic that was incredibly fascinating to me during my research and for that, I will always be thankful. In addition, I would like to thank Dominic Dirkx, who always welcomed my questions about and problems concerning Tudat with open arms. Without Dominic's help, the thesis would have been a much longer and more difficult process.

Furthermore, I would like to thank my parents, Sandra and Daniel, and my sister Emilie, for their unending support of my life choices. Despite being more than an eight hour flight from home, my family was always there to talk, support me or give me advice whenever I needed it. They have been my rock since well before my post-secondary studies and I can confidently say that I would not be the person I am today without them.

Thank you Anthony, Jaime Q, Jaime N, Tino and Pablo, as spending almost every day with you over the last two years has made this Master's degree go by extremely quickly, and you have all helped me feel at home in your native continent through our countless adventures together. I will never forget and always cherish our good times, and I hope our paths will cross many more times in the future.

Thank you Pat, Andrew, Pedro, Sean and Rob for being the best long distance friends anyone could ever need. You have supported me through countless conversations and Skype calls, forever giving me the best reason to come home.

To the rest of my friends and colleagues in Delft, thank you all for the memories that we have created while working towards the common goal of becoming aerospace engineers.

Contents

List of Figures

List of Tables

Nomenclature

Abbreviations

AC	Attitude control module
AV	Avionics
CEA	Chemical Equilibrium with Applications
CER	Cost estimation relationship
COM	Communications
CpF	Cost per flight
CT	Cost
DA	Direct ascent
DE	Differential Evolution
DHL	Data handling
DoD	Department of Defence
DRL	Downrange landing
EN	Engine
EPS	Electrical power subsystem
ESA	European Space Agency
EXP	Expendable
FM1	First Flight Model
FT	Full thrust, fuel tank
FUE	Fuel
GA	Genetic Algorithm
GNC	Guidance, navigation and control
GTOW	Gross take-off weight
HNS	Avionics harness
HTA	Hohmann transfer orbit
HTPB	Hydroxyl terminated polybutadiene
IHS	Improved Harmony Search
IS	Interstage
LEO	Low-Earth Orbit
LER	Length estimation relationship
LH2	Liquid hydrogen
LOX	Liquid oxygen
LpA	Launches per annum
LRE	Liquid rocket engine
LV	Launch Vehicle
M&PA	Management and product assurance
MAIT	Manufacturing, Assembly, Integration and Test

MDA	Multidisciplinary Design Analysis
MDO	Multidisciplinary Design Optimization
MECO	Main engine cut-off
MER	Mass estimation relationship
NAFCOM	NASA and Air Force Cost Model
NASA	National Aeronautics and Space Administration
NLR	Netherlands Aerospace Centre
OAT	One-at-a-time
OT	Oxidizer tank
OXI	Oxidizer
PA	Payload adapter
PaGMO	Parallel Global Multiobjective Optimizer
PF	Payload fairing
PIP	Pipes
PL	Payload
PLA	Payload adapter
PO	Project Office
PpF	Price per flight
PR	Propellant
PRE	Pressurizant
PS	Pressurization system
PSO	Particle Swarm Optimization
PT	Pressurizant tank
PV	Pipes and valves
PWR	Power
REQ	Requirement
RLV	Reusable Launch Vehicle
RP1	Rocket propellant-1
RSE	Relative standard error
RTLS	Return-to-launch-site
SA	Simulated Annealing
SC	Solid casing
SE	Standard Error
SH	Stage harness
SKI	Skirt
SLV	Small Launch Vehicle
SQP	Sequential Quadratic Programming
SRLV	Small Reusable Launch Vehicle
SRM	Solid rocket motor
SS	Stage structure

SSO	Sun-synchronous orbit	
TFU	Theoretical Flight Unit	
THM	Thermal control	
TL	Tool	
TPS	Thermal protection system	
TR	Trajectory	
TRC	Thrust cone	
Tudat	TU Delft Astrodynamics Toolbox	
TV	Thrust vector control	
TVC	Thrust vector control	
US 1976	United States Standard Atmosphere 1976	
VAL	Valves	
VEB	Vehicle Equipment Bay	

Greek Symbols

α	Angle of attack	[rad]
β	Nozzle convergent half angle	[°]
γ	Flight path angle	[rad]
Γ	Vandenkerckhove function	[-]
γ	Ratio of specific heats	[-]
ε	Expansion ratio	[-]
μ	Mean relative error	[%]
ρ_p	Propellant density	[kg·m^{-3}]
σ	Standard deviation of the mean	[%]
σ_t	Tank material stress	[Pa]
θ	Pitch angle	[°]
θ_n	Nozzle divergent half angle	[°]
ξ	Thrust correction factor	[-]

Roman Symbols

A_t	Throat area	[m^2]
a_x	Axial acceleration	[m·s^{-2}]
A_e	Nozzle exit area	[m^2]
C	Cost	[k€,k$]
c^*	Characteristic velocity	[m·s^{-1}]
C_F	Thrust coefficient	[-]
c_p	Profit rentention cost reduction factor	[-]
$C_{dev,a}$	Amortized development cost	[k€,k$]
C_{dev}	Development cost	[k€,k$]
C_{fac}	Facilities cost	[k€,k$]

C_{fleet}	Direct fleet operations cost	[k€,k$]
C_{low}	Lower TFU cost bound	[k€,k$]
$C_{man,n}$	Manufacturing cost of n^{th} unit	[k€,k$]
C_{man}	Manufacturing cost	[k€,k$]
C_{oh}	Overhead cost	[k€,k$]
$C_{ops,n}$	Operations cost of n^{th} unit	[k€,k$]
C_{ops}	Operations cost	[k€,k$]
C_{own}	Ownership cost	[k€,k$]
C_{rec}	Recovery cost	[k€,k$]
C_{trans}	Transportation cost	[k€,k$]
C_{upp}	Upper TFU cost bound	[k€,k$]
D_e	Nozzle exit diameter	[m]
D_s	Stage diameter	[m]
D_t	Nozzle throat diameter	[m]
d_{final}	Final downrange distance	[km]
d_{target}	Target downrange distance	[km]
E	Absolute mean relative error	[%]
f	Cost correction factor, fitness function	[-]
F_D	Drag force	[N]
F_T	Thrust force	[N]
FF	Fill factor	[-]
g_0	Earth's gravitational acceleration at sea level	[m·s^2]
h_{final}	Final altitude	[m]
h_{target}	Target altitude	[m]
I	Public damage insurance	[k€]
I_{sp}	Specific impulse	[s]
K_u	Percentage of unused propellant	[-]
k_{sm}	Interstage material correction factor	[-]
L_m	Manufacturing learning factor	[-]
L_0	Operations learning factor	[-]
L_{con}	Convergent nozzle section length	[m]
L_{div}	Divergent nozzle section length	[m]
$L_{fairing}$	Fairing length	[m]
$L_{interstage}$	Interstage length	[m]
L_{tanks}	Tank length	[m]
M	Mean molecular mass	[kg·mol^{-1}]
m	Mass	[kg]

$\dot{m}$	Propellant mass flow rate	[kg·s^{-1}]
M_f	Fuel mass	[kg]
$M_{avionics}$	Avionics mass	[kg]
M_{engine}	Liquid engine mass	[kg]
M_{EPS}	Power subsystem mass	[kg]
$M_{f,TPS}$	Fuel tank TPS mass	[kg]
$M_{fairing}$	Fairing mass	[kg]
M_{inert}	Inert mass	[kg]
$M_{interstage}$	Interstage mass	[kg]
$M_{intertank}$	Intertank mass	[kg]
$M_{ox,TPS}$	Oxidizer tank TPS mass	[kg]
M_{ox}	Oxidizer mass	[kg]
M_{pas}	Pad interface mass	[kg]
M_{PLA}	Payload adapter mass	[kg]
M_{PL}	Payload mass	[kg]
N	Number of stages	[-]
n	Number of samples	[-]
$N_{engines}$	Number of engines	[-]
OF	Oxidizer to fuel mass ratio	[-]
p	Multiplication factor, learning curve	[-]
P_c	Combustion chamber pressure	[Pa]
P_a	Ambient pressure	[Pa]
P_e	Nozzle exit pressure	[Pa]
P_{tank}	Tank pressure	[Pa]
q	Dynamic pressure	[Pa]
$\dot{Q}$	Convective heat flux	[W·m^{-2}]
Q_N	Vehicle complexity factor	[-]
R	Specific gas constant	[J·kg^{-1}K^{-1}]
R^2	Coefficient of determination	[-]
R_A	Universal gas constant	[J·mol^{-1}K^{-1}]
R_u	Longitudinal radius of the throat	[m]
S	Percentage of work subcontracted out	[-]
s_a	Semi-major axis score	[-]
s_e	Eccentricity score	[-]
S_{int}	Interstage surface area	[m^2]
SF	Sliver fraction	[-]
SF_t	Safety factor on tank wall thickness	[-]

t_b	Burn time	[s]
T_c	Combustion chamber temperature	[K]
t_c	Coast time	[s]
T_S	Specific transportation cost	[€·kg^{-1}]
V	Velocity	[m·s^{-1}]
v_e	Exhaust gas true exhaust velocity	[m·s^{-1}]
V_{ullage}	Ullage volume percentage	[-]
W	Work-year cost conversion	[k€]
$\bar{y}_i$	Model function value	[-]
y_i	Actual function value	[-]

1 Introduction

The rapid rise in production of small satellites in recent years has created a need for dedicated launch systems to bring these into orbit [1]. There are currently only three solutions for bringing small satellites into orbit [2]. The first involves having them share a ride alongside larger satellites in a dedicated launch vehicle. This method usually restricts the orbital parameters of the small satellite, as the launch orbit is dependent on the needs of the primary satellite, and costs anywhere between $200k (2014) and $325k (2014) for a 3U CubeSat [2]. A second solution is a cluster launch, where a collection of small satellites are launched to the same orbit as part of a rideshare agreement, with this method costing up to $110k (2014) per kg into orbit [2]. The final solution to the need for small satellite launches is the recent development of small launch vehicles (SLVs) . Both public space agencies and private companies have been developing small launch vehicles with payload capacities below 1000 kg in order to provide a lower cost alternative to the first two presented options [3]. With active and future SLVs averaging an advertised launch price of $29.9k (2018) per kg to low-Earth Orbit (LEO) [1], these solutions are promising for small satellite cost to orbit. The expendable version of the Falcon 9 offers $2.675k (2018) per kg to LEO for a maximum payload of 22800 kg, setting the benchmark for lowest price to orbit [1]. Nonetheless, a dedicated small launch vehicle, defined as a system capable of bringing up to 1000 kg of payload to a desired orbit, offers lower advertised prices compared to rideshare and cluster launches by over threefold [1].

An important detail regarding the advertised launch price of small launch vehicles is that only a handful of the service providers have demonstrated these reduced launch prices. Among currently active small launch vehicles, the Kuaizhou-1A from the China Aerospace Science and Technology Corporation leads the way at an advertised launch price of $20.54k (2018) per kilogram to orbit, followed by Rocket Lab's Electron at $33.55k (2018) per kilogram and Northrop Grumman's Minotaur I at $38.00k (2018) per kilogram [1]. However, several companies currently developing small launch vehicles are advertising even better rates, from the Indian Space Research Organization with its Small Satellite Launch Vehicle offering a launch price of $8.83k (2018) per kilogram, to ARCA Space Corporation with its HAAS 2CA at $10.27k (2018) per kilogram, and Vector's Vector-H offering a launch price of $12.39k (2018) per kilogram [1]. Additional information concerning target launch rates, payload range and target orbits are summarized in Table 1.1.

Table 1.1: Key parameters concerning small launch vehicle targets [1].

Key Parameters	**Value**	**Launch Vehicle**
Minimum price per kilogram	$8.83k/kg (2018)	ISRO SSLV
Maximum target launch rate	100/year	Vector-R
Payload range	5 kg - 1000 kg	SS-520-5/Firefly α
Target orbit	LEO SSO	-

In parallel, reusability of launch vehicles has become a topic of interest as of late due to its potential to reduce overall launch prices, especially when focusing on the first stage [4, 5]. Full reusability of a launch system has never been demonstrated, but partial reusability still provides the advantage of reducing production costs over the life cycle of the system due to reuse of software and hardware, dependent on factors such as launch rate, number of units produced, and number of reuses. Although historical horizontal landing reusable launch vehicles (RLVs) such as the Space Shuttle have proven to be much more costly than anticipated, with an expected launch cost of $450M (2010) actually totalling $1.55B (2010) per launch [6, 7], recent successes with vertical take-off, vertical landing from SpaceX with the Falcon 9 and Falcon Heavy launch vehicles have garnered new interest in reusability [5, 8, 9]. With SpaceX president Gwynne Shotwell stating "launch costs will decrease by about 30% because of reusable rockets [5]," reusable launch vehicles offer the potential for further decreases in satellite price per kilogram to low-Earth orbit.

In combination with a reusable system, launch prices could further decrease by up to 30% for small launch vehicles as well. However, this is all assuming that the advertised launch prices and statements made from SpaceX officials are indeed valid. From the literature study, historical data from the Space Shuttle indicates that winged orbital vehicle are much more costly than initially planned. Moreover, SpaceX's initial attempts at recovering the first stage of the Falcon 9 made use of a parachute system, but this method failed due the parachute's inability to reduce the first stage to reasonable speeds through the upper atmosphere, leading to burning up upon re-entry. Based on this historical precedent, retro-propulsion vertical take-off, vertical landing systems are the most promising solution for small, reusable launch vehicles. As the majority of the parameters affected by reusability are disadvantages, the greatest advantage comes in the form of potential reduction in launch price over the system's life. Higher development and operations cost are mitigated by lower production costs for the Falcon 9. From this information, it is concluded that the development of a small, reusable launch vehicle modelling tool should focus on cost minimization. An improvement on the reported average of $29.90k (2018) per kilogram to orbit of small launch vehicle manufacturers would present a cost-effective solution to orbit. As established in the literature study, two different launch vehicles are to be optimized for a payload of 100 kg and 500 kg to a Sun-synchronous orbit at an altitude of 650 km. As such, through a 30% reduction in launch prices, these systems are deemed cost-effective if they can achieve a price per launch below $2.00M (2018) and $10.0M (2018), respectively.

There currently exists no open-source tool for designing and costing small and reusable launch vehicles making it difficult to verify the claims made by industry professionals. An in-depth literature review of the past, previous and future markets of both small and reusable launch vehicles established the need for and confirmed the feasibility of modelling a small, reusable launch vehicle [1]. At the early design phases, public companies and private agencies could benefit from a tool that both predicts the cost of developing such a system given a specific mission and optimizes this system for minimum cost or maximum payload performance. Such a tool would also allow critical assessment of claims made by reusable and small launch vehicle developers. The reuse of an upper stage has recently been investigated, which yielded a reduction in launch cost of only 6.3% [10]. However, a small launch vehicle with reusable first stage has been investigated by Snijders and yielded promising results of up to 50% launch cost reduction for ten launches per year and ten first stage reuses, but in this study the expendable launch vehicle design was already set, and the model does not include development costs [11]. A tool capable of designing and optimizing a launch vehicle from basic propulsion parameters and that includes full life-cycle costs gives interested parties more design freedom and accuracy in their results. Vandamme, van Kesteren and Miranda have developed an open-source tool to design and optimize a small, air-launched solid, liquid and hybrid system, respectively [12–14]. These works are used as a starting point for this research as a greater focus can be set on the reusable launch vehicle, trajectory and cost models. The main research objective is presented as follows.

The research objective is to develop a tool capable of designing and optimizing a small, reusable launch vehicle, focusing on the retro-propulsion techniques employed by SpaceX for first stage re-entry, recovery and reuse.

This objective is achieved by adapting current design tools developed at the Delft University of Technology for launch vehicles, while adding supplementary functionality to the design tools to model the desired system. This leads to the following research question.

Is a small, reusable launch vehicle a cost-effective solution to bringing small satellites into low-Earth orbit, and if so, under what conditions?

To answer this question, a launch vehicle, trajectory and cost model must first be developed, before these can be integrated in an optimization environment to design the best potential design given a specific objective function. Chapter 2 presents a brief summary of the literature used as a starting point for this work, the development environment and its past uses, and the requirements for the tool and models that were developed. Chapter 3 details the launch vehicle propulsion, geometry and mass models including necessary verification and validation. Chapter 4 summarizes the ascent trajectory model adopted from previous works before detailing the reusable first stage trajectory model. The cost model is presented in Chapter 5 before the integration of the models into the tool is detailed in Chapter 6. The results for various cases are presented in Chapter 7 and a sensitivity analysis is then conducted in Chapter 8. Finally, conclusions and recommendations from the research are presented in Chapter 9 and Chapter 10, respectively.

2
Literature Study

The design of a small, reusable launch vehicle encompasses several fields, making the project highly multidisciplinary. This chapter presents a brief summary of past and present, small and reusable launch vehicle technologies to provide context for the research, in addition to the multidisciplinary design analysis and optimization environment, before detailing the requirements for the tool that has been developed. While the literature study includes a thorough analysis of the various disciplines [1], this literature review covers the most pertinent and relevant material for this research, presenting the main conclusions to be used in this work.

2.1. Small Launch Vehicles

A small launch vehicle is defined as a launch vehicle capable of bringing up to one metric ton of payload into low-Earth orbit [3]. An extensive survey of the retired, planned and operational small launch vehicles was previously conducted by the author [1]. From this survey, conclusions were made about preferred propulsion systems, the competitive price per kilogram to orbit, expected launch mass as a function of payload mass, and the geometry of a small launch vehicle. Along with setting a baseline on typical values found for these launch systems, the survey also reveals insight into mass trends that should be investigated in this work. The launch cost data is shown in Figure 2.1, while a summary of all the results is presented in Table 2.1, where "Mixed Data" indicates a launch vehicle with both solid and liquid stages. It is important to note that while the standard deviation can be used to describe the confidence in a normal distribution, it is used here to denote the variation in the set of values.

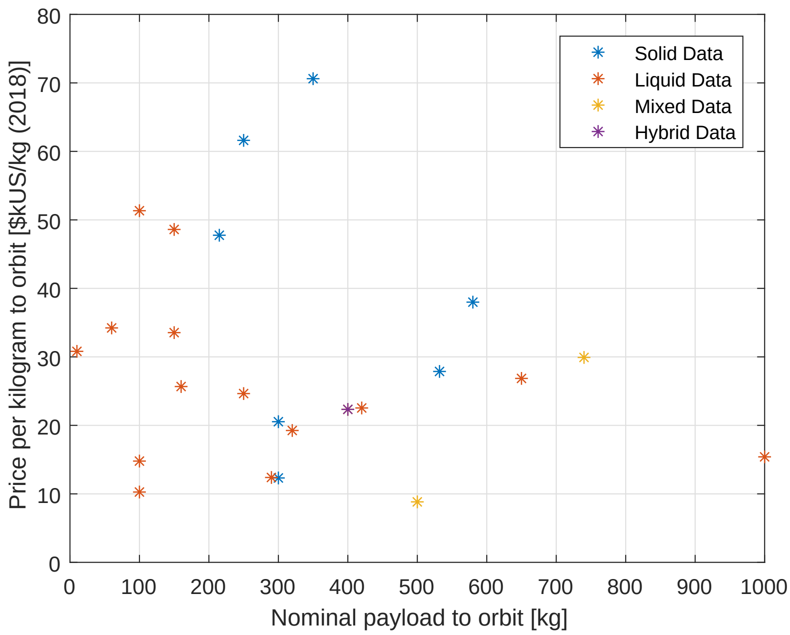

Figure 2.1: Cost per kilogram to orbit of surveyed small launch vehicles, separated by propulsion system [1].

Table 2.1: Small launch vehicle survey summary.

Information	Findings
Propulsion system	Liquid propulsion system preferred for payload below 200 kg Solid and mixed propulsion systems preferred for payload above 200 kg
Cost per kilogram to orbit	Minimum: \$8.83k (2018) Maximum: \$70.6k (2018) Average: \$29.9k (2018) Standard deviation: \$16.1k (2018)
Launch vehicle height	Minimum: 9.54 m Maximum: 34.0 m Average: 21.3 m Standard deviation: 5.86 m
Launch vehicle diameter	Minimum: 0.52 m Maximum: 3.00 m Average: 1.57 m Standard deviation: 0.56 m

From the above summary, conclusions can be made about the scope of the research. Trends seen in the propulsion systems indicate that liquid systems are preferred for payload masses below 200 kg, while solid and mixed systems are preferred for payload masses above 200 kg. Due to these trends, two reference missions with payload masses of 100 kg and 500 kg will be investigated to try to determine the reason behind these trends. The final orbit of these satellites will be a 650 km altitude Sun-synchronous orbit due to additional trends seen in small satellite mission [15]. Furthermore, the geometry of the small launch vehicle to be designed will be restricted to the range given in Table 2.1. This means that the diameter will be constrained between 0.5 m and 3.0 m, with more freedom given to length. Finally, as the average cost per kilogram to orbit is \$29.90k (2018), a small, reusable launch vehicle will be considered economically advantageous if the reduction in launch cost is greater than 30%, as per the benchmark set by SpaceX officials. This sets the target launch cost at below \$20.00k (2018) per kilogram, or a price per flight of \$2.00M for the 100 kg payload and \$10.0M for the 500 kg payload.

2.2. Reusable Launch Vehicles

As mentioned in the introduction, no small, reusable launch vehicle is currently on the market, thus a focus is set on all reusable launch vehicles. In the past, only four different orbital launch systems, namely the Space Shuttle, the Boeing X-37, the Falcon 9 and the Falcon Heavy, have reused flight hardware, with winged reusable systems such as the Space Shuttle proving to be more costly than expendable counterparts and negatively impacting launch rate [1].

Conversely, SpaceX have proven that retro-propulsion techniques for recovery and reuse have positively impacted launch costs and launch rate. SpaceX initially opted to recover the first stage of the Falcon 1 and Falcon 9 with parachutes decelerating the stage through the atmospheric re-entry. Two Falcon 1 and two Falcon 9 first stage recovery attempts failed with the first stage burning up upon re-entry before the parachutes could be deployed, because of excessive velocities reached by the stage. This led SpaceX to investigate, and eventually successfully perform, propelled vertical landings due to the protective plume caused by the engine exhaust which acts as a blanket over the first stage during re-entry, to the slower re-entry velocities, and to the added controllability compared to parachutes [16, 17]. Since the first successful vertical landing after orbital launch in 2015, the Falcon 9 has flown 54 more times, with 21 of those flights using a first stage used once or more than once in the past. SpaceX's Falcon Heavy is another partially reusable heavy-lift launch vehicle derived from the Falcon 9 rocket. With reusability in mind from the start of the design process, SpaceX has been able to offer very competitive prices for their launches. For instance, a reusable Falcon Heavy could be launched at a starting price of \$90M (2018), which is less than a quarter of the price of a \$400M (2018) Delta IV Heavy, its closest competitor in terms of payload capacity [8].

The reusable flight profile of a Falcon 9 is depicted as follows. After launch and upon second stage separation, cold gas thrusters flip the first stage such that the tail end of the stage is in line with its velocity vector. Then, the engine reignites in a boostback burn to bring the trajectory of the vehicle towards the landing site. Grid fins are then deployed to stabilize and control the stage during its re-entry. The engine is ignited once more to slow down the first stage, before the grid fins are used to steer the lift produced by the stage. Prior to landing, the landing legs are deployed and the first stage is ignited one last time to ensure a precise landing before the final touch down [18]. A close-up view of the Falcon 9 grid fins and landing legs are seen in Figure 2.2 and Figure 2.3, respectively.

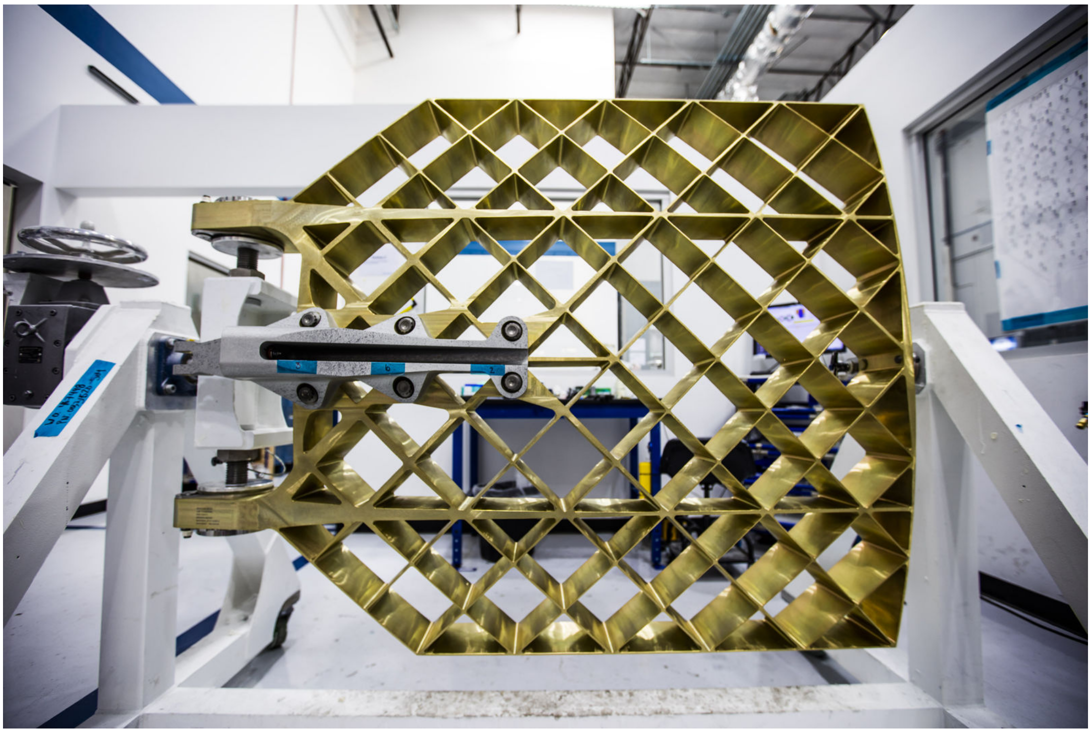

Figure 2.2: Close-up of Falcon 9 grid fins before painting [19].

Figure 2.3: Close-up of a Falcon 9 landing burn with landings legs deployed [19].

SpaceX has demonstrated a soft landing both on a drone ship in the Atlantic Ocean and back at the launch site. The latter scenario requires an additional burn to change the trajectory of the first stage more drastically, and requires more propellant. In fact, reusing a first stage reduces the payload capability of the launch vehicle, decreasing by 20% for a downrange landing (DRL) compared to 40% for a return-to-launch-site (RTLS) landing for a LEO payload [1]. Thus, SpaceX tailors its launch services based on the needs of the customer. If a customer books a launch beyond the reusability threshold, SpaceX will opt for the non-reusable version of the Falcon 9. The price difference between the reusable and expendable versions of the Falcon 9 is not documented, but if these are the same, the expendable version thus offers a lower price per kilogram. Assuming a company expects to make the same profit from a reusable launch compared to an expendable launch, this arises the question of determining the total life-cycle costs of a reusable launch vehicle compared to an expendable counterpart.

Blue Origin are also developing a heavy-lift launch vehicle named the New Glenn that will also employ retro-propulsion techniques for recovery. However, they have only demonstrated the technology sub-orbital flights, and little information regarding costs have been made public [1].

Both companies that have proven retro-propulsion landings using liquid rocket engines, as these have reignition and throttling capabilities which are essential during re-entry and landing, and which are extremely difficult to achieve with solid motors [20]. Thus, for the reusable system to be designed, a liquid first stage will be imposed, with the freedom to choose between solid and liquid propulsion for upper stages.

2.3. Multidisciplinary Design Analysis and Optimization

Multidisciplinary Design Analysis (MDA) is a process that aims to satisfy the coupling between various subsystems. Multidisciplinary Design Optimization (MDO) is a set of engineering design methods that aim to take advantage of the coupling between these various subsystems in order to reach an optimal solution. This section introduces the two concepts, details how MDA and MDO are used for the design and optimization of a small, reusable launch vehicle in this work, and elaborates on the tool used to implement these concepts.

As launch vehicle design is a highly multidisciplinary problem, Multidisciplinary Design Analysis and Optimization are commonly used in literature. Villanueva [21, 22], Castellini [23], Jodei [24], and van Kesteren [13] have all used MDO to model solid propellant launch vehicles, with each study selecting design parameters based on propulsion and geometry. Castellini [23], Akhutar [25], and Vandamme [12] have also used this technique for liquid launch vehicles, while Miranda has employed it for hybrid systems [14].

The general formulation of an MDO algorithm is as shown in Equation 2.1, where $f(x, y, z)$ is the objective function, and z_g and z_k are the global and local design variables, respectively, where the former refer to variables used throughout the disciplines such as sizes and masses while the latter are used within a single discipline and include chamber pressure, exit pressure and other propulsion variables. In addition, $g(x, y, z)$ are inequality constraints, $h(x, y, z)$ are equality constraints, $c(x, y, z)$ are the coupling functions between subsystems and $R(x, y, z)$ are the residual functions used to quantify the satisfaction of the individual state equations [13, 26]. A launch vehicle can be optimized for minimum launch wet or dry mass, maximum payload to orbit, or minimum launch cost, and the reason for this is further described in Chapter 7. Trajectory variables are usually considered as state variables x. Coupling variables usually include the dry mass, the specific impulse, and the length and diameter of each stage. Equality constraints deal with the specifics of the mission such as desired orbit and payload mass, while inequality constraints deal with maximum and minimum allowable values in a subsystem such as maximum chamber pressure, maximum load factor and minimum nozzle exit pressure [26].

$$
\begin{aligned}
&\text{minimize} && f(x, y, z) \\
&\text{with respect to} && z = [z_g, z_k] \\
& && g(x, y, z) \leq 0 \\
&\text{subject to} && h(x, y, z) = 0 \\
& && \forall i, \forall j \neq i, y_i = \{c_{ji}(x_j, y_j, z_j)\}_j \\
& && \forall i, R_i(x_i, y_i, z_i) = 0
\end{aligned}
\tag{2.1}
$$

The general process behind an MDO tool is depicted in Figure 2.4, where the lines connecting the boxes indicate coupling between the disciplines.

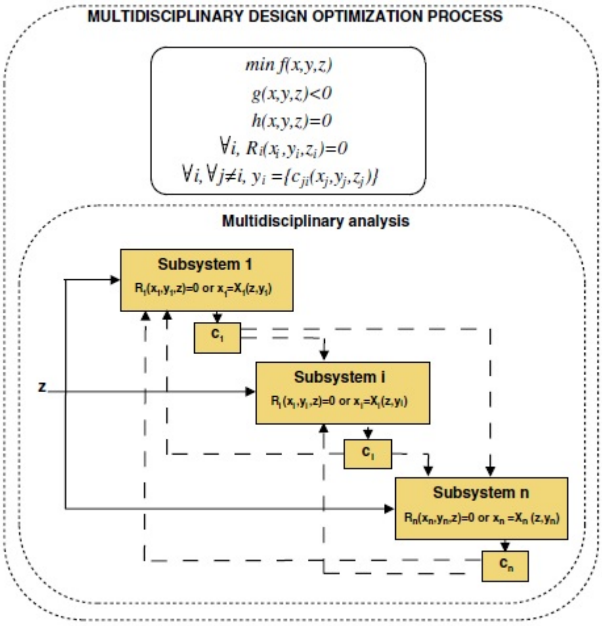

Figure 2.4: General process of a multidisciplinary design optimization [26].

The typical decomposition of MDA and MDO disciplines for launch vehicle design is seen in Figure 2.5. Given an optimization algorithm with an objective function, constraints and design variables, the various disciplines can be modelled in the order shown in the grey box through the coupling functions. After the trajectory has been modelled, the objective function and constraints are evaluated before this process is repeated until an optimal solution is found.

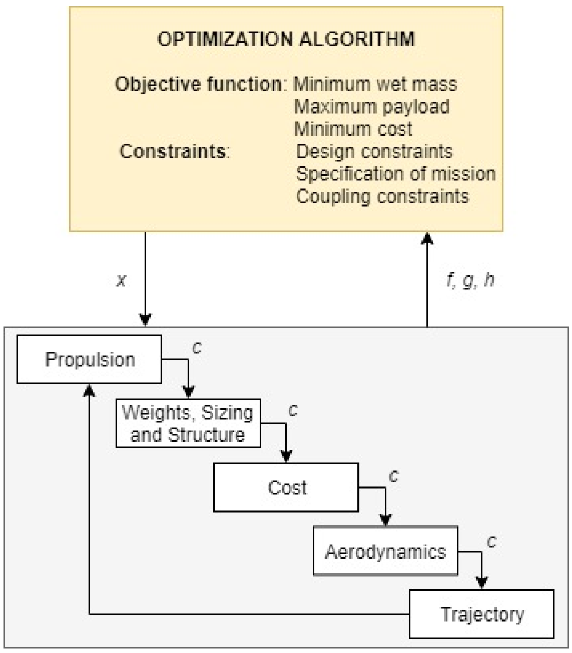

Figure 2.5: Typical breakdown of launch vehicle disciplines for MDO process.

2.4. Optimization Algorithms

The optimization methods can be separated into two types of algorithms, namely gradient-based algorithms and heuristic algorithms [13]. The former consists of differentiating the objective function and constraints to evolve the variables and to reach a local optimal solution. This method thus requires smooth, differentiable objective and constraint functions. Examples of gradient-based algorithms include Sequential Quadratic Programming (SQP) , Newton's Method and the Steepest Descent method. Conversely, heuristic algorithms perform a search of variables in a stochastic manner, providing the advantage of working with non-differentiable objective and constraint functions. For this reason, as well as the complex non-linearity of launch vehicle design, heuristic algorithms are preferred over gradient-based techniques [13, 26]. Examples of heuristic algorithms include the Genetic Algorithm (GA) , Particle Swarm Optimization (PSO) , Simulated Annealing (SA) and Differential Evolution (DE) . The general functioning of these algorithms is described below.

1. GA: Genetic algorithms use evolutionary processes from genetics to optimize a function, first establishing an initial population from the design variables converted to chromosomes in a binary notation. These populations are then evaluated through multiple generations, where the best chromosomes from each generation are kept until convergence is obtained in the solution [13].

2. PSO: In particle swarm optimization, candidate solutions are mimicked as flocks of birds or school of fish. These candidates move through the defined search space by following particles that have the lowest cost at every iteration of the optimization [13].

3. SA: Simulated annealing is designed based on processes in the metallurgical industry, where each point is considered as a state in a physical system and the objective function must minimize the internal energy of the system. For optimization, the process changes one variable at a time to determine its effect on the solution [26].

4. DE: A subset of genetic algorithms, differential evolution uses real numbers instead of chromosomes to evaluate the goodness of fit of each population [13].

Common advantages of PSO and SA is that these require less computational complexity when compared to GA and DE, as these methods only modify single agents between iterations as opposed to the majority or all of the population. However, this sometimes leads PSO and SA algorithms to be trapped in local optima, which does not happen with GA and DE [27]. Quantifying this computational complexity generally is difficult due to the differences in each optimization process, but is dependent on the size of the search space and of the population.

Although all of the heuristic algorithms mentioned above have been used in launch vehicle design in the past [26], the no free lunch theorem states, "any two optimization problems are equivalent when their performance is averaged across all possible problems," meaning that there is no clear optimal optimization routine for launch vehicle design [28]. This is demonstrated through the analysis conducted by Castellini as well as the comparison of methods conducted by Zitzler [23, 29]. Nonetheless, GA and DE techniques are more frequently used for launch vehicle optimization [21–23, 30–32], while PSO is more frequently used for pure trajectory optimization [33–35]. Furthermore, Vandamme and van Kesteren have demonstrated that DE outperforms PSO for likeliness of convergence and quality of optimal solution for solid and liquid small launch vehicles, respectively [12, 13].

The next section presents the development environment used during the research.

2.5. Development Environment

Before detailing the theory needed to model a small, reusable launch vehicle, this section presents the development environment in which the work is performed. As the base of this work is adopted from Vandamme, van Kesteren and Miranda, several models have already been implemented and validated in the tool [12–14]. This section also describes the models that have already been developed in the Tudat framework, as well as any modifications or improvements to the tool.

The TU Delft Astrodynamics Toolbox (Tudat) is a set of C++ libraries that is developed at the university and that has been used in the framework of a Master's thesis for launch vehicle modelling in the past [12–14]. One of the key strengths of Tudat is its ability to combine validated libraries such as gravity, atmospheric and aerodynamic models in a powerful simulator framework. The solid launch vehicle model developed in Tudat has also been validated, removing the need to start the work from the basic theory. Instead, a focus can be set on adapting the liquid launch vehicle model and including reusability and cost models to design and optimize a small, reusable launch vehicle. The Tudat software also includes the functionality to be used with the Parallel Global Multiobjective Optimizer (PaGMO) platform developed by the European Space Agency

(ESA) [36], which offers the advantages of having already been developed and validated. The PaGMO platform includes all of the aforementioned heuristic algorithms.

2.5.1. Existing Models

To simulate a small, reusable launch vehicle from the Earth's surface to a target orbit, several key models independent of the launch vehicle are necessary. This section provides a brief overview of the models that have already been implemented in the Tudat environment.

First, it is necessary to characterize the atmosphere surrounding the launch vehicle during flight to properly account for the forces acting on the launch vehicle. Tudat allows for the choice between difference existing atmospheric models, but to remain consistent with the previous studies done in this environment, the US Standard Atmosphere 1976 (US 1976) model is used. This model presents values for atmospheric parameters from the Earth's surface up to 1000 km at a latitude of 45° North, suitable for the LEO missions of interest. The US 1976 model uses the geometric altitude Z and the geopotential altitude H, where the latter is an adjustment to Z using the variation of gravity with elevation. The model divides the lower atmosphere (<86 km) into eight layers and the upper atmosphere (86 km to 1000 km) is divided into four sections to determine the temperature. The atmosphere is divided into the lower and upper atmosphere to determine the pressure at a given altitude, and the density of the air is then calculated using the ideal gas law [12]. This model has been validated from an altitude between -5 km and 1000 km.

Furthermore, a gravitational model is necessary to characterize the force of gravity on the launch vehicle, which is one of the main forces that acts on a launch vehicle during flight. The central gravity model is an approximation to the attraction law between two bodies that discards the mass of the launch vehicle, as it is negligible compared to the mass of the Earth [13]. A more detailed model that accounts for the non-spherical shape of the Earth with spherical harmonics has also been investigated to determine its impact on the gravitational forces acting on the launch vehicle, and the most dominant term was found to have a magnitude of 5μg [13]. Accounting for the spherical harmonics can also have a computing time up to fiftyfold that of the central gravity model, making it unattractive for calculation time [11]. Spherical harmonics are thus ignored due to their insignificant contribution to the gravitational forces and added computation time. The agreement between the central gravity and more complex spherical harmonics models serves to verify its functionality and validate its use for launch vehicle modelling.

Additional modules already implemented in Tudat include reference frame transformations, definition of the equations of motion and numerical integrators. The Tudat environment has been used extensively in published works since 2012, thus the additional modules mentioned above, which are applicable to a wide variety of astrodynamic problems, have all been validated. The reader is referred to the work of Vandamme and van Kesteren, as well as the documentation of the Tudat tool for more detailed explanations of these flight mechanics and environment models [12, 13, 37].

2.6. Tool Requirements

A list of requirements can be set for the models that were developed during the research based on the information gathered in the literature study. The requirements (REQ) are listen in Table 2.2, separated by their applicability to the launch vehicle (LV), trajectory (TR) or cost (CT) models. Furthermore, the reasoning behind the values chosen is as presented in the works under the "Source" column, or is an improvement on these works. All reported accuracies indicate the absolute relative error as defined in Section 3.5.

Table 2.2: List of requirements established for the models.

ID	Requirement	Source
REQ-LV-001	The tool shall be able to model the thrust of solid and liquid stages to within 10% accuracy.	[12], [13]
REQ-LV-002	The tool shall be able to model the specific impulse of solid and liquid stages to within 10% accuracy.	[12], [13]
REQ-LV-003	The tool shall be able to model the propellant mass of solid and liquid stages to within 10% accuracy.	[12], [13]
REQ-LV-004	The tool shall be able to model the inert mass of launch vehicle stages to within 10% accuracy.	[12], [13]
REQ-LV-005	The tool shall be able to model the length of launch vehicle stages to within 10% accuracy.	[12], [13]
REQ-LV-006	The tool shall be able to model the GTOW of launch vehicles to within 10% accuracy.	[12], [13]
REQ-TR-001	The tool shall be able to simulate the launch vehicle to within 3% of the desired altitude.	[12], [13]
REQ-TR-002	The tool shall be able to simulate the launch vehicle to an eccentricity less than 0.1.	[12], [13]
REQ-TR-003	The tool shall be able to simulate the launch vehicle to within 1° of the desired inclination	[12], [13]
REQ-TR-004	The tool shall be able to simulate the reuse landing altitude to within 1m of the desired value.	[38]
REQ-TR-005	The tool shall be able to simulate the reuse landing velocity to less than 5m/s.	[38]
REQ-TR-006	The tool shall be able to simulate the reuse desired downrange distance to within 5km.	[38]
REQ-CT-001	The tool shall be able to model the price per flight of solid and liquid launch vehicles to within 20% accuracy.	[39, 40]

From Table 2.2 as well as the information gathered in the literature study, requirements for the tool (TL) to be developed can be derived, shown in Table 2.3.

Table 2.3: List of requirements established for the tool.

ID	Requirement
REQ-TL-001	The tool shall be developed in the Tudat environment, coded in C++.
REQ-TL-002	The tool shall model and optimize return-to-launch-site and downrange landing reusable launch vehicles, as well as expendable launch vehicles to the accuracies shown in Table 2.2.
REQ-TL-003	The tool shall be able to model a reusable launch vehicle in less than 0.5 seconds.
REQ-TL-004	The tool shall be able to simulate the ascent and descent of a reusable launch vehicle in less than 1 second.
REQ-TL-005	The tool shall be able to output the physical launch vehicle parameters necessary for analysis and comparison purposes.
REQ-TL-006	The tool shall be able to output the full simulation time history of the ascent and descent trajectories in a text file.
REG-TL-007	The tool shall output the optimal objective function and optimal design parameters in a text file.
REQ-TL-008	The inputs of the tool shall be read from user-modifiable text files.

The following chapters deal with the actual models used and developed in the study, starting with the launch vehicle model in Chapter 3.

3
Launch Vehicle Propulsion, Geometry and Mass

The first step in simulating a small, reusable launch vehicle is to model the launch vehicle that will be optimized for flight. As mentioned in the Introduction, the first stage of a reusable launch vehicle must be a liquid stage due to its ability to reignite and throttle throughout the atmosphere and especially during landing. Nonetheless, it may be advantageous to use solid-propelled upper stages, as these have proven to be less expensive in the past [1].

This chapter deals with the theory necessary to model the propulsion, geometry and mass of both solid and liquid stages, as well as the launch vehicle in full. Additionally, information regarding geometry and mass of the reusability elements of launch vehicles is included. Finally, the concepts of verification and validation are introduced, before their application to solid and liquid stages and launch vehicles, as well as the reusability models, is presented.

3.1. Propulsion

Modelling a stage and, inherently, a launch vehicle, starts with modelling the propulsion of such a stage. As done in many previous studies, the main design parameters are related to the propulsion subsystem. This is advantageous as most geometry and mass models rely on propulsion subsystem information such as thrust, F_T and specific impulse, I_{sp} , and both solid and liquid launch vehicles can be built from the same design parameters.

To model the propulsion of solid and liquid stages, ideal rocket theory is used as a starting point [41]. The thrust provided by an ideal rocket motor or engine is given by Equation 3.1, where $\dot{m}$ is the propellant mass flow rate, v_e is the true velocity of the exhaust gases, A_e is the nozzle exit area, P_e is the nozzle exit pressure and P_a is the ambient pressure.

$$F_T = \dot{m} v_e + A_e (P_e - P_a) \tag{3.1}$$

Additionally, the specific impulse is calculated using Equation 3.2, where g_0 is the Earth's gravitational acceleration at sea level.

$$I_{sp} = \frac{v_e}{g_0} \tag{3.2}$$

In Multidisciplinary Design Analysis and Optimization, "design variables should be selected to represent an overall description of the design, as they also significantly affect the objective function and constraint values" [24]. In the previous works that this research is building upon, the design parameters were chosen due to the ability to model the performance of a launch vehicle stage in parallel with another important tool [12–14]. The free NASA Chemical Equilibrium with Applications (CEA) tool is used to calculate complex chemical equilibrium product concentrations from a set of reactants and determines thermodynamic and transport properties for the product mixture [42]. This tool has been used and validated in previous works [12–14], setting the building block from which to build upon for the solid and liquid stages. Furthermore, the specific choice of parameters in this study allows for the design of both solid and liquid stages simultaneously through the optimization of parameters that affect the performance of the vehicle. In the case of a given solid motor or liquid engine, a tabulated input of performance can be used, which would lead to a different set of design parameters.

The design parameters used in this work are summarized in Table 3.1. Note that the last three entries are only used as design parameters for liquid stages.

Table 3.1: Propulsion design parameters for launch vehicle stage modelling.

Symbol	**Description [units]**
P_c	Combustion chamber pressure [Pa]
P_e	Nozzle exit pressure [Pa]
D_s	Stage/case diameter [m]
D_e	Nozzle exit diameter [m]
t_b	Burn time [s]
t_c	Coast time [s]
OF	Oxidizer to fuel mass ratio [-]
Propellant	Propellant choice [-]
$N_{engines}$	Number of engines [-]

Given a combustion chamber pressure and the type of propellant used, important values such as the combustion chamber temperature T_c, the ratio of specific heats γ and the combustion gas mean molecular mass M are output using CEA. All of the above information can be used to develop the launch vehicle propulsion model. First, the Vandenkerckhove function, Γ, and the specific gas constant R using the universal gas constant R_A of 8314 J·K^{-1}·mol^{-1} are calculated in Equation 3.3 and Equation 3.4, respectively.

$$\Gamma = \sqrt{\gamma}\left(\frac{2}{\gamma+1}\right)^{\frac{\gamma+1}{2(\gamma-1)}} \tag{3.3}$$

$$R = \frac{R_A}{M} \tag{3.4}$$

Next, the expansion ratio ε can be calculated as done in Equation 3.5.

$$\varepsilon = \frac{A_e}{A_t} = \frac{\Gamma}{\sqrt{\frac{2\gamma}{\gamma-1}\cdot\left(\frac{P_e}{P_c}\right)^{\frac{2}{\gamma}}\left(1-\left(\frac{P_e}{P_c}\right)^{\frac{\gamma-1}{\gamma}}\right)}} \tag{3.5}$$

The throat area A_t can also be calculated using Equation 3.5, before calculating the mass flow rate as shown in Equation 3.6.

$$\dot{m} = \frac{P_c\cdot A_t\cdot\Gamma}{\sqrt{R\cdot T_c}} \tag{3.6}$$

The characteristic velocity c^* and the thrust coefficient C_F are then calculated as in Equation 3.7 and Equation 3.8, respectively.

$$c^* = \frac{1}{\Gamma}\sqrt{R\cdot T_c} \tag{3.7}$$

$$C_F = \Gamma\sqrt{\frac{2\gamma}{\gamma-1}\left(1-\left(\frac{P_e}{P_c}\right)^{\frac{\gamma-1}{\gamma}}\right)} \tag{3.8}$$

Finally, the exhaust velocity is calculated using Equation 3.9.

$$v_e = c^*\cdot C_F \tag{3.9}$$

Using the equations above, the thrust and specific impulse of an ideal solid or liquid propulsion system can be determined. To correct for the non-ideal behaviour of real solid rocket motors and liquid engines, a correction factor ξ is introduced in the thrust calculation, as shown in Equation 3.10. The value for ξ is based on regression and is determined in Section 3.5. In the case of nozzle divergence, the correction factor only applies to the momentum thrust term in Equation 3.10, but since the factor is determined from regression data, its multiplication with the total thrust or momentum term is irrelevant, only affecting its magnitude.

$$F_T = \xi \left(\dot{m} v_e + A_e (P_e - P_a) \right) \tag{3.10}$$

Equation 3.1 to Equation 3.10 are applicable for both solid and liquid stages. The following section deals with geometry and mass modelling of these stages.

3.2. Geometry and Mass

The main differences between solid and liquid stages arise in the geometry and mass modelling of these systems. Solid and liquid rocket stages are described in the following sections.

3.2.1. Solid Rocket Stage

The geometry and mass of a solid rocket stage can be determined from key outputs of the propulsion subsystem. The length and mass of these systems are generally formulated as in Equation 3.11 and Equation 3.12, respectively.

$$L_{SRM} = L_{case} + L_{con} + L_{div} \tag{3.11}$$

$$M_{SRM} = M_P + M_{nozzle} + M_{case} + M_{igniter} \tag{3.12}$$

As shown in the work of van Kesteren [13], the characteristic velocity, and thus the performance, of various solid propellants varies by less than 1% over a range of chamber pressure from 30 bar to 100 bar. For this reason, as well as being the most commonly used solid propellant and showing slight performance improvements compared to poly-butadiene acrylonitrile [41], hydroxyl terminated polybutadiene (HTPB) is used for modelling solid rocket motors.

First, the propellant mass of a solid rocket motor can be calculated using Equation 3.13, where SF is the percentage of unburned propellant resulting from the solid grain geometry, known as the sliver fraction. This value is set to 3% from typical values in literature [43]. In fact, a 3% sliver fraction is an upper limit value, as technological advancements in grain design have resulted in slivers less than 1% [43].

$$M_P = (\dot{m} \cdot t_b) \cdot (1 + SF) \tag{3.13}$$

The length of a solid motor case can be determined as shown in Equation 3.14 under the assumption that the wall and insulation of the motor case is equal to 1% of the motor diameter, which has been validated for length and mass models [13], and where ρ_p is the density of the propellant and FF is the percentage of the total volume occupied by the solid grain, known as the fill factor. The value of fill factor in this study is set to a nominal value of 95% [43], and it has been shown that a 5% variation in this value affects GTOW by less than 0.5%, well within the requirements of the tool [13].

$$L_{case} = \frac{M_p}{\rho_p \cdot \pi \left(\frac{0.99 D_s}{2} \right)^2 \cdot FF} \tag{3.14}$$

The length of the convergent and divergent sections of the solid motor nozzle can be calculated using Equation 3.15 and Equation 3.16, respectively, where D_t is the diameter of the nozzle throat, R_u is the longitudinal radius of the throat, β is the convergent half angle and θ_n is the divergent half angle. This model assumes a conical nozzle but corrections to the lengths for bell nozzles are presented in Section 3.5.

$$L_{con} = \frac{D_s - D_t}{2 \sin(\beta)} \tag{3.15}$$

$$L_{div} = R_u \sin(\theta_n) + \frac{D_e - D_t - 2(R_u - R_u \cos(\theta_n))}{2 \tan(\theta_n)} \tag{3.16}$$

For the mass estimation of a solid rocket stage, the reader is referred to the work of van Kesteren, as this model was directly adopted for solid stage mass estimation [13]. The solid rocket motors were validated for a thrust between 6.5 kN and 2.2 MN, and their accuracies are shown in Table 3.5.

3.2.2. Liquid Rocket Stage

For liquid rocket stages, the length and mass of these systems are generally formulated as in Equation 3.17 and Equation 3.18, respectively, where the variables are defined later in this section.

$$L_{LRE} = L_{engine} + L_{tanks} \tag{3.17}$$

$$M_{LRE} = M_P + M_{engine} + M_{tanks} + M_{TPS} + M_{intertank} \tag{3.18}$$

In contrast to solid stages, the choice of propellant in liquid stages has a greater impact on the performance of the stage. Two common choices for liquid-propelled rockets include liquid oxygen (LOX) as the oxidizer and either liquid hydrogen (LH2) or rocket propellant-1 (RP1) as the fuel [12]. This study uses the CEA database created by Vandamme to model the propulsion of both types of liquid-propelled stages.

The option to use either type of fuel is left as a design parameter for liquid stages as both offer different advantages. Liquid hydrogen has a higher specific impulse than RP1 by more than 100 s, is a better engine coolant, and is environmentally-friendly because the exhaust gas is water vapour. However, LH2 must be kept at cryogenic temperatures, making it difficult to handle and impractical for long-term storage. Liquid hydrogen is also more than ten times less dense than RP1, which leads to larger tanks. Conversely, RP1's lower specific impulse and increased exhaust toxicity is counterbalanced by its stability at room temperature and increased density [41]. Minor differences must be made when modelling the two different types of propulsion systems, as detailed later in this section.

Similar to solid stages, the propellant mass of liquid stages can be determined using Equation 3.19, where K_u is a percentage of unused propellant, usually found in pipes, valves, or wetting tank walls. For liquid stages, K_u is set to 0.32% [23], but is also subject to a sensitivity analysis in Chapter 8, as it has been shown to vary between 0.16% and 0.48% in a launch vehicle survey [44].

$$M_P = (\dot{m} \cdot t_b) \cdot (1 + K_u) \tag{3.19}$$

The geometry and mass of the remaining liquid stage components can now be determined. The engine length and mass can be determined using the following relationships, where a distinction is made between RP1 and LH2 engines. In addition, the engine mass estimation relationship includes the thrust chamber assembly, turbo-pumps, propellant feed system and miscellaneous parts such as the gas generator or pre-burner system, manifolds, and the electrical, control and instrumentation systems [45]. The length and mass relationships validity range, R^2 and relative standard error (RSE) are presented in Table 3.2, where the latter indicates that there is a 95% probability that the actual value is in range of the estimated value, plus or minus twice the percentage [41]. Additional relationships are available to reduce the uncertainty, but the sole dependence on thrust of Equation 3.20 and Equation 3.21 make these universally adaptable, and also meet the requirements of Section 2.6 as shown in Section 3.5.

$$L_{engine} = \begin{cases} 0.1362 {F_T}^{0.2279} & \text{if RP1} \\ 0.1667 {F_T}^{0.2238} & \text{if LH2} \end{cases} \tag{3.20}$$

$$M_{engine} = \begin{cases} 1.104 \cdot 10^{-3} F_T + 27.702 & \text{if RP1} \\ 1.866 \cdot 10^{-10} {F_T}^2 + 0.00130 F_T + 77.4 & \text{if LH2} \end{cases} \tag{3.21}$$

Table 3.2: Validity range, R^2 and relative standard error of engine length and mass estimation relationships.

Relationship	Validity Range	Fuel	R^2	RSE
Length	20 kN - 8.0 MN	RP1	0.783	17.6%
	50 kN - 3.5 MN	LH2	0.890	10.6%
Mass	20 kN - 8.0 MN	RP1	0.897	25.8%
	50 kN - 3.5 MN	LH2	0.993	13.6%

Using the OF ratio and the total propellant mass, the oxidizer mass M_{ox} and fuel mass M_f can be calculated. Using their respective densities, the total length of the tanks can be determined using Equation 3.22, derived from the volume of such tanks with cylindrical bodies and spherical end caps as seen in Figure 3.1 where the grey area accounts for empty volume as shown by Vandamme [12]. The tanks are assumed to have the same diameter as the stage. Below, V_{ullage} represents the ullage volume, and is set to 10% of the total tank volume [23], subject to a sensitivity analysis in Chapter 8.

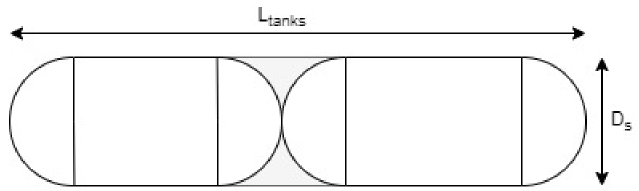

Figure 3.1: Propellant tank layout.

$$L_{tanks} = \left(\frac{M_{ox}}{\rho_{ox}} + \frac{M_f}{\rho_f} + \frac{\pi {D_s}^3}{6}\right) \cdot (1 + V_{ullage}) \cdot \frac{4}{\pi {D_s}^2} \tag{3.22}$$

The thickness of both the oxidizer and fuel tanks can be calculated using Equation 3.23, where P_{tank} is the tank pressure, SF_t is a safety factor on the thickness and σ_t is the tank material stress.

$$t_{tank} = \frac{P_{tank} SF_t D_s}{2\sigma_t} \tag{3.23}$$

With the wall thickness, the volume of the oxidizer and fuel tank walls can be calculated, before multiplying this value with the tank material density to determine the tank mass. Additionally, the tanks need thermal protection systems (TPS) if they are held at cryogenic temperatures. The relationships used to determine their masses are detailed in Equation 3.24 and Equation 3.25 [23].

$$M_{ox,TPS} = 0.9765\left(\pi D_s L_s + \pi {D_s}^2\right) \tag{3.24}$$

$$M_{f,TPS} = \begin{cases} 0 & \text{if RP1} \\ 1.2695\left(\pi D_s L_s + \pi {D_s}^2\right) & \text{if LH2} \end{cases} \tag{3.25}$$

The mass of the intertank, which is the structure between the two separate tanks in a stage can be determined using Equation 3.26 [23].

$$M_{intertank} = \begin{cases} 5.4015\pi {D_s}^2 \left(3.2808 D_s\right)^{0.5169} & \text{if stage 1} \\ 3.8664\pi {D_s}^2 \left(3.2808 D_s\right)^{0.6025} & \text{otherwise} \end{cases} \tag{3.26}$$

The total inert mass of a liquid stage can thus be calculated by summing all of the aforementioned components except for the propellant mass.

3.3. Launch Vehicle Model

After modelling the propulsion and building a solid or liquid stage, the launch vehicle model follows. Solid and liquid launch vehicles are built in a similar fashion, and unless otherwise noted, the assembly of a launch vehicle is the same for these different stages. When no uncertainty is provided for the mass estimation relationships, the data used to created these was not readily available. Nonetheless, they are validated in Section 3.5 when the launch vehicle models are compared to existing systems.

First, the length and mass of an interstage connecting two successive stages must be determined. A distinction is made between solid and liquid launch vehicles, as well as lower and upper stages. The length of an interstage of a solid stage is given by the length of the converging and diverging portion of the nozzle, as well as a fixed distance of 0.1 m as validated by van Kesteren [13]. The length of a liquid stage interstage is given by the length of the engine added to $0.2D_s$, as validated by Castellini [23]. For both types of launch vehicles, the upper-most stage interstage length, which is actually the vehicle equipment bay (VEB), is equal to an additional $0.287D_s$ [23]. These equations are summarized in Equation 3.27.

$$L_{interstage} = \begin{cases} L_{conv} + L_{div} + 0.1 & \text{if solid stage} \\ L_{engine} + 0.2D_s & \text{if liquid stage} \\ L_{conv} + L_{div} + +0.287D_s & \text{if solid upper stage} \\ L_{engine} + 0.287D_s & \text{if liquid upper stage} \end{cases} \tag{3.27}$$

Additional contributions to the length of the launch vehicle includes the length of the payload fairing. A length estimation relationship was developed from 23 existing launch vehicles as a function of the payload diameter. This relationship is shown in Equation 3.28, has an R^2 value of 0.8682 and a relative standard error 16.1%. The data used to create the length estimation relationship is shown in Appendix A.

$$L_{fairing} = 1.1035{D_s}^{1.6385} + 2.3707 \tag{3.28}$$

The mass of the payload fairing can be estimated using the relationship in Equation 3.29. This relationship was also developed from the data in Appendix A, has an R^2 value of 0.8653 and an RSE of 32.0%.

$$M_{fairing} = 49.3218(L_{fairing}D_s)^{0.9054} \tag{3.29}$$

Further distinctions must be made between lower and upper stages for the interstage mass. Separated into three different types, the interstage mass differs between first stages, middle stages, and the upper stage VEB. The mass estimation relationships for interstages are shown in Equation 3.30, where k_{sm} is 1.0 for classical Al-alloys based structures and 0.7 for advanced composite based structures, and S_{int} is the surface area of the interstage [23]. In this work, k_{sm} is fixed to 1.0.

$$M_{interstage} = \begin{cases} k_{sm} \cdot 7.7165 \cdot S_{int}\,(3.3208D_s)^{0.4856} & \text{if stage 1} \\ k_{sm} \cdot 5.5234 \cdot S_{int}\,(3.3208D_s)^{0.5210} & \text{if upper stage} \end{cases} \tag{3.30}$$

The mass of the pad interface which connects the first stage to the launch pad prior to launch is given by Equation 3.31 [23].

$$M_{pad} = \begin{cases} 25.736\pi \frac{{D_s}^2}{4}\,(3.2808D_s)^{0.5498} & \text{if stage 1} \\ 0 & \text{otherwise} \end{cases} \tag{3.31}$$

The mass of the VEB is equal to the mass of an upper stage interstage as well as the sum of the avionics and power subsystems mass. The mass estimation relationships for these subsystems are shown in Equation 3.32 and Equation 3.33 [23].

$$M_{avionics} = 0.25 \cdot (246.76 + 1.3183 \cdot D_s \cdot L_{vehicle}) \tag{3.32}$$

$$M_{EPS} = 0.3321 M_{avionics} \tag{3.33}$$

The final elements that contribute to the mass of the launch vehicle are the payload M_{PL} and the payload adapter M_{PLA}. Given a payload mass, the mass of the payload adapter can be calculated using Equation 3.34 [23].

$$M_{PLA} = 0.00477536{M_{PL}}^{1.01317} \tag{3.34}$$

With the given design parameters and additional information about the structure material and material properties, a full launch vehicle model can now be created. The validation of the propulsion, geometry and mass models for individual stages and launch vehicles is described in Section 3.5.

3.4. Reusability Geometry and Mass Model

Elements that must be added to a first stage in order to make it reusable include landing legs and associated hydraulics, cold gas thrusters for high-altitude controllability under zero main-engine thrust conditions and grid fins for added controllability. While these components affect the geometry and mass of a launch vehicle, conclusions from literature are that changes to the geometry are insignificant [1]. For retro-propulsion reusability, these assumptions are valid because the landing legs and grid fins are stowed against the body of the launch vehicle pre-deployment and do not affect the aerodynamics of the vehicle, while the cold gas thrusters are stored inside the first stage [46]. This can be seen in Figure 3.2, where the schematic of the deployment of the Falcon 9 landing legs shows very minimal changes to the cylindrical shape of the launch vehicle [47].

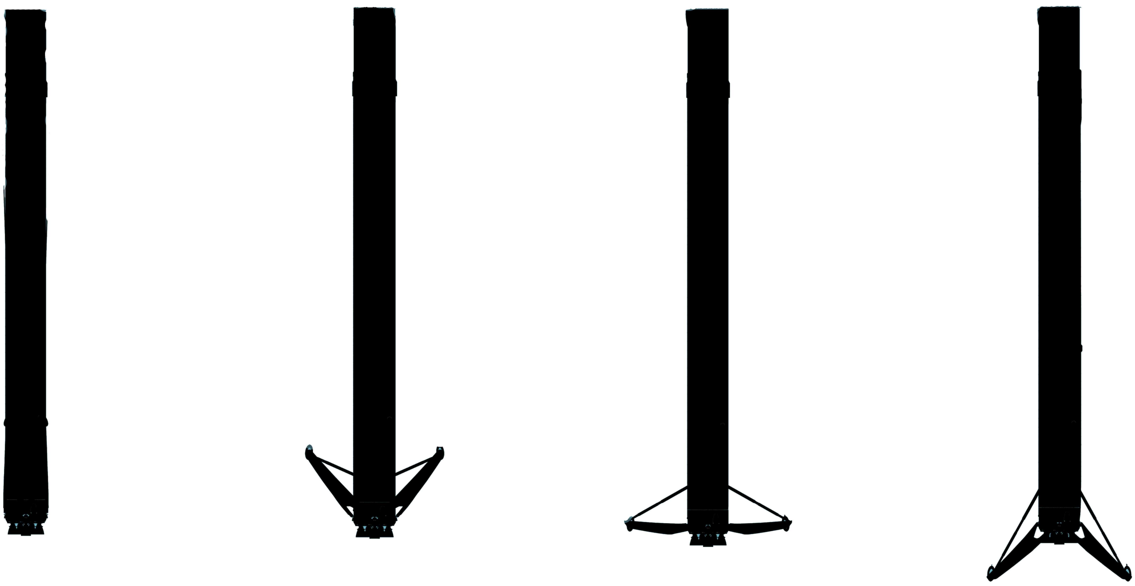

Figure 3.2: Schematic of Falcon 9 landing leg deployment.

Extensive aerodynamic analysis of the launch vehicle is beyond the scope of this research. Nonetheless, the direct effect of the stowed landing legs on the aerodynamic coefficients can be determined through more detailed computational fluid dynamics simulations, which is left as a recommendation.

The mass models for these systems is derived as follows. A study conducted by Tartabini assumes an added inert mass of 10.0% for a reusable first stage compared to an expendable counterpart [48]. An estimated landing gear mass of 2100 kg from Blau for the Falcon 9 v1.1, which equals a 10.0% increase in inert mass, validates this assumption [49]. Furthermore, this assumption also holds true for interplanetary landers, with a Mars-lander landing gear increasing the dry mass by 9.41% in a study conducted by Price, Manning and Sklyanskiy [50]. As an initial estimate, the reusable hardware mass is assumed to equal 10.0% of the first stage inert mass, where the cold gas thruster and grid fin masses can be considered negligible [46], being lumped within this 10.0%.

3.5. Verification and Validation

Larson *et al.* define verification as “proof of compliance with design solution specifications and descriptive documents” and validation as “proof that the product accomplishes the intended purpose based on stakeholder expectations” [51]. For both, a combination of tests, demonstrations, analysis, inspections, simulations and/or modelling lead to the proof of the final product. This step is crucial to first ensuring that the small, reusable launch vehicle is verified at each step in the design with existing models and products, before validating that it can accomplish its intended goal. The accuracy presented in Section 2.6 thus serves as a baseline to determine the validity of the models. As done in previous works [12–14], instead of leaving design variables to be optimized, these will be predefined with known values to then compare the outputs of the models with the expected outputs to determine their accuracy. This section deals with the validation of the propulsion, geometry and mass models of solid and liquid stages and launch vehicles.

The important statistical figures used in this study, along with RSE, include the relative mean error μ, the absolute relative error E, and standard deviation σ, as described by van Kesteren [13]. These statistical figures are determined using Equation 3.35 through Equation 3.37, where y_i is the actual value found in literature, $\bar{y}_i$ is the model value and n is the number of samples. The mean relative error first provides a measure of how the model can predict the actual value. The absolute mean error is almost identical, but evaluates the absolute error, which is a better indication of how the model is expected to vary compared to the actual value. The absolute mean error is thus used as the measure of accuracy in the model requirements and in the sensitivity analysis as presented in Chapter 8. Finally, the standard deviation is a measure of the variation in the set of values, as mentioned in Section 2.1.

$$\mu = \frac{100\%}{n} \cdot \sum_{i=1}^{n} \frac{\left(y_i - \bar{y}_i\right)}{y_i} \tag{3.35}$$

$$E = \frac{100\%}{n} \cdot \sum_{i=1}^{n} \frac{\left|y_i - \bar{y}_i\right|}{y_i} \tag{3.36}$$

$$\sigma = 100\% \cdot \sqrt{\frac{1}{n-1} \sum_{i=1}^{n} \left(\mu - \frac{\left(y_i - \bar{y}_i\right)}{y_i}\right)^2} \tag{3.37}$$

Although much of the code used for solid rocket stage propulsion modelling was adopted from van Kesteren [13], it was deemed necessary to validate the model again after the transfer of the code from the old Tudat environment into the new one. Nine existing solid rocket motors ranging in thrust from 7.6 kN to 465.1 kN were used to model the ideal rocket behaviour of solid rocket motors. Then, the correction factor ξ_{solid} was determined to minimize the average relative error and standard deviation between the existing solid rocket motors and the model. The chosen value for ξ_{solid} is 0.93630, and the results from the analysis are presented in Table 3.3. The statistical values for these are summarized in Table 3.5.

The same process for validating liquid rocket engines was undertaken. First, ideal rocket theory was used to determine the mean relative error in vacuum thrust between ideal engines and actual engines. Then, a correction factor of ξ_{liquid} of 0.92744 was used to minimize the error and essentially account for the discrepancies between ideal rocket theory and real engines. This single correction factor can be used for both RP1 and LH2 engines with expansion ratios ranging from 16 to 280, making it applicable to a wide range of liquid engines and reducing the number of variables in the model. The results from the liquid engine analysis, as well as the related statistical figures, are presented in Table 3.4 and Table 3.6, respectively. For brevity, only the corrected values are shown in Table 3.4.

Table 3.3: Solid rocket stage propulsion validation data. In the brackets beside the solid rocket motor, a 1 indicates that the motor includes thrust vector control (TVC) while a 0 indicates no thrust vector control.

	Design Parameter					**Actual Values**			**Ideal Rocket Theory**			**Corrected Values**		
SRM (TVC)	P_c [bar]	P_e [bar]	D_s [m]	D_e [m]	t_b [s]	I_{sp} [s]	F_T [kN]	M_p [kg]	I_{sp} [s]	F_T [kN]	M_p [kg]	I_{sp} [s]	F_T [kN]	M_p [kg]
Orion 50S (0) [52]	56.1	0.18327	1.27	1.424	75.3	292.3	465.1	12163.0	314.5	496.0	12467.8	294.5	464.4	12467.8
Orion 50 (1) [52]	55.8	0.11403	1.27	0.860	75.6	290.2	114.6	3025.0	321.4	124.6	3076.8	301.0	116.7	3076.8
Orion 38 (1) [52]	39.4	0.08654	0.965	0.526	67.7	287.0	32.2	771.0	320.0	34.7	771.1	299.6	32.5	771.1
STAR 31 (0) [52]	49.1	0.08823	0.765	0.728	45.0	293.5	82.3	1286.0	323.1	70.9	1037.1	302.5	66.4	1037.1
STAR 48A (0) [52]	37.4	0.14280	1.245	0.637	87.2	283.4	77.2	2430.0	311.6	74.3	2183.0	291.7	69.6	2183.0
STAR 30E (0) [52]	37.0	0.06612	0.762	0.584	51.1	290.4	35.1	631.0	322.8	34.1	567.5	302.3	32.0	567.5
STAR 27 (0) [52]	38.8	0.08627	0.693	0.485	34.4	287.9	25.4	334.0	319.8	29.3	331.4	299.4	27.5	331.4
STAR 17A (0) [52]	46.2	0.09234	0.442	0.349	19.4	286.7	16.0	112.0	321.5	16.7	105.6	301.0	15.6	105.6
STAR 13B (0) [52]	56.7	0.15450	0.345	0.204	14.8	285.0	7.60	41.2	317.2	8.90	43.8	297.0	8.40	43.8

Table 3.4: Liquid rocket engine propulsion validation data. The mass of propellant shown below is normalized for a single engine, despite the Falcon 9 v1.1 having 9 first-stage engines.

	Design Parameter							**Actual Values**			**Corrected Values**		
LRE (Launch Vehicle)	P_c [bar]	P_e [bar]	D_s [m]	D_e [m]	t_b [s]	OF [-]	Prop.	I_{sp} [s]	F_T [kN]	M_p [kg]	I_{sp} [s]	F_T [kN]	M_p [kg]
HM7B (Ariane 5) [53, 54]	37.0	0.03816	5.40	0.99	945	5.0	LH2	446.0	64.8	14900.0	448.9	63.8	13735.1
LE5B (H-IIB) [55, 56]	36.0	0.02646	4.00	1.71	499	5.0	LH2	447.0	137.0	16600.0	454.1	141.6	15907.4
LE7A (H-IIA) [57, 58]	121.0	0.22773	4.00	1.82	390	5.9	LH2	438.0	1098.0	100000	432.9	1109.9	102249
RL10B2 (Delta IV 4) [59, 60]	44.0	0.01130	4.00	2.15	850	5.88	LH2	465.5	110.1	21320.0	462.9	112.5	21121.5
RL10A42 (Atlas V) [61, 62]	42.0	0.04450	3.05	1.17	842	5.5	LH2	451.0	99.2	20830.0	445.7	100.8	19467.2
Vinci (Ariane 6) [63, 64]	61.0	0.01846	5.40	2.15	800	5.8	LH2	467.0	180.0	31000.0	461.4	180.3	31972.9
Vulcain 2 (Ariane 5) [65, 66]	109.0	0.23414	5.4	1.76	540	5.3	LH2	439.0	1113.0	170000	434.3	1061.7	135005
RD191 (Angara 1.2) [67, 68]	262.6	0.74681	2.90	1.45	215	2.6	RP1	337.5	2084.9	128000	332.6	2107.1	139278
YF100 (Long March 7) [69, 70]	180.0	0.55180	2.25	1.34	180	2.6	RP1	335.0	1340.0	75000.0	330.7	1297.6	72217.7
Merlin 1D (Falcon 9 v1.1) [71]	97.2	0.52850	3.70	1.07	180	2.34	RP1	320.0	742.4	43966.7	318.4	708.1	40934.5
RD120 (Zenit) [72, 73]	178.1	0.12962	3.90	1.95	315	2.6	RP1	350.0	912.0	82487.0	349.8	885.5	81537.9
RD58M (Zenit) [74, 75]	79.0	0.02073	3.70	1.40	650	2.82	RP1	361.0	85.0	15850.0	357.9	86.0	15962.4

Table 3.5: Solid rocket stage propulsion validation data relative error, absolute relative error and standard deviation. The correction factor, ξ_{solid}, used here is 0.93630.

	μ [%]	E [%]	σ [%]
Ideal vacuum thrust	4.45	8.96	9.32
Corrected vacuum thrust	-2.21	6.86	8.72
Ideal specific impulse	10.6	10.6	1.25
Corrected specific impulse	3.57	3.57	1.17
Propellant mass	-3.96	6.28	7.59

Table 3.6: Liquid rocket engine propulsion validation data relative error, absolute relative error and standard deviation. The correction factor, ξ_{liquid}, used here is 0.92744.

	μ [%]	E [%]	σ [%]
Ideal vacuum thrust	7.26	7.26	2.82
Corrected vacuum thrust	-0.53	2.28	2.62
Ideal specific impulse	7.19	7.19	0.94
Corrected specific impulse	-0.59	0.96	0.87
Propellant mass	-3.08	5.56	6.73

The absolute relative error below 10% for both solid and liquid propulsion values serves to validate the use of the propulsion model in the design of a small, reusable launch vehicle, as per the requirements set in Section 2.6.

The solid rocket stage length and inert mass validation data, as taken from van Kesteren's study, are shown in Table 3.7. The absolute mean error below 10% for both the length and inert mass serve to validate the solid rocket stage model.

Table 3.7: Solid rocket stage length and mass relative error, absolute relative error and standard deviation. The correction to length includes a factor for a submerged bell nozzle, while the inert mass correction factor of 1.3 is used [13].

	μ [%]	E [%]	σ [%]
Original length	40.1	40.1	23.2
Corrected length	11.7	7.15	11.5
Original inert mass	17.2	-16.6	11.9
Corrected inert mass	12.4	-2.76	13.8

Next, the liquid engine length and mass relationships are validated with the same existing engines as before, as seen in Table 3.8.

Table 3.8: Liquid rocket engine length and mass validation data.

		Actual Values		**LER and MER Values**	
Liquid Engine (Launch Vehicle)	ϵ	L_{engine} [m]	M_{engine} [kg]	L_{engine} [m]	M_{engine} [kg]
HM7B (Ariane 5) [53]	83.10	2.010	165.0	1.983	161.1
LE5B (H-IIB) [55]	110.0	2.790	269.0	2.370	265.2
LE7A (H-IIA) [57]	51.90	3.700	1800.0	3.757	1750.2
RL10B2 (Delta IV 4) [61]	280.0	4.153	301.0	2.251	226.0
RL10A42 (Atlas V) [61]	84.00	2.286	168.0	2.196	210.3
Vinci (Ariane 6) [63]	240.0	4.200	280.0	2.502	317.9
Vulcain 2 (Ariane 5) [65]	45.10	3.050	1300.0	3.720	1667.9
RD191 (Angara 1.2) [68]	37.00	4.000	2290.0	3.761	2354.0
YF100 (Long March 7 K2)	35.00	-	-	3.368	1460.2
Merlin 1D (Falcon 9 v1.1) [76]	21.40	2.920	476.0	2.934	809.4
RD120 (Zenit) [72]	114.5	3.872	1125.0	3.087	1005.3
RD58M (Zenit) [77]	280.0	2.270	340.0	1.814	122.6

The statistical values for the above engines are presented in Table 3.9. Although the absolute relative error and standard deviation are larger than for the performance values, the mean relative error of -11.7% for length and 3.07% for mass suggest that the relationships used are still applicable. In fact, the two engines that are underestimated in length by more than 40%, namely the RL10B2 and the Vinci, have an expansion ratio that is more than double the rest of the LH2 engines (280 and 240, respectively). These two engines also have shorter stowed lengths, being 2.20m for the RL10B2 [59], which is much closer to the estimated length. To mitigate this error, a constraint will be placed on the expansion ratio of LH2 engines during the optimization. When these two engines are excluded from the analysis, the mean relative error is reduced to -4.74% and the absolute mean error is reduced to 10.6%.

Table 3.9: Liquid rocket engine length and mass relative error, absolute relative error and standard deviation.

	μ [%]	E [%]	σ [%]
Liquid engine length	-11.7	16.1	18.6
Liquid engine mass	3.07	36.9	47.7

With the validated propulsion, geometry and mass of liquid rocket engines, the construction of the stages as a whole can now be completed. As mentioned in Section 3.2.2, the length of a liquid rocket stage is given by the sum of the engine length and tank lengths. Furthermore, the inert mass of a liquid stage is given by the sum of the tank, engine, interstage, thermal protection system, intertank, thrust structure and pad interface masses. It is important to note that for this validation, the interstage length and masses are included in the individual stage mass calculations. The liquid stage validation results are presented in Table 3.10.

Table 3.10: Liquid rocket stage validation data.

	Actual Values		**Model Values**	
Launch Vehicle (Stage #)	L_s [m]	$M_{s,inert}$ [kg]	L_s [m]	$M_{s,inert}$ [kg]
Ariane 5 (2) [78]	4.71	4540.0	7.97	4511.2
H-IIB (2) [79]	11.00	4000.0	9.59	2356.2
H-IIA (1) [80]	37.20	11200.0	32.81	9685.1
Delta IV 4 (2) [60]	12.20	2850.0	10.35	2351.7
Atlas V - Centaur (2) [62]	12.68	2316.0	12.96	1519.0
Ariane 6 (2)	-	-	10.79	4761.3
Ariane 5 (1) [66]	23.80	14700.0	28.51	13531.7
Angara 1.2 (1) [67]	25.70	9800.0	29.36	7422.9
Long March 7 (K2 Booster) [81]	27.00	6000.0	24.52	5633.1
Falcon 9 v1.1 (1) [49]	45.70	23100.0	43.78	20036.9
Zenit (2) [82]	10.40	9017.0	14.39	4572.4
Zenit (3) [82]	5.60	3861.0	6.11	1630.3

The important statistical values for the liquid rocket stages are presented in Table 3.11. The discrepancies between actual and calculated values for length can be attributed to the fact that, for most stages, it is not stated whether or not the interstage length is included, and may sometimes be omitted from the reported values. In addition, some stages such as the first and second stages of the Ariane 5 do not include engine length in their reported values whereas these are considered in the model, leading to additional ambiguity. Furthermore, the model consistently underestimates the inert mass of a liquid rocket stage. This trend is consistent with the results obtained by Vandamme, before a correction factor was applied to the inert mass [12]. Thus, this method is used again as it provides estimates within the range set in the requirements of the tool. Using the mean relative error of the inert mass, a correction factor of 1.31862 is multiplied by the original inert mass to yield a mean relative error of 0.00%.

Table 3.11: Liquid rocket stage length and mass relative error, absolute relative error and standard deviation.

	μ [%]	E [%]	σ [%]
Liquid stage length	9.08	18.7	24.6
Liquid stage mass	-24.2	-24.2	18.0

When analyzing launch vehicles, the process of validating each individual component of the launch vehicle (apart from the engine) was not conducted, as the mass estimation relationships used in this work come from sources where these were individually validated in their respective works. Therefore, a focus is set on validating the geometry and mass models of launch vehicles as a whole. As mentioned previously, the solid launch vehicle model was adopted from van Kesteren and for brevity purposes, its validation will not be elaborated on again [13]. Nonetheless, validation of liquid launch vehicles is crucial, as the equations and relationships used to model the vehicles are created by the author or adopted from various sources. Expendable liquid launch vehicle validation was done for Zenit, Falcon 9 v1.1, Falcon 9 FT, the first two stages of Long March 6, and the first stage of Falcon 1c. The last two were included in the launch vehicle validation because they are both classified as small launch vehicles and, since the results presented in Table 3.10 serve as both a validation and calibration set, it is important to validate other liquid stages and launch vehicles outside of this calibration set [23]. The design parameters and results for the first two stages of Long March 6 and the first stage of Falcon 1c are presented in Table 3.12 and Table 3.13, respectively, and the relative errors are found in Table 3.14. Although no inert mass data is public for these stages, the validation has already been done with the other stages in Table 3.10. The remaining liquid launch vehicle validation is found in Appendix B, and further validates the models used.

Table 3.12: Long March 6 and Falcon 1c design parameters used for validation.

	Design Parameter						
Launch Vehicle (Stage #)	P_c [bar]	P_e [bar]	D_s [m]	D_e [m]	t_b [s]	OF [-]	Prop.
Long March 6 (1) [83]	180.0	0.5518	3.350	1.338	180.0	2.60	RP1
Long March 6 (2) [83, 84]	120.0	0.1205	2.250	0.946	290.0	2.50	RP1
Falcon 1c (1) [71, 85]	61.4	0.4682	1.676	0.960	169.0	2.17	RP1

Table 3.13: Long March 6 and Falcon 1c validation data.

	Actual Values					**Model Values**				
Launch Vehicle (Stage #)	I_{sp} [s]	F_T [kN]	M_p [kg]	L_s [m]	$M_{s,inert}$ [kg]	I_{sp} [s]	F_T [kN]	M_p [kg]	L_s [m]	$M_{s,inert}$ [kg]
Long March 6 (1) [83]	335.0	1340.0	76000.0	15.0	-	330.7	1297.6	72217.7	14.6	5635.3
Long March 6 (2) [83, 84]	341.5	180.0	15150.0	7.30	-	346.6	180.1	15409.9	7.97	1038.2
Falcon 1c (1) [71, 85]	304.8	482.6	27102.0	15.9	-	309.7	470.7	26262.9	16.9	1812.6

Table 3.14: Long March 6 and Falcon 1c validation data relative errors.

	Error [%]				
Launch Vehicle (Stage #)	I_{sp}	F_T	M_p	L_s	$M_{s,inert}$
Long March 6 (1)	-1.28	-3.17	-4.98	-2.53	-
Long March 6 (2)	1.49	0.05	1.72	9.18	-
Falcon 1c (1)	1.62	-2.48	-3.10	6.16	-

The relative error below 10% for all parameters in Table 3.14 serves to validate the launch vehicle model and calibration set. The final aspect needing validation is the reusable launch vehicle model. For this, the expendable and reusable versions of the Falcon 9 Full Thrust (FT) were compared in terms of individual stage inert and wet mass, as well as GTOW and payload capacity. While SpaceX does not disclose much of its proprietary data, various sources were used to reconstruct the geometry and mass of the expendable and reusable launch vehicles, as depicted in Section 3.4.

The reusable launch vehicle mass model is first validated using a ΔV budget comparison. Since the only difference in the expendable and reusable Falcon 9 FT is the additional hardware, the maximum propellant capacity of the first stage does not change. Assuming the expendable and reusable mission ΔV are nearly equal, the two variables that can change to satisfy these conditions are the leftover propellant mass for boost-back, re-entry and landing, and the payload mass. The ΔV fractions of the Falcon 9 FT [38, 86] are compared to the model results and the results from Woodward who does not use mass estimation relationships for his Falcon 9 FT launch vehicle model but whose results show good agreement with actual values [38].

Table 3.15: Reusable launch vehicle geometry and mass model validation.

	Falcon 9 FT Expendable			**Falcon 9 FT RTLS**		
	Actual	Woodward	Model	Actual	Woodward	Model
First stage inert mass [kg]	22200.0	20821.8	27062.7	24420.0	23426.4	29769.0
Payload mass [kg]	22800.0	22800.0	22800.0	13680.0	14820.0	13680.0
Leftover propellant [%]	0.00	0.00	0.00	0.21	0.17	0.17
$\Delta V_{1,ascent}$ [m/s]	3740.0	3693.7	3986.4	2554.2	2913.3	2893.3
ΔV_2 [m/s]	5502.0	5378.7	5217.4	6682.0	6406.3	6312.8
$\Delta V_{1,ascent}$ [%]	40.5	40.7	43.3	27.7	31.3	31.4
ΔV_2 [%]	59.5	59.3	56.7	72.3	68.7	68.6
Total ΔV_{ascent} [m/s]	9242.0	9072.4	9203.8	9236.2	9319.6	9206.1

With a mean ΔV fraction absolute relative error of 7.62% and mean relative error of -2.29% between the actual Falcon 9 FT and the model, the preliminary reusable launch vehicle model is validated. The model also shows close agreement with Woodward's model (E of 3.27% and μ of -0.70%), further validating the method used. The large first stage inert mass of the model compared to the actual value may be due to innovative manufacturing techniques employed by SpaceX, as the mass estimation relationship employed on the Merlin engines is overestimated by more than 50%. As the Falcon 9 has nine first-stage engines, this error affects the total inert mass significantly, as seen in Table 3.15. Future models could account for these innovative manufacturing techniques to better estimate the mass of these engines.

With a validated launch vehicle model, it is now possible to simulate this launch vehicle to orbit. The method used for this simulation, as well as the recovery trajectory, is presented in Chapter 4.

4
Trajectory Model

After modelling the launch vehicle, it is important to be able to simulate this system to a given orbit to satisfy the requirements of a mission, usually restricted by that payload's final semi-major axis, eccentricity, inclination, argument of perigee and longitude of the ascending node. As fine-tuning of the final orbit is not the focus of the research as with similar previous studies [12–14], only the first three orbital parameters are of interest to determine the accuracy of the final orbit.

In this section, the method used to model the launch vehicle to its intended orbit is first detailed. Then, the trajectory model for the retro-propulsion reusability is explained, before the ascent and descent trajectory constraints are presented. Finally, the verification and validation of the descent trajectory is detailed.

4.1. Nominal Ascent Trajectory

The nominal ascent trajectory is adopted from the work of van Kesteren and Miranda [13, 14]. Two types of ascent trajectories are commonly used when modelling a launch vehicle to orbit, namely a direct ascent (DA) and a Hohmann transfer ascent (HTA) [87]. In the first model, the trajectory is selected such that the summit point coincides with the target satellite orbit before the final stage is accelerated to the required orbital velocity. In the Hohmann transfer ascent, the upper stage reaches a parking orbit at an altitude of approximately 200 km, before the upper stage engines are reignited into a Hohmann transfer orbit [87]. A direct ascent approach is selected as the best option for the study at hand for reasons that are discussed hereafter. The two different trajectories are depicted in Figure 4.1.

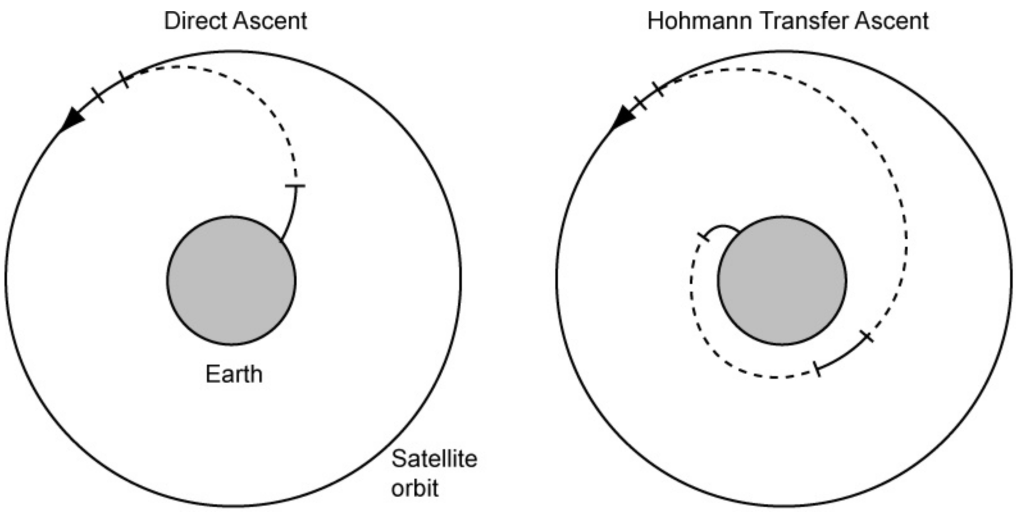

Figure 4.1: Sketch of direct ascent and Hohmann transfer ascent trajectories [87].

Although the Hohmann transfer ascent minimizes the required energy to orbit, the direct ascent trajectory offers more advantages for this study, listed below [87].

1. The direct ascent trajectory does not require re-ignition of the engines, which is advantageous for upper stage solid motors.
    1.1. Solid upper stages are investigated in Chapter 7 to determine if this is indeed an advantage within the scope of this study.

2. Shorter coasting periods in a direct ascent are better for cryogenic propellants to avoid boil-off.
   2.1. The period of a parking orbit is approximately 100 minutes, and the opportunity to raise the orbit comes once per period after one orbital revolution [88]. This is an order of magnitude greater than the time to reach the target orbit with a direct ascent.
3. Problems with attitude control are reduced when using a direct ascent compared to a Hohmann transfer ascent.
4. The steeper trajectory of the direct ascent allows for launch vehicle tracking from the launch site as opposed to a global network of tracking stations with the Hohmann transfer ascent.
5. The steeper direct ascent trajectory is better for first stage recovery, reducing the total distance travelled from the main engine cut-off (MECO) to the launch site.

In addition, a study by Kreiter showed that there was a 8.45% payload mass increase for the 1966 Mars Opportunity using an Atlas-Centaur launch vehicle for a direct ascent compared to a Hohmann transfer ascent [89]. Furthermore, Hohmann transfer ascents are more commonly used for satellites with geostationary, interplanetary, or other non-LEO target orbits, while direct ascent is preferred for LEO target orbits [90]. A direct ascent is thus chosen for the main launch vehicle trajectory as a result of the combination of the above advantages and the use of this algorithm in previous works in the same environment [13, 14].

To model the direct ascent, a parametric control law is used. For the first stage, five discrete pitch angles points, including the initial pitch, are selected to model the ascent, while for the remaining stages, only three discrete points are used. The first stage points are located at 0%, 5%, 20%, 60% and 100% of the burn time, while the upper stage points are located at 0%, 50% and 100% of the burn time. Finer tuning of the trajectory can be accomplished with added pitch points.

The parametric control law has been verified and validated by van Kesteren [13]. To do so, the model was compared to a separate simulation tool used for the ALOSS project by the Netherlands Aerospace Centre (NLR) . In this validation process, van Kesteren showed that the drag loss difference between the NLR tool and his model was overestimated by less than 10.0%, yet the final altitude and velocity agreed within 0.50%.

4.2. Reusable Descent Trajectory

There are two different trajectory options for retro-propulsion recovery. The first is the downrange landing option, where the reusable first stage lands on a separate landing pad or barge downrange from the launch site. This method requires two different burns, namely a re-entry burn as the stage re-enters the atmosphere, and a landing burn, where the stage is brought to near-zero velocity at the target landing altitude. The second option is the return-to-launch-site method, where an additional boostback burn is needed to alter the trajectory of the first stage after separation from the rest of the launch vehicle to redirect it towards the launch site. The first option is depicted in Figure 4.2 while the latter is shown in Figure 4.3 (not to scale).

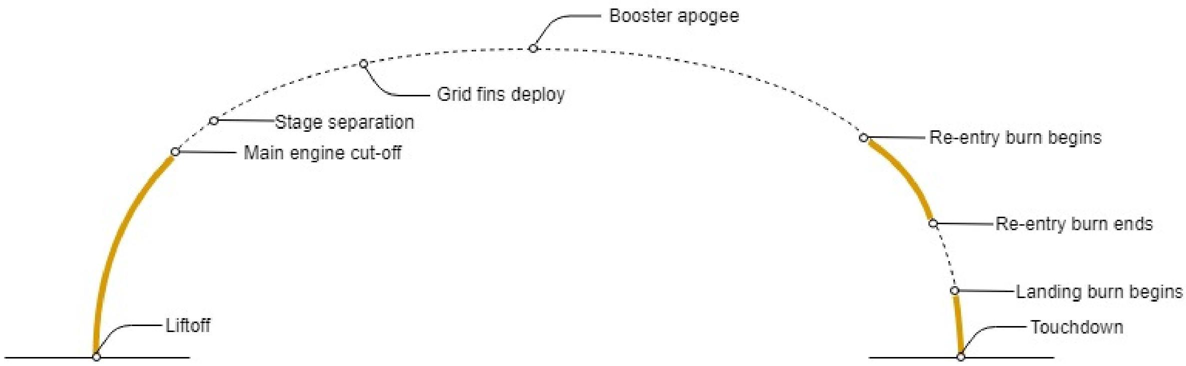

Figure 4.2: Downrange landing flight profile.

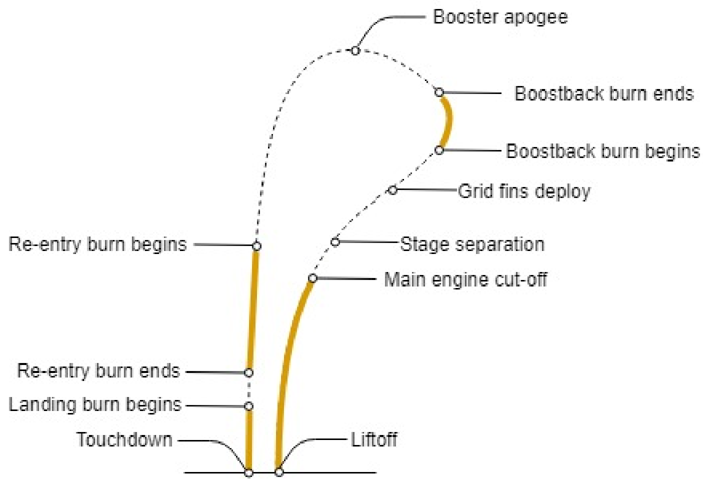

Figure 4.3: Return-to-launch-site flight profile.

Since guidance is not the focus of this research, it is assumed that the on-board attitude control system and cold-gas thrusters can meet the requirements of reorienting the first stage to the desired attitude before performing the recovery manoeuvres. The reorientation involves pitching over the first stage such that the thrust vector is opposite to the velocity vector before the main engines are reignited. For both methods, a simple approach is used to slow down the rocket to zero velocity at the desired landing altitude. Aside from the boostback burn, the first stage will have an angle of attack of 180°, meaning the thrust vector will be directly opposite to the velocity vector. Additional assumptions for the reusable trajectory are listed below.

1. The pitch angle during the boostback manoeuvre will be set to 190°, as this value has been shown to replicate the Falcon 9 boostback trajectory in previous studies [38, 91, 92].
2. The boostback manoeuvre time will vary between 20 s and 60 s, as with previous Falcon 9 missions [93].
3. The re-entry burn will begin between an altitude of 80 km and 50 km and will end between an altitude of 55 km and 30 km. Previous missions have a similar range for re-entry burn altitudes, and the wide range in these values is due to the difference in return-to-launch-site and downrange landing conditions [93].
4. The landing burn will begin below an altitude of 15 km, as with previous Falcon 9 missions [93].

The constraints places on both the ascent and reuse trajectories are presented in the following section.

4.3. Trajectory Constraints

As with the launch vehicle geometry and mass models, constraints must be put in place for the trajectory to meet realistic values during flight. For the trajectory, these constraints can be separated into two categories, namely path constraints and boundary constraints. The former are conditions that must be met at every time step during the integration, while the latter are to be met at boundaries of the integration [23]. The two types of constraints relevant to the research are presented in this section.

The first path constraint is the maximum dynamic pressure, q_{max}, which is reached when the pressure change due to increasing velocity is greater than that due to decreasing air density. The dynamic pressure of the launch vehicle is given by Equation 4.1.

$$q = \frac{1}{2}\rho V^2 \tag{4.1}$$

The maximum dynamic pressure during ascent has a wide range among existing launch vehicles, varying between 27.0 kPa for Falcon 9 RTLS missions to up to 90.0 kPa for the PSLV C-19, with the Ariane V and Pegasus values in the middle at 57.0 kPa and 57.5 kPa, respectively [13, 38]. To remain consistent with the previous studies using the same framework as this research, an upper limit for q_{max} is set to 90.0 kPa. During descent, the q_{max} values from literature can be used as a reference. Wilken *et al.* and Sippel et al. set the re-entry q_{max} to 200 kPa, as derived from upper limits in previous SpaceX missions [94, 95]. This value is chosen as the maximum for this study as well.

Another path constraint already implemented in the Tudat tool is the axial acceleration constraint, which should not exceed 10g for ascent, as per van Kesteren's study [13]. This value is similar to the range between 10g and 14g found in literature for small launch vehicle design [21, 22]. For the descent, this constraint is not as strict, with a limit imposed of a maximum of 20g as per the work of Snijders on reusable launch vehicles [11]. The axial acceleration is calculated using Equation 4.2.

$$a_x = \frac{F_T - F_D}{m} \tag{4.2}$$

Furthermore, the angle of attack should not exceed 30° during ascent, as limited by the Missile DATCOM module. This is especially important in the denser portions of the atmosphere where drag and lift forces are significant.

The final path constraint that is applied to the trajectory model is the convective heat flux, $\dot{Q}$, calculated from the free-stream enthalpy convective model as seen in Equation 4.3 [31]. During the ascent, this value should not exceed 1135 W/m^2 after the fairing jettison in order to protect the payload, as per the works of Vandamme and van Kesteren [12, 13]. During descent, this value is unconstrained as per the work of Sippel due to the complexity in analytically calculating this value during re-entry, and is left as a recommendation for further study [95].

$$\dot{Q} = \frac{1}{2}\rho v^3 \tag{4.3}$$

The boundary constraints are dependent on the target orbit and reusable trajectory of choice. Nonetheless, commonalities between the trajectories exist. The reusable first stage is constrained to land within 1m of its desired altitude, and at a velocity below 5 m/s. This is a significant improvement on the constraints of Woodward, who imposed an error of 100 m and 90 m/s for altitude and velocity, respectively [38]. As attitude control is beyond the scope of this work, the uncontrolled first stage is constrained to land within 5 km of the desired landing location, with precision landing left as a recommendation for future study. A final constraint of having the altitude larger than the downrange distance at MECO is imposed for reusable launch vehicles.

The application, verification and validation of the trajectory model is presented in the following section.

4.4. Trajectory Model Verification and Validation

As the nominal trajectory module was adopted from van Kesteren and was validated in his work [13], this model is not revalidated. However, it is important to verify and, to the best extent possible, validate the reusable trajectory model for both recovery options before applying it to a small, reusable launch vehicle.

First, the DRL trajectory is verified and validated with the Falcon 9 FT launch vehicle using the flight profile from the SES-10 mission launched on March 30, 2017 from Kennedy Space Center Launch Complex 39 Pad A. The input data used for the simulation are presented in Table 4.1 and the results are shown in Table 4.2. The mission data have been reconstructed from the SES-10 mission YouTube webcast, and collected by Murphy [93]. In addition, 12% of the total first stage propellant was saved for the reuse flight, with three engines burning during the re-entry burn and a single engine burning during the landing burn.

Table 4.1: Downrange landing trajectory input data.

Parameter	**Stage 1**	**Stage 2**
Design Parameters		
P_c [bar]	108.0	108.0
P_e [bar]	0.8520	0.04875
D_s [m]	3.66	3.66
D_e [m]	0.988	2.97
t_b [s]	172.0	346.0
t_c [s]	11.0	-
OF [-]	2.38	2.38
Propellant [-]	RP1/LOX	RP1/LOX
$N_{engines}$ [-]	9	1
Launch Vehicle and Trajectory Data		
Payload Mass [kg]	5282.0	
Initial FpA [°]	89.50	
Initial Latitude [°]	28.61	
Initial Longitude [°]	-80.60	
Initial Azimuth [°]	85.00	
Fairing Jettison Time [s]	169.0	
Pitch Angles [°]	89.38 88.52 77.35 48.70 40.68	42.97 0.00 0.00

Table 4.2: Downrange landing trajectory validation data.

Parameter	**SES-10 Mission**	**Trajectory Model**	**Error [%]**
Stage 1 Ascent			
MECO Time [s]	158.0	158.0	0.00
MECO Altitude [km]	63.63	65.09	2.29
MECO Downrange Distance [km]	86.89	89.17	2.62
MECO Velocity [m/s]	2314	2242	-3.14
Maximum Dynamic Pressure [kPa]	30.49	27.14	-11.0
Stage 1 Descent			
Re-entry Burn Initial Altitude [km]	71.71	72.00	0.40
Re-entry Burn Final Altitude [km]	54.75	38.50	-29.7
Landing Burn Initial Altitude [km]	13.37	12.40	-7.26
Landing Altitude [km]	0.00	0.01	-
Landing Velocity [m/s]	0.00	0.42	-
Downrange Landing Distance [km]	626.9	555.7	-11.36
Stage 2			
Final Altitude [km]	218.0	217.7	-0.16
Final Eccentricity [-]	0.001	0.025	-
Final Inclination [°]	-	34.42	-

The process employed here serves as a verification of the first stage trajectory upon re-entry and landing. Calibration, or tuning, of the ascent pitch angles was conducted in order to obtain the similar MECO conditions, as the pitch profile is not made public. It was also deemed necessary to throttle the first stage to 80% of the maximum thrust between 3 km and 15 km of altitude during the ascent, as done during this mission, to achieve better agreement in the maximum dynamic pressure and MECO values. This throttling was adopted for the rest of the work. Then, the descent parameters were chosen to meet the proper landing requirements as detailed in Section 2.6. Aside from the maximum dynamic pressure, re-entry burn final altitude and downrange landing distance, the DRL trajectory model values agree within 10% of the reported mission data. The large discrepancy between the actual and modelled re-entry burn final altitude can be explained by the lack of aerodynamic modelling of the grid fins. Although included in the mass model, the capabilities of the Missile DATCOM software do not allow for the inclusion of grid fins. As the aerodynamic data for the Falcon 9 are not made public, it is not possible to quantify the exact influence of the grid fins on the aerodynamics. Nonetheless, the behaviour of the first stage during recovery is as expected, and the model can accurately recreate the landing conditions, verifying and validating the DRL trajectory module. In future iterations, an aerodynamic analysis of grid fins as a function of Mach number and angle of attack can be incorporated in the aerodynamic module.

Again using the Falcon 9 FT model, the RTLS trajectory is now validated using the flight profile from the CRS-10 mission launched on February 19, 2017 from Kennedy Space Center Launch Complex 39 Pad A [96, 97]. The inputs for the simulation are presented in Table 4.3, while the actual values and model results are compared in Table 4.4. In addition, 17% of the total first stage propellant was saved for the reuse flight, as validated in Table 3.15 of Section 3.5, with three engines burning during the boostback and re-entry burns and a single engine burning during the landing burn.

Table 4.3: Return-to-launch-site landing trajectory input data.

Parameter	**Stage 1**	**Stage 2**
Design Parameters		
P_c [bar]	108.0	108.0
P_e [bar]	0.8520	0.0488
D_s [m]	3.66	3.66
D_e [m]	0.988	2.97
t_b [s]	162.0	302.0
t_c [s]	9.0	-
OF [-]	2.38	2.38
Propellant [-]	RP1/LOX	RP1/LOX
$N_{engines}$ [-]	9	1
Launch Vehicle and Trajectory Data		
Payload Mass [kg]	2490.0	
Initial FpA [°]	89.50	
Initial Latitude [°]	28.61	
Initial Longitude [°]	-80.60	
Initial Azimuth [°]	50.80	
Fairing Jettison Time [s]	152.0	
Pitch Angles [°]	89.38 88.52 83.08 65.89 46.41	65.89 0.00 0.00

Table 4.4: Return-to-launch-site trajectory validation data.

Parameter	**CRS-10 Mission**	**Trajectory Model**	**Error [%]**
Stage 1 Ascent			
MECO Time [s]	143.0	138.0	-3.50
MECO Altitude [km]	63.00	72.72	15.4
MECO Downrange Distance [km]	48.00	42.22	-12.0
MECO Velocity [m/s]	1650	1837	11.3
Maximum Dynamic Pressure [kPa]	27.00	25.99	-3.74
Stage 1 Descent			
Boostback Time [s]	50.00	48.95	-2.10
Re-entry Burn Initial Altitude [km]	51.40	62.00	20.62
Re-entry Burn Final Altitude [km]	36.10	36.00	-0.28
Landing Burn Initial Altitude [km]	5.76	13.12	127.8
Landing Altitude [km]	0.00	0.01	-
Landing Velocity [m/s]	0.00	0.66	-
Downrange Landing Distance [km]	14.83	0.68	-
Stage 2			
Final Altitude [km]	414.0	409.6	-1.06
Final Eccentricity [-]	0.001	0.077	-
Final Inclination [°]	51.64	51.37	-0.52

A few remarks can be made about the RTLS validation data in Table 4.4. First, it is unknown when the payload fairing is separated from the second stage, and in the simulation the fairing was jettisoned at the same time as the second stage ignition. As the fairing accounts for extra dry mass, this is certainly a factor in the discrepancy between the MECO values. Additionally, as mentioned previously, the exact pitch profile of the Falcon 9 FT is not known, which may explain the errors between MECO altitude, downrange distance and velocity. Moreover, although the re-entry and landing burn initial altitudes are much larger than the actual CRS-10 mission values, the behaviour at the end of the re-entry burn and at landing are as expected and meet the requirements from Section 2.6. Finally, the distance between Kennedy Space Center Launch Complex 39 Pad A and Landing Zone 1 (the landing site for the reusable first stage) is 14.83 km. As guidance and control is not the focus of this research, a return-to-launch-site recovery is assumed to land within 5 km of the launch site. Therefore, although differences between the actual CRS-10 mission values and the simulated model differ by more than 10% for certain values, the behaviour of the recoverable first stage is as expected, serving to verify and validate the RTLS trajectory model for its use in this research.

To further demonstrate the agreement of the RTLS trajectory model with the flight profile of a Falcon 9 FT RTLS mission, the first stage altitude is plotted as a function of downrange distance in Figure 4.4, normalized for comparison purposes. Comparing this figure to the version produced by Brendel in Figure 4.5 in his study of optimal guidance for reusable launch vehicles further verifies the RTLS trajectory model [92], not in terms of quantitative results but in terms of the expected trajectory for a return-to-launch-site vehicle.

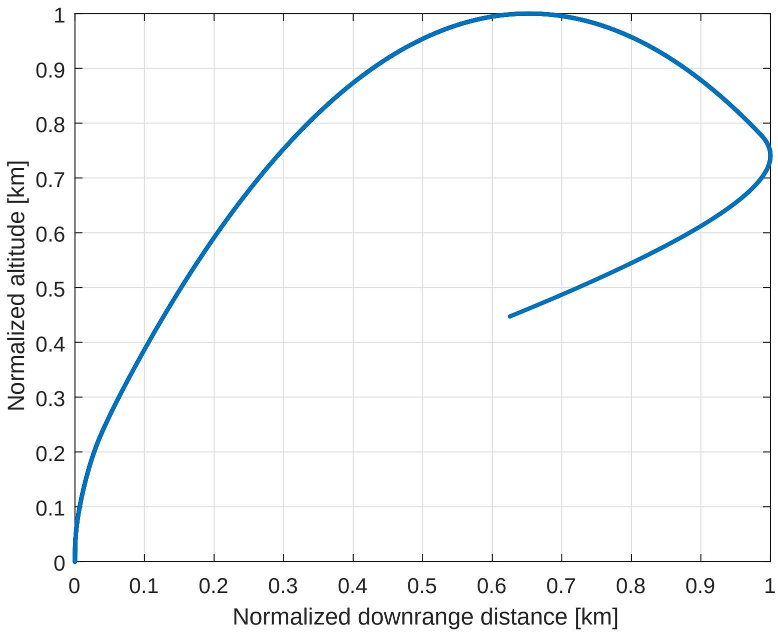

Figure 4.4: Altitude as a function of downrange distance of the modelled reusable first stage after MECO.

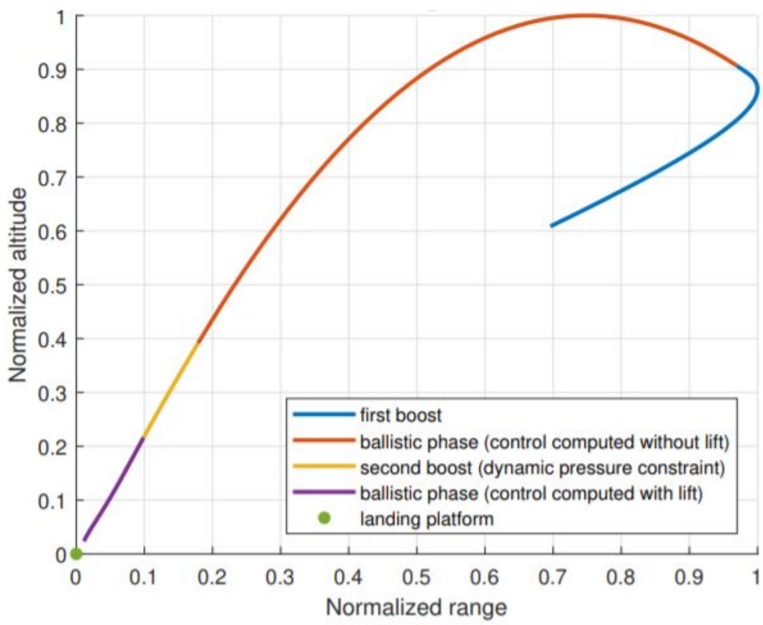

Figure 4.5: Altitude as a function of downrange distance of the reusable first stage from Brendel [92].

If proprietary Falcon 9 FT is ever made public, additional requirements could be placed on the re-entry trajectory to further demonstrate its validity along the flight path. Nonetheless, tuning the ascent pitch profile to match the actual MECO states was sufficient in verifying the re-entry behaviour of the first stage for both the return-to-launch-site and downrange landing cases, as well as validating their use based on the landing requirements set in Section 2.6.

The following chapter presents the cost model developed to determine the price per flight of a small, reusable launch vehicle.

5
Cost Model

As mentioned in the Introduction, there is a need to reduce the launch costs of small launch vehicles. To do so while accounting for reusability, it is important to accurately estimate the price per launch of a conceptual small, reusable launch vehicle to determine its price-reduction capabilities. This chapter presents the small launch vehicle cost model adapted from Drenthe [39, 40], first detailing how the flight unit cost estimate is calculated before explaining how this is used to calculate the development, manufacturing and operations costs of the launch vehicle. The following sections detail the changes made to the model and its applicability to the multidisciplinary design analysis environment. Subsequently, the reusability cost model and its verification and validation are presented.

5.1. Launch Vehicle Cost Model

Several cost estimation tools are used in the aerospace industry that can be used to cost launch vehicle systems, developed by both academics and space agencies. However, most of these are subject to strict governmental regulations and are not made available to the public, especially outside of the United States. These include the *Unmanned Space Vehicle Cost Model*, the *Small Satellite Cost Model*, *Price-H* and *TruePlanning* by PRICE^{TM} Systems Solutions, *aces* by 4cost, *SSER^{TM}-H* by Galorath Incorporated, the *NASA and Air Force Cost Model* and the *Aerospace Launch Vehicle Cost Model* from the Department of Defence (DoD) [40]. In fact, Koelle's TransCost cost estimation model is the only publicly available tool that can be used to estimate launch vehicle costs. The *TransCost Model for Space Transportation Systems Cost Estimation and Economic Optimization* is a dedicated launch vehicle system model encompassing the development, production and operations phases of expendable and reusable launch vehicles [98]. The accuracy of the cost estimation relationships is stated as being within ±20% of the cost data range. Despite its acclaim and widespread use, TransCost has been shown to overestimate the cost of small launch vehicles, sometimes by up to 140% [13, 40].

To make up for *TransCost*'s inaccuracies for small launch vehicles, Drenthe has developed a parametric model for estimating costs of a small launch vehicle in its early phases of development [39, 40], capable of estimating the price per flight of a commercial launch vehicle to within 20% of actual prices. Drenthe's method is a hybrid cost estimation method that combines Koelle's *TransCost* method with the Theoretical First Unit method. The former was used as a basis for CERs but was reconstructed at the subsystem level, compared to the system level costing of TransCost. These formed a basis for the Flight Unit (FU, NASA), or Theoretical First Unit (T1, NASA/ESA), another parametric approach to cost modelling in early design phases used in NAFCOM and TruePlanning as well as by ESA and NASA.

In general, the cost per flight of a launch vehicle is the sum of its development, manufacturing and operations costs, as depicted in Equation 5.1 [39]. This is elaborated on in more detail in the following sections.

$$CpF = C_{dev} + C_{man} + C_{ops} \tag{5.1}$$

Prior to validating Drenthe's model with the outputs from the Multidisciplinary Design Analysis values, minor modifications were made to ensure consistent use of the methodology used in this work. These modifications are presented in the following sections, organized in the same order as the work presented in Drenthe's thesis [39]. Additionally, any variables presented with an uncertainty are subject to a sensitivity analysis in Chapter 8.

5.1.1. Flight Unit Cost Estimate

Drenthe breaks down the solid and launch vehicle equipment as per Table 5.1 and Table 5.2, respectively. The parts are identified by their unit, equipment and part IDs through the first, second and third, and finally last three letters (if applicable).

Table 5.1: Solid launch vehicle breakdown.

Unit	Equipment	Part	Part ID
Stage	Solid Casing (incl. nozzle)		S-SC-
	Thrust Vector Control		S-TV-
	Stage Harness		S-SH-
Interstage	Interstage Structure		I-IS-
Payload	Payload Adapter		P-PA-
	Payload Fairing		P-PF-
Avionics	Avionics	Comms	A-AV-COM
		Power	A-AV-PWR
		Data Handling	A-AV-DHL
		GNC	A-AV-GNC
		Avionics Harness	A-AV-HNS
Attitude Control	Attitude Control Module		C-AC-

Table 5.2: Liquid launch vehicle breakdown.

Unit	Equipment	Part	Part ID
Stage	Pressurizant Tank		S-PT-
	Fuel Tank		S-FT-
	Oxidizer Tank		S-OT-
	Stage Structure	Thrust Cone	S-SS-TRC
		Skirt	S-SS-SKI
		Thermal Control	S-SS-THM
	Engine(s)		S-EN-
	Thrust Vector Control		S-TV-
	Propellant	Fuel	S-PR-FUE
		Oxidizer	S-PR-OXI
		Pressurizant	S-PR-PRE
	Pressurization System		S-PS-
	Pipes & Valves	Pipes	S-PV-PIP
		Valves	S-PV-VAL
	Stage Harness		S-SH-
Interstage	Interstage Structure		I-IS-
Payload	Payload Adapter		P-PA-
	Payload Fairing		P-PF-
Avionics	Avionics	Comms	A-AV-COM
		Power	A-AV-PWR
		Data Handling	A-AV-DHL
		GNC	A-AV-GNC
		Avionics Harness	A-AV-HNS
Attitude Control	Attitude Control Module		C-AC-

Some of the structural elements presented in Chapter 3, namely the pad interface, intertank and thrust structure, are not accounted for in the mass breakdown presented in Table 5.1 and Table 5.2. However, the mass estimation relationships account for these additional components. As these are all structural elements, which all have the same cost estimation relationships [40], these elements are costed using the structural CERs. Moreover, in the case of a reusable launch vehicle, since the majority of the mass comes from the landing legs, these are also assumed to fall in the scope of a structural element and are costed as such. Given an expendable and reusable launch vehicle with comparable masses without the reusable hardware, the reusable system will thus have a higher flight unit cost due to the additional costs associated with the reusable hardware. Additional propellant needed for descent also increases the size of the propellant tanks, which also increases the flight unit cost of a reusable system compared to an expendable system.

The full list of the cost estimation relationship coefficients used in the model, which take the form of Equation 5.2, are presented in Table 5.3 along with their respective RSE and the log of the standard error (SE) . The latter is used in the sensitivity analysis presented in Chapter 8. The Origin column indicates whether the CER was taken from Drenthe or from the NASA and Air Force Cost Model [99]. It should be noted that there is no difference in the cost estimation relationships between expendable and reusable launch vehicles. This is a result of the simplicity of the reusable launch vehicle and trajectory models, as larger propellant tanks and additional structures are taken into account in the cost estimation relationships. Furthermore, as advanced control is beyond the scope of this research, the reusable control system is not more complex than what is used during ascent, making this cost estimation relationship applicable to both types of systems.

$$C = a \cdot m^b \tag{5.2}$$

Table 5.3: Cost estimation relationship coefficients for individual launch vehicle elements.

Equipment Element Name	***a* value**	***b* value**	**RSE [%]**	**SE (log)**	**Origin**
Solid Casing, including propellant	90.72782	0.44422	12.9	0.1282	Drenthe
Pressurizant Tank	19.99465	0.71253	27.6	0.2711	Drenthe
Fuel Tank	19.99465	0.71253	27.6	0.2711	Drenthe
Oxidizer Tank	19.99465	0.71253	27.6	0.2711	Drenthe
Thrust Cone	2.799300	0.91199	12.6	0.1253	Drenthe
Skirt	2.799300	0.91199	12.6	0.1253	Drenthe
Thermal Control	2.799300	0.91199	12.6	0.1253	Drenthe
Engine(s)	31.48271	0.78811	35.8	0.3469	Drenthe
Thrust Vector Control	33.90978	0.60977	13.7	0.1359	Drenthe
Pressurizant System	11.50618	1.06948	49.8	0.4708	Drenthe
Pipes	8.958770	0.68815	34.3	0.3333	Drenthe
Valves	8.958770	0.68815	34.3	0.3333	Drenthe
Stage Harness	27.45211	0.44623	34.9	0.3393	Drenthe
Payload Adapter	26.01794	0.70000	7.95	0.0794	NAFCOM
Payload Fairing	23.59239	0.70000	9.93	0.0991	NAFCOM
Comms	51.11253	0.80000	One data point	-	NAFCOM
Power	42.01174	0.80000	Two data points	-	NAFCOM
Data Handling	141.6820	0.80000	7.06	0.0705	NAFCOM
GNC	69.05491	0.82458	23.8	0.2346	Drenthe
Avionics Harness	27.45211	0.44623	34.9	0.3393	Drenthe
Attitude Control Module	257.8420	0.75000	29.1	0.2854	NAFCOM
Interstage Structure	6.70369	0.68041	19.3	0.1909	Drenthe

With the above cost estimation relationships, the Theoretical Flight Unit (TFU) cost can be estimated as per the method employed by Drenthe [39, 40]. The following section details the modifications made to the development cost estimates.

5.1.2. Development Cost Estimate

The approach taken to estimate the development cost is the same as the approach detailed by Drenthe [40]. As there is insufficient knowledge of system specifics at the early design phase, a parametric relationship approach to determine the development costs of a system is used. These relationships are derived from the Flight Unit cost per launch vehicle element, and are divided in two major contributors, namely the design and development effort and building and testing work performed on system and subsystem models.

Drenthe's model uses certain underlying assumptions in the development cost estimate due to limitations and lack of project data encountered during the early stages of design. First, each subsystem element is assumed to be the first of its kind to be produced, whereas it is highly likely that many of the components in the launch vehicle have been previously manufactured. This can be alleviated in later stages of the design where each specific launch vehicle element can be estimated one-by-one. In addition, the level-of-effort costs associated with the development costs are highly dependent on the experience of the team, and were chosen as the average expected value as per the effort of the Space Shuttle management case. Finally, there is an inherent uncertainty associated with the input mass data used to validate the development costs, but this is alleviated in Chapter 8 through a sensitivity analysis. Nonetheless, Drenthe has shown that the underlying assumptions about profit retention of subcontractors and percentage of work subcontracted out have a relative magnitude of less than 2.5% on the development cost [39].

The underlying assumptions used in Drenthe's model regarding model philosophy, subcontractorship and learning cost improvement remain the same in this work. This includes the assumptions made for the Management and Product Assurance (M&PA) which are modelled as level-of-effort costs, which are in turn modelled as a percentage of the theoretical first unit. These assumptions are summarized in Table 5.4.

Table 5.4: Additional assumptions used to model the development cost [39].

Input	**Value**	**Reasoning**
Management and Product Assurance	5.25%	As per the work of Drenthe, derived from historical project performance
Profit retention cost reduction factor	0.9695	Factor introduced by Koelle as a function of number of subcontracts [100]
Percentage of work subcontracted out	20%	Estimate from SpaceX
Subcontractor profit	8%	Typical value for ESA

The only modifications made to the development cost model is the use of certain cost factors applied to the costing equations for normalization, as per Koelle's widely used TransCost model [100]. There are fourteen different cost factors that can be applied throughout the different phases of costing, with many potentially increasing or reducing the development cost by up to 50% [100]. The factors relevant to the development phase and their applied range are listed below.

1. $f_{0,dev}$, the system engineering/integration factor.
   This factor is applicable to the development phase to account for the complexity added due to multiple stages. It is equal to 1.04^N, where N is the number of stages.

2. f_1, the technical development factor.
   This factor is used to normalize the equations based on the technology's flight proven status. In this study, a value of 1.0 is used for expendable systems as an average of the expected 0.9 to 1.1 range, and a value of 1.2 is used for reusable systems as an average of the expected 1.1 to 1.3 range.

3. f_3, the team experience factor.
   This factor accounts for the level of experience of the team developing the system. In this study, a value of 1.0 is used as an average of the expected variations from 0.9 to 1.1.

4. $f_{10,dev}$, the cost engineering factor.
   When cost engineering principles are taken into the design of a system, the costs of this system is reduced compared to a "business-as-usual" approach, which are governmental contracts that focus more on maximization of performance rather than minimization of cost [38]. With this in mind for the small, reusable launch vehicle, this factor is set to 0.8 as an average of the expected 0.75 to 0.85 range.

5. $f_{11,dev}$, the commercial venture factor.
   As the system being designed is a commercial launch vehicle, it is not subject to the same restrictions from governments and customers. Thus, this reduces the development cost by a factor of 0.5.

From the list above, it is evident that the factors can both increase and reduce the development cost of a launch vehicle depending on the system, but a commercial company is likely to always see a reduction in development costs. Therefore, the development cost changes from Equation 5.3 to Equation 5.4 using the updated model, where c_p is the profit retention cost reduction factor, PO is the Project Office costs and $MAIT$ are the Manufacturing, Assembly, Integration and Test costs [39].

$$C_{dev} = c_p \cdot (PO + MAIT) \tag{5.3}$$

$$C_{dev} = c_p \cdot (PO + MAIT) f_{0,dev} f_1 f_3 f_{10,dev} f_{11,dev} \tag{5.4}$$

The detailed steps needed to calculate the development cost are provided in Appendix C. The use of the above factors is verified and validated in Section 5.2.

5.1.3. Manufacturing Cost Estimate

Again, the approach taken by Drenthe is adopted in the estimation of the manufacturing cost of a launch vehicle. The only modifications made to the model are the use of additional cost factors, consistent with the approach presented by Koelle [100]. In the manufacturing cost model, only two of these factors are applicable. These are listed below.

1. $f_{10,man}$, the cost engineering factor.
   As with the development cost, the manufacturing costs see the same reduction of 0.8 when cost engineering principles are included in the design phases.

2. $f_{11,man}$, the commercial venture factor.
   As with the development cost, the commercial nature of the system being designed induces a reduction in the manufacturing cost. For this phase, this factor has a value of 0.55.

In addition to the above factors, another modification made to the manufacturing cost estimate is that the manufacturing cost of a reusable first stage is averaged over its number of reuses. Therefore, a trade-off between the learning curve associated with producing more units and the reduced manufacturing cost per unit occurs. The manufacturing learning factor L_m is given by Equation 5.5 as a function of n units and the learning curve p, with the latter set to 0.9 as per Drenthe's work [39, 40]. The effect of uncertainty in this design parameter and the effect of number of units manufactured and number of reuses is investigated further in Chapter 7.

$$L_m = n^{\frac{\ln p}{\ln 2}} \tag{5.5}$$

Similar to the development cost, the manufacturing cost equation changes from Equation 5.6 to Equation 5.7 using the updated model, where $FM1$ is the First Flight Model cost.

$$C_{dev} = c_p \cdot (FM1 \cdot L_m + M/PA\%) \tag{5.6}$$

$$C_{dev} = c_p \cdot (FM1 \cdot L_m + M/PA\%) f_{10,man} f_{11,man} \tag{5.7}$$

An underlying assumption in this section is that a constant number of units are manufactured in a certain period of time, which is not an ideal case [39]. Variations in manufacturing times and efficiency can be taken into account in later stages of the design when actual production intervals are known. Additionally, the learning curve used in this model is independent of the period between the manufacturing of separate units, which is unrealistic yet applicable at the conceptual design stage [39].

5.1.4. Operations Cost Estimate

As the operations costs are derived from TransCost in Drenthe's model, no additional factors need to be included in the cost estimate. However, as the data used in Drenthe's model is outdated, some of the values were modified to better represent their current state. The variables of interest in the operations costs, as well as their values in Drenthe's model and the updated expendable and reusable model, are presented in Table 5.5.

Table 5.5: Operations cost variables and values.

Parameter	Symbol	Units	Drenthe Model [39]	Expendable	Reusable
Country productivity factor	f_8	-	1.0	1.0	1.0
Commercial venture factor	$f_{11,ops}$	-	0.5	0.5	0.5
Assembly and integration factor	f_c	-	0.7 - 0.85	0.7 - 0.85	0.7 - 0.85
Launch vehicle type factor	f_v	-	0.8	0.8	0.8
Launches per year	LpA	-	var	var	var
Vehicle complexity factor	Q_N	-	0.4N	0.4N	0.7N
Average learning factor operations	L_0	-	$f(n_{units})$	$f(n_{units})$	$f(n_{units})$
Work-year costs	W	k€	286425	301200	301200
Number of stages	N	-	2-3	2-3	2-3
Fuel and oxidizer mass	M_p	kg	var	from MDA	from MDA
Gross take-off weight (GTOW)	M_0	Mg	var	from MDA	from MDA
Pressurizant mass	M_{pres}	kg	var	from MDA	from MDA
Mass mixture ratio	OF	-	var	from MDA	from MDA
Public damage insurance	I	k€	100	100	100
Payload mass	M_{PL}	kg	var	from MDA	from MDA
Payload charge site fee	c_{PL}	€ kg^{-1}	5.51	5.51	5.51
Launch site fees	F	k€	1220	1220	1220
Specific transportation cost	T_S	€ kg^{-1}	5.365	5.365	5.365
Percent of work subcontracted out	S	-	20%	20%	20%

The launch site fees are equal for all cases as any additional costs associated with landing are assumed to be included in the recovery costs. Important values to further detail in Table 5.5 are listed below.

1. f_c: This factor has a value of 0.7 for horizontal assembly and of 0.85 for vertical assembly then transport to launch pad. Depending on the launch vehicle being validated or designed, this value is subject to change.

2. Q_N: The vehicle complexity factor increases for reusable launch vehicles and is a function of the number of stages, N.

3. L_0: The learning factor for operations is the same learning factor as the one in manufacturing, calculated as a function of the number of units produced.

4. W: The work-year costs is updated to reflect its actual conversion to euros in 2015.

Along with the direct and indirect operations costs adopted from Drenthe's model, there is the need to account for recovery and refurbishment of reusable stages. As these two cost factors are typically the highest source of uncertainty in cost models and there is a lack of reported data from existing systems [100, 101], initial estimates are provided from literature.

The recovery costs have been modelled as a percentage of direct and indirect operations costs [100, 101], or by using a bottom-up approach and costing each individual phase of recovery [102]. The former method is more commonly used to establish a general range of recovery costs, whereas the latter method seeks to precisely determine the cost drivers behind recovery. In the work of Stappert *et al.*, the cost of recovery C_{rec} is separated into the direct operations cost of the fleet C_{fleet}, the ownership cost C_{own}, the facilities cost C_{fac}, the transportation costs C_{trans} and an overhead cost C_{oh}, as depicted in Equation 5.8 [102].

$$C_{rec} = C_{fleet} + C_{own} + C_{fac} + C_{trans} + C_{oh} \tag{5.8}$$

The fleet costs include fuel costs, docking, navigation, cargo handling and berthing fees. The ownership costs include depreciation, interest and insurance rates, crew, maintenance and repair costs. Facility costs include cranes, additional harbour facilities and supply vessels, while any post-processing transportation to the facility are included in the transportation costs [102]. Although the specifics of how each of these elements are calculated are not detailed, the total estimates for SpaceX downrange landing and return-to-launch-site missions are provided. Using this bottom-up approach, the recovery per launch of a DRL mission is estimated to be \$667.8k (2018) compared to \$243.7k (2018) for a RTLS mission. In this study, initial estimates for the recovery costs are modelled as a function of direct and indirect operations costs as per the works of Wertz and Koelle [100, 103], and are then compared with the estimates provided by Stappert *et al.* [102].

Typically, the refurbishment cost is modelled as a percentage of the average manufacturing cost of a single launch vehicle [40, 100, 103, 104]. This is in line with the metric used by SpaceX official Gwynn Shotwell, who has stated that the cost of refurbishing the Falcon 9 first stage which originally flew the CRS-8 mission was "substantially less than half" of what it would have cost to build a new one [105]. Studies vary this refurbishment fraction between 5% and 50%, and as a safe upper limit, a first estimate for refurbishment cost is estimated to be 50% of the average manufacturing cost.

A summary of all the segments that make up operations costs are presented in Table 5.6.

Table 5.6: Operations cost estimation relationships. The variables used and their respective units are presented in Table 5.5.

	Segment	**CER**
Direct Operations Costs	Ground Operations	$W \cdot 8 \cdot M_0^{0.67} LpA^{-0.9} N^{0.7} f_c f_v L f_8 f_{11,ops} / 1000$
	Propellant Cost	$\left(\frac{M_p}{r+1} c_f + \left(M_p - \frac{M_p}{r+1}\right) c_{ox} + M_{pres} c_{pres}\right) / 1000$
	Flight & Mission Operations	$W \cdot 20 \cdot Q_N LpA^{0.65} L f_8 / 1000$
	Transportation Costs	$T_S M_0$
	Fees and Insurance Costs	$I + F + c_{PL} P / 1000$
Indirect Operations Costs	Indirect Operations Costs	$(40S + 24) LpA^{-0.379} W / 1000$
Reusability Costs	Recovery Costs	$0.5 C_{ops}$
	Refurbishment Costs	$0.5 C_{man,av}$

The following section explains how the development, manufacturing and operations costs are used to calculated the cost per flight of a launch vehicle.

5.1.5. Cost per Flight

The cost per flight of a launch vehicle are calculated by amortizing the development costs over a fixed number of flights. This amortized development cost $C_{dev,a}$ is added to the n^{th} unit's manufacturing and operations cost, $C_{man,n}$ and $C_{ops,n}$ respectively, to determine the cost per flight of the vehicle CpF, as seen in Equation 5.9 [40]. This equation is an extension of Equation 5.1 for the n^{th} unit in a set.

$$CpF = C_{dev,a} + C_{man,n} + C_{ops,n} \tag{5.9}$$

As per the methodology employed by Drenthe, the estimate for price per flight PpF is calculated assuming a nominal profit margin of 8%, as seen in Equation 5.10 [40]. This profit margin has an inherent uncertainty associated to it, but when comparing the optimized expendable and reusable launch vehicles, this uncertainty is nullified.

$$PpF = 1.08 \cdot CpF \tag{5.10}$$

As the model adopted from Drenthe has been modified, additional validation is needed to ensure the accuracy of these modifications. This validation is presented in the following section.

5.2. Cost Model Verification and Validation

Verifying and validating the changes made to the small launch vehicle cost model as well as the added reusability is a crucial step to ensuring accurate results when performing the optimization for cost. Additionally, it is important to demonstrate that the cost model is verified and valid when using the mass outputs of the Multidisciplinary Design Analysis tool, and not only with the reported mass values from literature as done by Drenthe [39].

The cost model was first integrated into the Tudat environment, as it was adopted from Drenthe in a Microsoft Excel file. To verify its implementation within the new environment, the development, manufacturing and operations costs were compared for the Falcon 1, Falcon 9 and Pegasus XL with the values reported in Drenthe's work. This step yielded perfect agreement between the Tudat output and Microsoft Excel files. Then, the cost model was integrated within the MDA tool. All cost outputs from the model developed by Drenthe are expressed in k€ (2015) unless otherwise stated. Any conversions from these units can be calculated using the Historical EUR/USD Exchange Rates and USD Inflation Table from Appendix D and Appendix E, respectively.

The main challenge that arises when validating the cost model with the MDA tool is needing of knowing all of the propulsion design parameters of a given stage. For instance, as shown in Chapter 3, it is possible to model the Falcon 1c first stage, but lack of public information regarding the Kestrel engine makes it impossible to validate the second stage of this launch vehicle. As such, the life-cycle cost of the Falcon 1c is determined by using the MDA outputs for the first stage while assuming that the mass breakdown of the second stage as reported by Drenthe holds true [39].

Using the same design parameters as Table 3.12, the mass data for the Falcon 1c first stage can be determined before using these values in the updated cost model. The flight unit, development and manufacturing costs of the old and updated model are compared in Table 5.7. As the modelled Falcon 1c is heavier than the reported mass values used in Drenthe's model (first stage inert mass of 1812.6 kg compared to Drenthe's estimate of 1623.0 kg), the flight unit cost is higher in the updated model. Nonetheless, the additional cost factors in the development and manufacturing costs actually reduce these. The Falcon 1c development cost is estimated to be $90M (2010). Drenthe's model estimates this value to be 95.2M€ (2015), which is equivalent to $97.2M (2010) using the Historical EUR/USD Exchange Rates and the NASA 2018 Inflation Index [39, 106]. The modified model estimates the Falcon 1c development cost to be 88.5M€ (2015), which is equivalent to $90.3M (2010). This results in a reduction of relative error from 8.0% to 0.3%. Moreover, the Falcon 1c manufacturing cost is estimated to be 8.62M€ (2015), or $7.65M (2005), using Drenthe's model and 8.31M€ (2015), or $7.37M (2005), using the new modified model. Compared to the estimated $5.90M (2005), there is a reduction in relative error from 29.7% to 24.9%, again verifying the changes made to the cost model.

A similar procedure was done to validate the updated cost model for the Pegasus XL, using the design parameters in Table 5.8 to construct the launch vehicle. The only modifications made between the Falcon 1c cost model and the Pegasus XL cost model were changing $f_{10,dev}$ and $f_{10,man}$ from 0.8 to 1.0, and changing $f_{11,dev}$ from 0.5 to 0.55 and $f_{11,man}$ from 0.55 to 0.7. These were changed to their upper-limit values as per the range provided by Koelle because the company is more than 30 years old [100]. As with the Falcon 1c model, the flight unit cost of the Pegasus XL is higher in the MDA compared to Drenthe's model. Nonetheless, the relative error between the vehicle development cost, reported as $50.0M (1988), is reduced from 14.0% for Drenthe's model to -10.4% with the MDA, which is equivalent to $57.0M (2010) and $44.8M (2010), respectively. These results are summarized in Table 5.9.

Finally, the modifications to the cost model, as well as the added reusability costs, are verified using reported data from the Falcon 9 FT as Drenthe's model has also shown to be applicable for launch vehicles outside the target payload range of 100 kg to 700 kg [39]. The expendable Falcon 9 FT's development cost is significantly reduced in the updated model from a value of 407.1k€ (2015) to 286.8k€ (2015), equivalent to a change from $415.7M (2010) to $292.8M (2010). Comparing this to the estimated development cost of $300.0M (2010) [39, 107], a significant improvement of the development cost estimate is provided with the updated model, as seen in Table 5.10. Updating the operations mass values with the Multidisciplinary Design Analysis values, the price per flight assuming an 8% profit on the cost per flight can also be compared to the actual value of $62.0M (2010) and Drenthe's estimates. For 20 launches per year, Drenthe's model yields a price per flight of $72.4M (2010), while the update model returns a price per flight value of $57.1M (2010), resulting in a reduction in relative error from 16.8% to -7.90%, validating the ensemble of changes made in the development and manufacturing cost models. Furthermore, the same process can be applied to compare the price per flight of an expendable and reusable Falcon 9 FT. Using the 10% increase in inert mass for reusable hardware, there is an increase in both flight unit and development costs as seen in Table 5.11. Assuming a total of 100 units, 20 launches per year and 4 reuses of the first stage for a return-to-launch-site reuse, which is a conservative estimate based on recent successes from SpaceX, there is a decrease in price per flight from $54.8M (2015) to $35.1M (2015), equivalent to a 35.9% decrease in price per flight. This decrease agrees with the estimate provided by Shotwell of price reduction of "approximately 30%" [5]. The agreement between the reduction in price per flight for a reusable launch vehicle compared to an expendable one serves to verify the reusable cost model, as well as validating it as per the requirements of Section 2.6.

Although the number of validation cases is limited, the improved accuracy of the updated model compared to Drenthe's model, as well as the agreement to within 20% of reported values as set in the requirements, serves to validate the cost model used in this study. Furthermore, the lack of available validation data does not undermine the value of the models. As shown in previous studies, the verification of the models with available data is sufficient to then use these in a comparison study. While certain parameters and factors have an inherent uncertainty, the comparison of two designs using the same model is justified [11, 13, 14].

With the validated launch vehicle, trajectory and cost models, their implementation within a Multidisciplinary Design Analysis and Optimization framework is described in the next section.

Table 5.7: Falcon 1c flight unit, development and manufacturing cost comparison between models (FY 2015). The * symbol indicates values that were adopted from Drenthe's model.

	Flight Unit Costs [k€]		**Development Cost [k€]**		**Manufacturing Average Unit Cost [k€]**	
	Drenthe Model	MDA Model	Drenthe Model	MDA Model	Drenthe Model	MDA Model
Vehicle Cost	13 160	22 243	95 201	83 438	8 620	7 647
M&PA	-	-	4 621	4 041	418	370
Stage 1	10 001	19 084	68 840	57 658	6 233	5 309
Stage 2	3 159	3 159*	21 739	21 739*	1 968	1 968*

Table 5.8: Pegasus XL design parameters used for validation.

	Design Parameter				
Solid Rocket Motor (Stage #)	P_c [bar]	P_e [bar]	D_s [m]	D_e [m]	t_b [s]
Orion 50S XL (1) [52]	75.15	0.2531	1.275	1.422	68.6
Orion 50 XL (2) [52]	70.26	0.1777	1.275	0.861	69.4
Orion 38 (3) [52]	45.23	0.0991	0.965	0.526	68.5

Table 5.9: Pegasus XL flight unit, development and manufacturing cost comparison between models (FY 2015).

	Flight Unit Costs [k€]		**Development Cost [k€]**		**Manufacturing Average Unit Cost [k€]**	
	Drenthe Model	MDA Model	Drenthe Model	MDA Model	Drenthe Model	MDA Model
Vehicle Cost	15 783	19 987	114 188	89 752	10 338	9 163
M&PA	-	-	5 543	4 349	501	444
Stage 1	9 803	13 529	67 479	55 399	6 110	5 902
Stage 2	3 919	4 257	26 976	17 433	2 442	1 857
Stage 3	2 061	2 201	14 190	12 571	1 285	960

Table 5.10: Falcon 9 FT flight unit, development and manufacturing cost comparison between models (FY 2015).

	Flight Unit Costs [k€]		**Development Cost [k€]**		**Manufacturing Average Unit Cost [k€]**	
	Drenthe Model	MDA Model	Drenthe Model	MDA Model	Drenthe Model	MDA Model
Vehicle Cost	87 373	147 844	407 140	286 764	47 480	34 212
M&PA	-	-	19 437	13 565	2 290	1 648
Stage 1	77 462	130 773	319 486	217 275	40 511	29 088
Stage 2	9 911	17 071	68 218	55 924	4 679	3 476

Table 5.11: Falcon 9 FT flight unit, development and manufacturing cost comparison between expendable and reusable models (FY 2015).

	Flight Unit Costs [k€]		**Develpoment Cost [k€]**		**Manufacturing Average Unit Cost [k€]**	
	Expendable	Reusable	Expendable	Reusable	Expendable	Reusable
Vehicle Cost	147 844	152 627	286 764	330 796	31 325	5 719
M&PA	-	-	13 565	15 669	1 508	276
Stage 1	130 773	135 556	217 275	254 119	26 448	2 074
Stage 2	17 071	17 071	55 924	61 008	3 369	3 369

6
Software Implementation

Despite building from the works of Vandamme, van Kesteren and Miranda [12–14], the Tudat development environment was completely revamped in 2016. This means that the existing modules had to be recoded in the new environment as the old models were no longer compatible, before all of the new models could be integrated into the software. This section details the minor improvements made to the existing software, before detailing how the various disciplines and optimization algorithms were integrated into the Multidisciplinary Design Analysis and Optimization framework. Then, the general architecture of the tool is presented, before any additional inputs and assumptions, as well as important outputs of the tool, are listed.

6.1. Minor Modifications and Improvements

Along with the modules already implemented in the Tudat framework that remain unedited, a few modifications and additions were made for compatibility and ease of use.

In previous works, the US Air Force Missile DATCOM software has been used to predict the aerodynamic forces on a launch vehicle [12–14, 23]. The Missile DATCOM software is a semi-empirical aerodynamic prediction code that calculates aerodynamic forces, moments and stability derivatives from a variety of axisymmetric and non-axisymmetric missile configurations, with the option to add fins and wings. As the program was originally coded in FORTRAN, Vandamme made a Missile DATCOM database to reduce computational loads that had an error of less than 0.01% compared to the original Missile DATCOM for any given objective value. Although difficult to validate due to lack of public information of commerical launch vehicle aerodynamics, the module has reported errors of ±20% for the axial and normal force coefficients, as well as a 20% error on the coefficients for Ariane V and Vega [13]. Nonetheless, the uncertainty in the force coefficients have been shown to affect the GTOW of a small launch vehicle by less than 0.1%, which is acceptable within the scope of this research [13].

The Missile DATCOM database was previously read directly from the Tudat environment to output the force and moment coefficients as a function of the launch vehicle length, diameter, Mach number and angle of attack. Due to a major upgrade to the Tudat environment in 2016, this code was no longer compatible with the database and had to be updated for the purposes of this work. As the Tudat tool includes a *readTabulatedAerodynamicCoefficientsFromFiles* function, the best solution to make the database compatible with the environment was to use this function. To do so, a MatLab code was developed to transform the Missile DATCOM database text files into a Tudat-compatible format. The database itself was not modified, only the way it is accessed. If a new length and diameter configuration is added to the Missile DATCOM database, it suffices to enter the path of the output *for004.dat* file into the MatLab script to convert it to the proper format.

The Tudat environment also allows the user to save up to 46 different dependent variables at each time step of the integration, ranging from the body altitude and speed, to aerodynamic angles such as angle of attack and heading angle, to dynamic pressure and forces acting on the body. To evaluate the final state of both the upper stage of the launch vehicle and the reused first stage, the semi-major axis, eccentricity, inclination and downrange distance of the body were added as dependent variables.

Finally, an issue was encountered when trying to implement the thrust pitch guidance as it had been done in the past. From Figure 6.1, it can be seen that the angle of attack α is the difference between the pitch angle θ and the flight path angle γ. The issue was that the Tudat implementation did not agree with this, and after consulting with Tudat expert Dr. Dominic Dirkx, it was concluded that the best solution would be to implement aerodynamic guidance instead of thrust guidance. Thus, the new guidance algorithm controls the angle of attack of the launch vehicle by subtracting the flight path angle from the desired pitch angle, which now returns the expected values along the flight profile. This did not affect the inputs or outputs of the trajectory module, but only the way the angle of attack is calculated.

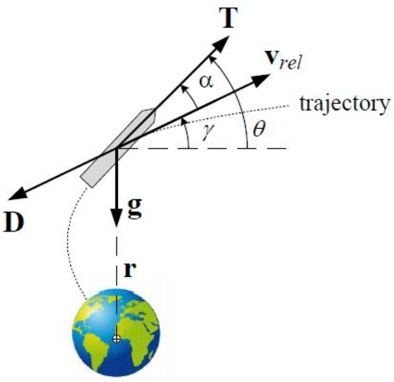

Figure 6.1: Sketch of important trajectory angles [108].

6.2. Objective Function, Constraint Handling and PaGMO

This section presents the two optimization loops needed for a reusable launch vehicle, from detailing how the design constraints are handled to the implementation of the objective function for both optimizations.

6.2.1. Cost Optimization

As mentioned in Section 2.5, the Parallel Global Multiobjective Optimizer platform developed by the European Space Agency is used in parallel with the Tudat environment for optimization purposes. Due to the reasons presented in Section 2.4 and its use in works of Vandamme and van Kesteren [12, 13], a differential evolution algorithm from PaGMO is selected for the primary optimization loop.

The fitness of the function describes how good a particular set of design parameters are with respect to the objective. In an optimization process, the fitness function is minimized to find the optimal configuration. The improvements made to the fitness function of the optimizer by Miranda [14] is adopted in this work. The improvements are twofold, namely the computation time is reduced from more than a day to less than four hours, and the convergence process occurs more rapidly from up to 10000 generations to less than 6000 generations. Hence, a piecewise objective function is used to minimize the cost of a launch vehicle.

The problem is divided into four different cases, as per the work of Miranda [14]. These cases are listed below, in order of improving fitness.

1. The vehicle is infeasible, as constraints placed on the vehicle are violated.
2. The vehicle is feasible, but violate path constraints during the trajectory simulation.
3. The vehicle is feasible and does not violate path constraints, but the target orbit is not reached before all propellant is used.
4. The vehicle is feasible and reaches the target orbit.

From the four different cases, the fitness function, f, can be established as follows. If the vehicle is infeasible, the fitness function is evaluated as in Equation 6.1.

$$f = 1 \cdot 10^6 \tag{6.1}$$

If the vehicle violates a path constraint, the fitness function is evaluated as in Equation 6.2, where h_{final} is the altitude at which the path constraint is violated and h_{target} is the target mission altitude.

$$f = -1 \cdot 10^3 \cdot h_{final}/h_{target} \tag{6.2}$$

If the target orbit is not reached before all the fuel is used, the fitness is evaluated as in Equation 6.3, where s_a and s_e are the semi-major axis and eccentricity scores given by Equation 6.4 and Equation 6.5, respectively, and p is a multiplier given by Equation 6.6.

$$f = -1 \cdot 10^6 \cdot (s_a + s_e) \cdot p \tag{6.3}$$

$$s_a = \left| \frac{a_{final}}{a_{target}} \right| \tag{6.4}$$

$$s_e = 1 - \left(e_{final} - e_{target}\right) \tag{6.5}$$

$$p = \begin{cases} 2.0 & \text{if } h_{final} > 0 \\ 4.0 & \text{if } h_{final} > 0.6 h_{target} \\ 8.0 & \text{if } h_{final} > 0.8 h_{target} \\ 16.0 & \text{if } h_{final} > 0.9 h_{target} \end{cases} \tag{6.6}$$

If the launch vehicle reaches the target orbit, the fitness function is evaluated as in Equation 6.7, aiming to minimize cost or GTOW. The purpose of this research is to optimize a small, reusable launch vehicle for cost, yet the option to minimize GTOW is also included for completeness and potential expansion of the tool in future research, as results in Chapter 7 show a correlation between minimum GTOW and minimum cost.

$$f = \begin{cases} -1 \cdot 10^{10} + 10 \cdot C & \text{for cost} \\ -1 \cdot 10^{10} + 10000 \cdot GTOW & \text{for GTOW} \end{cases} \tag{6.7}$$

The convergence of the differential evolution algorithm for the given objective function is presented graphically in Figure 6.2. Only the generations that are evaluated according to Equation 6.7 are shown.

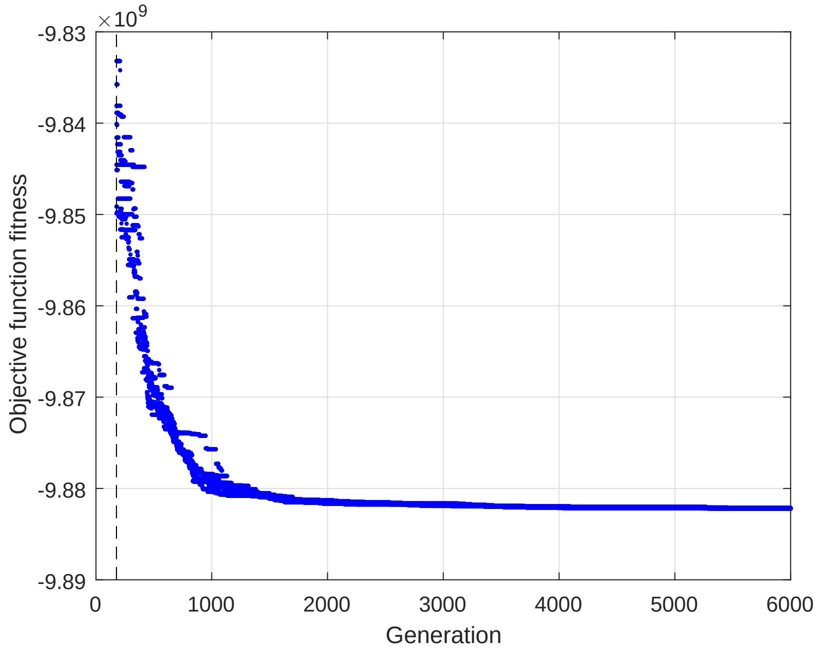

Figure 6.2: Evolution of fitness function for optimization of an expendable, two-stage solid launch vehicle. The mission target was an altitude of 650 km and an eccentricity below 0.1.

It can be seen through the dashed vertical line at generation 177 in Figure 6.2 that the launch vehicle is not minimized for cost only for the first 177 generations. After this point, the optimizer focuses on minimizing for cost, as desired.

6.2.2. Reuse Trajectory

After a small, reusable launch vehicle is optimized for cost, a second optimizer loop is run to determine the boostback, re-entry and landing burn conditions that will meet the requirements of the reuse trajectory. The problem uses the termination conditions of the optimal launch vehicle at the end of its first coast phase as a starting point, with boostback time, initial and final altitude of re-entry burn, and initial altitude of landing burn as design variables. In the case of a return-to-launch-site reuse, preliminary simulations of a Sun-synchronous orbit reuse showed that no satisfactory condition for the downrange distance could be met. This reason for this arises from the target orbit of the launch vehicle. In a near-equatorial launch with low-inclination target, the first stage flies along the direction of the rotation of the Earth, with no need for additional guidance when returning to the launch site. However, with a Sun-synchronous orbit, the first stage flies perpendicular to the direction of rotation of the Earth. Over the first stage burn and coast times and reuse trajectory time, the launch site has rotated out of the plane of flight of the first stage. Therefore, an additional variable, namely the yaw angle of the stage, is added as a design parameter for return-to-launch-site reuses in order to minimize the distance to the intended landing target.

An innovative approach is taken to minimize the difference between the first stage's actual and target landing altitude, velocity and downrange distance. While all of the aforementioned optimization algorithms within PaGMO are single-objective, the improved harmony search (IHS) algorithm has been developed to accept multiple objective functions, therefore making it a multi-objective solver.

First developed in 2007, the improved harmony search algorithm was developed by Mahdavi *et al.* and is a metaheuristic algorithm said to mimick the improvisation process of musicians [109]. "In the metaphor, each musician (i.e., each variable) plays (i.e., generates) a note (i.e., a value) for finding a best harmony (i.e., the global optimum) all together" [110]. It was developed in order to improve the quality of solution of the original harmony search algorithm and other heuristic and deterministic methods [111]. It has also been shown to outperform genetic algorithms in terms of quality of solutions for various types of mathematical problems. The algorithm, already integrated within PaGMO, presented the most user-friendly solution for evaluating the ideal solution for reuse trajectories. Instead of evaluating a fitness function that minimizes the sum of all three desired terminal states, the improved harmony search can minimize all three separately. This is advantageous, as different requirements set on the terminal altitude, velocity, and downrange distance allow for individual optimization on each parameter. A simple example is used to illustrate this advantage. From the given requirements of the reuse trajectory, the downrange distance error has an order of magnitude that is twice as large as the landing altitude and velocity. A first stage that lands at zero altitude, zero velocity and 50m downrange meets the requirements of the mission. However, a first stage that reaches zero velocity and zero downrange distance at an altitude of 50m does not meet the requirements. A fitness function that evaluates the sum of these requirements would be the exact same in the case of a single-objective optimization, but the multi-objective IHS allows the distinction to be made across the three requirements.

The altitude fitness function, f_1, velocity fitness function, f_2, and downrange distance, d, fitness function, f_3, are defined as in Equation 6.8, Equation 6.9 and Equation 6.10, respectively. In Equation 6.10, Δd is defined as the absolute difference between the final and target downrange distance, $|d_{final} - d_{target}|$.

$$f_1 = p \cdot (h_{final} - h_{target}) \tag{6.8}$$

$$f_2 = p \cdot v_{final} \tag{6.9}$$

$$f_3 = p \cdot \Delta d \tag{6.10}$$

Above, p is a multiplier that is given by the conditions in Equation 6.11. These values were chosen arbitrarily, as they helped with the convergence of the fitness function.

$$p = \begin{cases} 1.0 \cdot 10^{12} & \text{if } V_{final} > 400 \text{ m/s and } \Delta d > 50 \text{ km} \\ 1.0 \cdot 10^{9} & \text{if } V_{final} > 100 \text{ m/s and } \Delta d > 10 \text{ km} \\ 1.0 \cdot 10^{6} & \text{if } V_{final} > 40 \text{ m/s and } \Delta d > 5 \text{ km} \\ 1.0 & \text{otherwise} \end{cases} \tag{6.11}$$

The convergence of the improved harmony search algorithm for the given objective function is presented graphically in Figure 6.3. The slight increase in f_2 between generation 700 and 1500 can be attributed to the reduction in f_1 and f_3 in this interval.

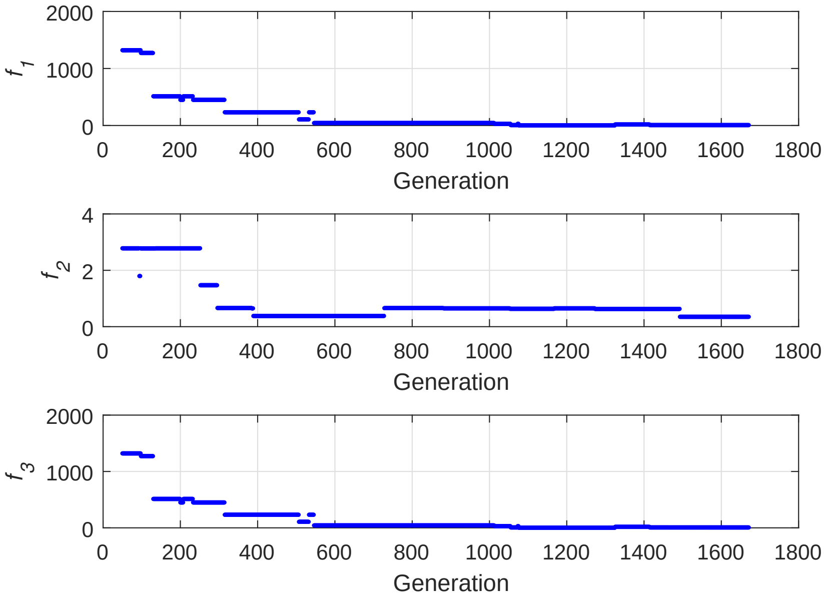

Figure 6.3: Evolution of fitness function for optimization of a return-to-launch-site reuse trajectory. The vehicle is an RP1-propelled 9-engine liquid rocket.

6.3. Tool Architecture

The combination of the models presented in earlier chapters can be summarized through a flowchart, as seen in Figure 6.4. In this figure, a few important blocks should be highlighted. First, all green blocks on the left side of the diagram represent an input to the simulation, which include the design parameters, the vehicle and trajectory constraints, and the initial conditions of the launch. The yellow blocks refer to the external databases, namely the CEA database and the Missile DATCOM database. Finally, the purple blocks represent a decision step, where the answer of the question within the block determines what happens next in the simulation.

The primary Multidisciplinary Design Optimization routine works as follows. First, the first generation of design parameters are chosen at random and fed into the optimization algorithm. These design parameters are then used to construct the stages and the launch vehicle. Once the launch vehicle is created, a decision block is encountered that decides whether or not the system violates any launch vehicle constraints. If it does, the simulation is terminated and the objective function is evaluated. If it does not, the cost of the launch vehicle is calculated before the Earth's environment is created. From the initial conditions and the geometry and mass of the launch vehicle, the environment and force models are created with the help of the Missile DATCOM database, before the equations of motion are set and the state of the system is propagated. At each time step, the propagator determines if a path constraint was violated. Once a constraint is violated or the termination conditions have been achieved, the objective function is evaluated based on the final orbit of the system and the price per flight.

Once the launch vehicle has been optimized, a second optimizer loop is started to determine the reuse parameters that give the desired landing state of the first stage. The functioning of this module is similar to the first, except it uses the terminal state of the optimized first stage as a starting point. A schematic of this process is seen in Figure 6.5.

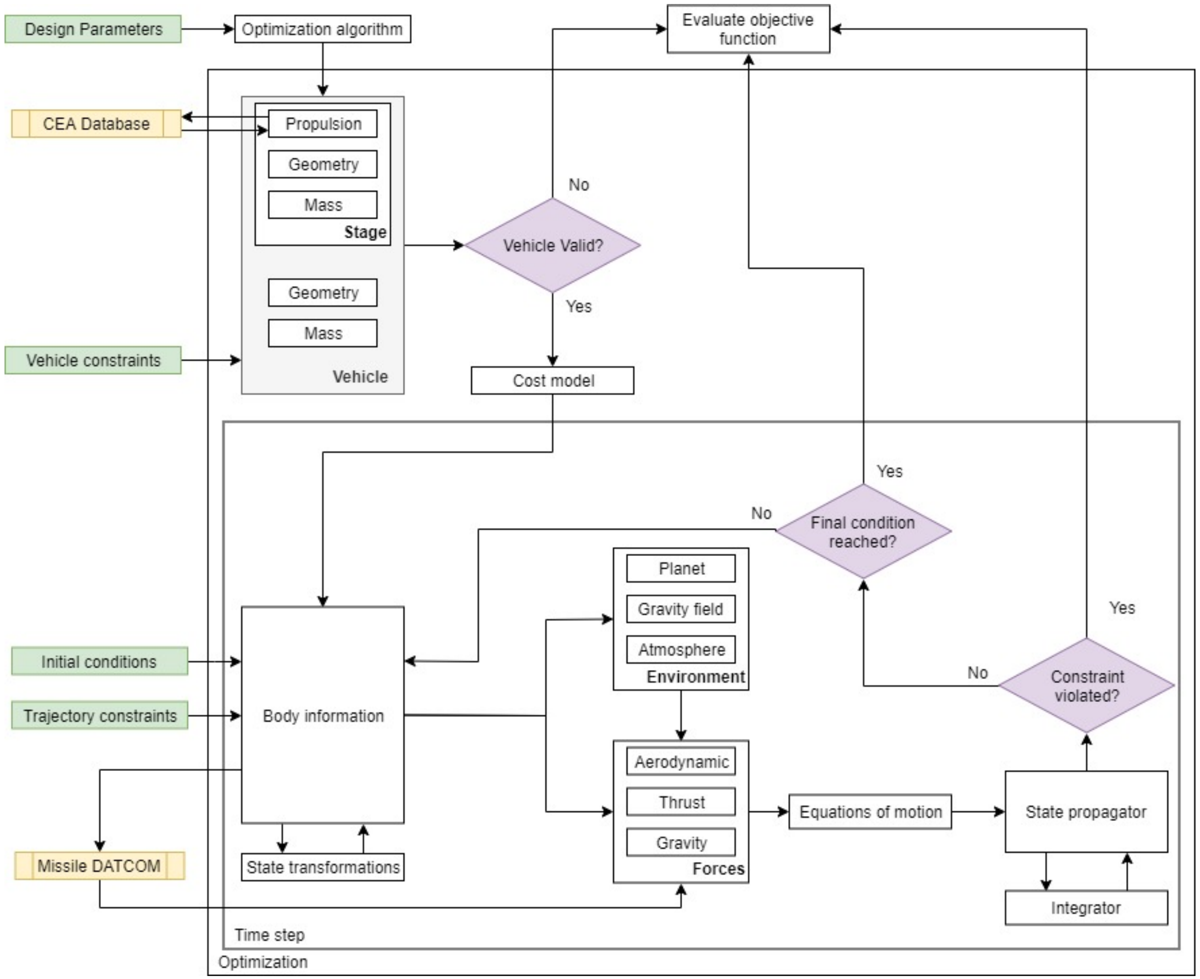

Figure 6.4: Top-level flowchart of the primary MDO tool used in this research.

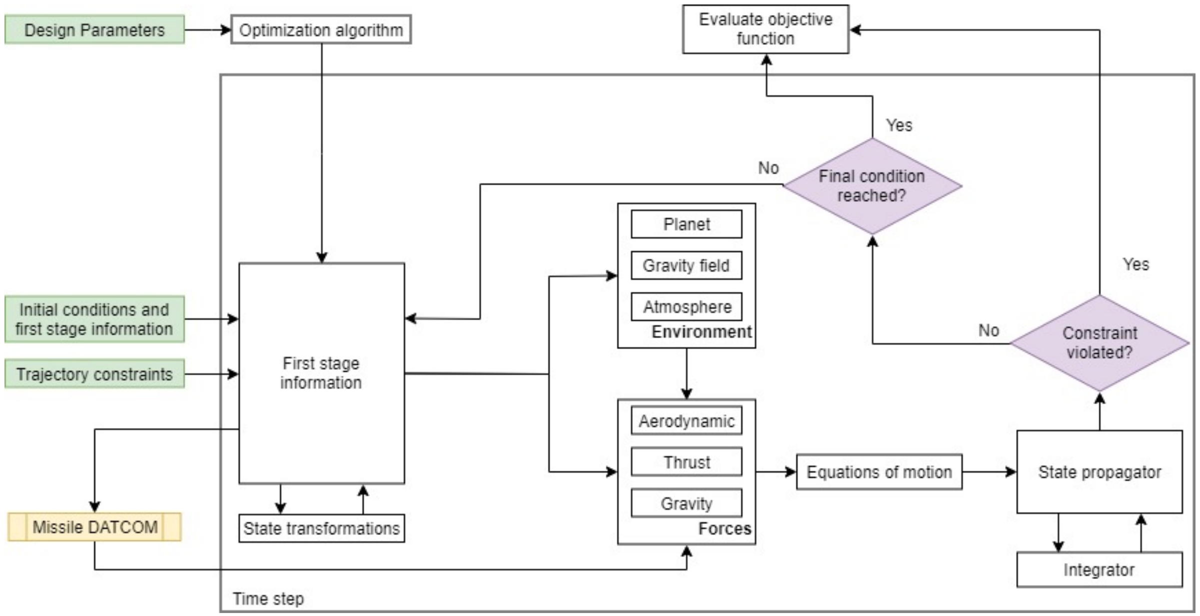

Figure 6.5: Top-level flowchart of the reuse MDO tool used in this research.

6.4. List of Inputs, Outputs and Assumptions

In addition to the aforementioned databases used as inputs to the tool, additional files with important inputs to the simulation are needed. These files define the simulation in greater detail, as there are many variables that have been mentioned in previous sections whose values were not established. This section lists these variables with their respective values, and also details the outputs of the tool.

From the information presented in Chapter 3, text files are used to configure the constants needed to build a solid and liquid stage. These constants are presented in Table 6.1 for solid stages and in Table 6.2 for liquid stages. These parameters have been set as constants in the model as sensitivity analyses varying these parameters have shown negligible (less than 1%) effects on GTOW and cost, or have shown best agreement for validation [12, 13].

Table 6.1: Additional inputs and assumptions used to model solid stages, as per the work of van Kesteren [13].

Input	**Value**	**Reasoning**
Motor case fill factor	95%	As used by Vandamme, van Kesteren and Miranda [12–14]
Available space for propellant	99%	Insulation starts at 99% of casing diameter
Insulation layer thickness	3 mm	As used by Castellini and van Kesteren [23]
Insulation material density	850 kg·m^{-1}	Ethylene-propylene-diene copolymer is assumed
Wall thickness safety factor	1.4	Design safety factor [41]
Case material density	2200 kg·m^{-1}	Carbon fibre composite is assumed
Case material allowable stress	800 MPa	Carbon fibre composite is assumed
Nozzle convergent half angle	30°	As used by van Kesteren
Nozzle divergent half angle	15°	As used by van Kesteren

Table 6.2: Additional inputs and assumptions used to model liquid stages, as per the work of Vandamme [12].

Input	**Value**	**Reasoning**
Propellant tank fill factor	95%	As used in previous works [12–14]
Wall thickness safety factor	1.4	Design safety factor [41]
Propellant tank pressure	4 bar	As used by Vandamme
Injector pressure drop fraction	1.0%	As used by Vandamme, added to tank pressure
Tank material density	2700 kg·m^{-1}	Aluminium Alloy 2014-T6 is assumed
Tank material allowable stress	400 MPa	Aluminium Alloy 2014-T6 is assumed
Reserved propellant percentage	10% to 17%	Fixed values of 10% for DRL and 17% for RTLS
Additional reusable stage mass	10% of $M_{s,inert}$	As established in Chapter 3

Next, as per the method described in Chapter 4, three text files are used to set-up the trajectory. The first text file contains all of the initial conditions of the launch vehicle, including the payload mass, initial flight path angle, latitude, longitude, azimuth, altitude and velocity. The target altitude and inclination are also included in this text file, all summarized in Table 6.3. The second file includes a list of the pitch angle points, as per the direct ascent trajectory described in Section 4.1. Finally, a text file containing the path constraints described in Section 4.3 is included in the directory. In the case of a reusable launch vehicle, an additional text file is used to define the return trajectory parameters, namely the boostback time, the initial and final altitudes of the re-entry burn, the initial landing burn altitude, the constant yaw angle, and the boostback burn pitch angle, which is held constant at 190°.

Table 6.3: Nominal trajectory input parameters for SSO launch from Plesetsk.

Input	**Value**
Payload mass [kg]	500.0 kg
Initial flight path angle [rad]	1.562 rad
Initial latitude [deg]	62.93°
Initial longitude [deg]	40.57°
Initial azimuth [deg]	280.0°
Initial altitude [m]	84.0 m
Initial velocity [m/s]	1.0 m/s
Target altitude [m]	650000 m
Target inclination [deg]	98.00°

For the cost model, three text files are used to divide the CER constants from Section 5.1.1, the cost correction factors presented throughout Chapter 5, and the operations constants presented in Section 5.1.4. Nominally, 20 launches per year, 100 total launches and, when applicable, 10 first stage reuses are assumed.

Finally, the directory includes a text file with the optimization bounds for the optimization process. A summary of this text file used for modelling a two-stage, RP1-propelled, 9 engine launch vehicle is shown in Table 6.4. For the various launch vehicle configurations, the trajectory bounds were held constant, as their range was sufficient to always converge to an optimal solution. The main differences that arise due to different configurations include changing the OF ratio to vary between 5.0 and 6.5 and changing the Fuel value to 0 for LH2-propelled stages. For solid upper stages, the OF and Fuel design parameters do not apply, and the number of engines is set to 1.

Table 6.4: List of optimization design parameter bounds.

Design Parameter	**Range**
Pitch Point 1	86° - 90°
Pitch Point 2	80° - 90°
Pitch Point 3	65° - 85°
Pitch Point 4	30° - 80°
Pitch Point 5	40° - 80°
Pitch Point 6	30° - 70°
Pitch Point 7	0° - 10°
Pitch Point 8	0° - 0.1°
$P_{c,1-2}$	30 bar - 200 bar
$P_{e,1}$	0.05 bar - 1 bar
$P_{e,2}$	0.001 bar - 0.1 bar
$D_{s,1-2}$	1 m - 2.5 m
$D_{e,1-2}$	0.2 m - 2 m
$t_{b,1}$	120 s - 200 s
$t_{b,2}$	250 s - 500 s
$t_{c,1}$	5 s - 30 s
OF_{1-2}	2.2 - 2.6
Fuel	1
$N_{engine,1}$	9
$N_{engine,2}$	1

The outputs of the simulations include two text files with the time history of each stage. The first text file includes the time evolution of the state in the Earth-Centred-Inertial frame, as well as the mass evolution of the launch vehicle. The second text file includes the dependent variable history of the launch vehicle. The dependent variables are listed below with their respective units in square brackets, and the time evolution of each are presented for a specific example in Appendix F.

1. Altitude [m]
2. Relative speed of vehicle with respect to the Earth [m/s]
3. Flight path angle [rad]
4. Heading angle [rad]
5. Angle of attack [rad]
6. Longitude [rad]
7. Latitude [rad]
8. Semi-major axis [m]
9. Eccentricity [-]
10. Inclination [rad]
11. Downrange distance [km]
12. Dynamic pressure [Pa]
13. Aerodynamic heat rate [W/m^2]
14. Thrust acceleration [m/s^2]
15. Aerodynamic acceleration [m/s^2]

Additionally, the user is able to output any variable of interest in the Application Output window of the Tudat environment. Variables that are of interest in this study is each stage's thrust force, engine mass, propellant mass, inert mass, length, and theoretical first unit cost, as well as the launch vehicle fairing mass, inert mass, GTOW, length and price per flight.

The outputs of an optimization also includes two text files per generation, listing the objective function fitness per population member in one file and the design parameters for that member in the second.

Now that the models have been presented and their implementation has been detailed, the main results of the study are presented in the following chapter.

7
Results

In earlier chapters, the models necessary to designing and optimizing a small, reusable launch vehicle are described. This section the important results of the tool concerning the optimization of launch price to orbit for these systems.

The first section details a wide range of potential designs that can be modelled with the tool in order to obtain key insights into cost drivers for such systems. By doing so, several potential designs are eliminated from the analysis due to preliminary trends in the results. Then, the most feasible design for cost-effective solutions to orbit is determined, before trends in optimal designs are analyzed. Subsequently, the effect of certain design choices such as intended orbit, launch site, and operations costs on the price per launch are investigated. Important to note that, unless otherwise noted, all costs are reported in FY2018.

7.1. Potential Designs

As the tool that has been developed is very versatile and allows for a range of different designs, it is important to compare these in order to determine the best solution for a cost-optimized, small, reusable launch vehicle.

As the first stage of such a system is constrained to be a liquid stage, there are two possible configurations for a two-stage SRLV, namely a liquid first stage and liquid second stage, or a liquid first stage and solid second stage. Both of these designs can be optimized for a return-to-launch-site and downrange landing recovery, and can be compared to an optimized expendable (EXP) counterpart. A three-stage small, reusable launch vehicle (SRLV) presents more options for stage configurations, which can be seen in Figure 7.1. Additionally, each liquid stage use either RP1 or LH2 as fuel, and the liquid first stage may have 1, 5 or 9 engines as these are designs currently being employed in the industry. Finally, all of these potential configurations should be optimized for the two mission cases, namely a 100kg and 500kg payload. All of these potential designs are summarized in Figure 7.1.

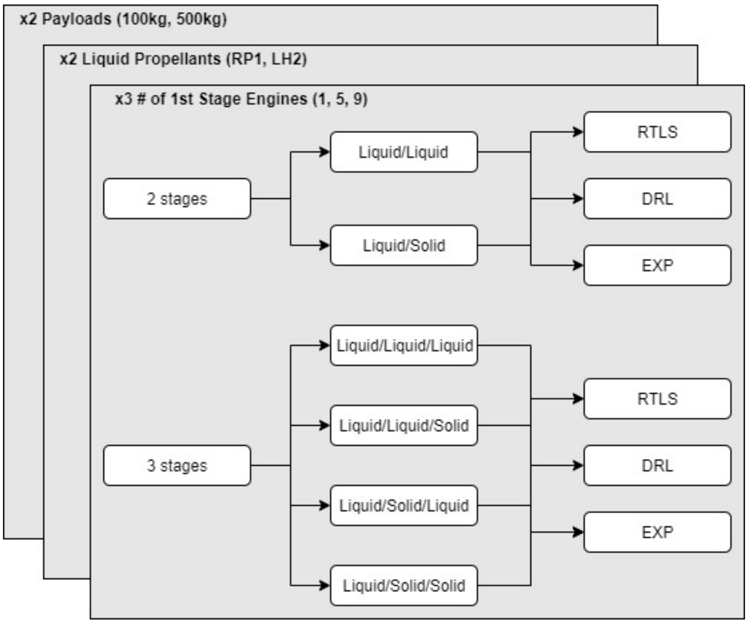

Figure 7.1: List of potential configurations for a small, reusable launch vehicle.

As the list of configurations would mean more than 200 optimized designs, it was deemed necessary to eliminate certain options based on preliminary trends. First, a comparison of two-stage and three-stage launch vehicles was conducted. Expendable RP1 1-engine and RP1 9-engine launch vehicles were compared in this study. The optimization results for these launch vehicles can be seen in Table 7.1, where certain conclusions can be made between these two systems. First, three-stage launch vehicles have a higher price per flight compared to the two-stage alternative. In the case of a three-stage 9-engine configuration, the first stage is comparable to the two-stage counterpart. This means that the second stage requires more thrust to carry the mass of the third stage to orbit, which increases the total inert mass of that stage resulting in a higher TFU second stage cost. The added third stage adds to this total, making the price per flight of a three-stage 9-engine launch vehicle more than its two-stage alternative. In the case of a single engine configuration, the three-stage launch vehicle's first stage is optimized for better first stage performance than the first stage of a two-stage vehicle. This increase in first stage TFU cost is counterbalanced by a smaller, less expensive second stage. However, this lowered second stage TFU cost does not balance the added cost of a third stage, resulting in a higher price per flight of the three-stage vehicle compared to the two-stage configuration. In general, it can be seen that the first stage of these launch vehicles represents a major portion of the cost, with a cost of approximately ten times that of the upper stages. Therefore, a significant reduction in three-stage first stage costs would be necessary to make these advantageous over two-stage vehicles, which is not the case for the optimal designs presented below.

Table 7.1: Comparison of optimized two-stage and three-stage launch vehicles for two different engine configurations.

Parameter	**2 Stage 9-engine**	**3 Stage 9-engine**	**2 Stage 1-engine**	**3 Stage 1-engine**
		Stage 1		
F_T [kN]	494.4	491.5	382.8	429.0
M_{engine} [kg]	795.1	791.9	450.3	501.3
M_p [kg]	22400	19911	14457	18247
L_{stage} [m]	19.50	18.58	18.88	23.85
M_{inert} [kg]	2017.9	1967.1	1293.2	1458.6
TFU [k$]	21864	21825	13564	14614
		Stage 2		
F_T [kN]	26.43	56.78	22.82	18.53
M_{engine} [kg]	56.88	90.39	52.90	48.16
M_p [kg]	3458.9	3486.0	2776.2	1231.9
L_{stage} [m]	4.980	5.407	5.150	3.466
M_{inert} [kg]	243.68	312.85	192.22	159.18
TFU [k$]	1658.6	2109.1	1457.0	1269.2
		Stage 3		
F_T [kN]	-	23.49	-	21.60
M_{engine} [kg]	-	53.64	-	51.55
M_p [kg]	-	1708.4	-	1610.5
L_{stage} [m]	-	3.680	-	3.935
M_{inert} [kg]	-	210.23	-	170.77
TFU [k$]	-	1499.0	-	1344.0
		Total		
$M_{fairing}$ [kg]	228.1	217.1	176.0	170.9
M_{inert} [kg]	3146.1	3384.8	2301.3	2621.2
GTOW [kg]	29158	28648	19672	23858
L [m]	28.78	32.24	27.87	35.35
PpF [k$]	11889.2	12265.7	10254.1	10833.3

The results from the above study show that three-stage launch vehicles are more expensive to launch than a two-stage counterpart with a similar stage configuration. From this preliminary analysis, all three-stage launch vehicles are excluded from further study, eliminating two thirds of the launch vehicle possibilities.

Next, a cost comparison was conducted between the 100 kg and 500 kg payloads. In the analysis, an expendable two-stage RP1 1-engine and RP1 9-engine were optimized for both payload classes. Table 7.2 presents the optimal configurations for the four different launch vehicles.

Table 7.2: Comparison of optimized 100kg and 500kg payload launch vehicles for two different engine configurations.

Parameter	**500kg 9-engine**	**100kg 9-engine**	**500kg 1-engine**	**100kg 1-engine**
		Stage 1		
F_T [kN]	494.4	239.6	382.8	206.05
M_{engine} [kg]	795.1	513.8	450.3	255.2
M_p [kg]	22400	9658.5	14457	7845.4
L_{stage} [m]	19.50	11.11	18.88	13.59
M_{inert} [kg]	2017.9	1176.9	1293.2	735.91
TFU [k$]	21864	16386	13564	10488
		Stage 2		
F_T [kN]	26.43	17.14	22.82	13.17
M_{engine} [kg]	56.88	46.63	52.90	42.25
M_p [kg]	3458.9	1959.6	2776.2	1510.5
L_{stage} [m]	4.980	3.944	5.150	3.974
M_{inert} [kg]	243.68	181.763	192.22	135.23
TFU [k$]	1658.6	1352.2	1457.0	1146.0
		Total		
$M_{fairing}$ [kg]	228.1	197.3	176.0	149.5
M_{inert} [kg]	3146.1	1785.0	2301.3	1241.3
GTOW [kg]	29158	13532	19672	10717
L [m]	28.78	19.08	27.87	21.16
PpF [k$]	11889.2	10110.1	10254.1	8991.88
Price per kg [k$/kg]	23.78	101.1	20.51	89.92

It is interesting to note what makes up the majority of the TFU cost. The ratio of the engine mass to inert mass of each stage, as well as the ratio of the engine TFU cost to stage TFU cost are presented in Table 7.3. When analyzing the first stages, it can be seen that nine engines make the stage more massive and thus, their contribution to the total TFU cost, which is approximately 50%, is greater than the 1-engine configurations, which is below 35%. When analyzing the second stages, it can be seen that a higher engine mass ratio directly correlates to a greater engine TFU cost ratio. As the engines are such important cost drivers in the launch vehicles, the use of the same engines for first and second stages could reduce the price per flight of such systems, which is left as a recommendation for future study.

Table 7.3: Comparison of mass and TFU cost breakdown of optimized 100kg and 500kg payload launch vehicles.

Parameter	**500kg 9-engine**	**100kg 9-engine**	**500kg 1-engine**	**100kg 1-engine**
		Stage 1		
M_{engine}/M_{inert}	39.4%	43.7%	34.8%	34.7%
$\text{TFU}_{engine}/\text{TFU}$	52.8%	49.9%	34.1%	28.1%
		Stage 2		
M_{engine}/M_{inert}	23.3%	25.7%	27.5%	31.2%
$\text{TFU}_{engine}/\text{TFU}$	54.6%	57.3%	58.7%	62.5%

Again, certain important conclusions can be made when comparing the different launch vehicles when optimized for the two payloads of interest. As can be expected, both vehicles optimized for the 100 kg case are lighter and smaller than their 500 kg counterpart. This reduces the TFU cost of each stage and, by extension, the price per flight of the smaller launch vehicle. However, as the focus of the study is to investigate reductions in price per kilogram to orbit for small launch vehicles, this measure is more important than the price per flight. When these are compared, the value for a 100 kg payload is more than four times greater than the price per kilogram to orbit of a 500 kg payload. This can be explained by the cost breakdown shown in Table 7.4 and Figure 7.2. Although the development cost of the 100 kg launch vehicles is reduced due to the smaller TFU costs, these only represent up to 5% of the total price per launch. The development and average manufacturing costs of the 500 kg class is approximately 30% higher than the 100 kg alternative for both configurations, yet the operations costs are only approximately 5% higher. This overall gain in total launch price for the 100 kg case does not balance the fivefold decrease in payload mass.

Table 7.4: Cost breakdown comparison between two different launch vehicles optimized for a 500kg and 100kg payload.

Parameter	**500kg 9-engine**	**100kg 9-engine**	**500kg 1-engine**	**100kg 1-engine**
$C_{dev,a}$ [k$]	495.44	387.85	517.11	400.51
$C_{man,n}$ [k$]	5288.7	4026.4	3915.0	3032.3
$C_{ops,n}$ [k$]	5224.4	4947.0	5062.4	4893.0

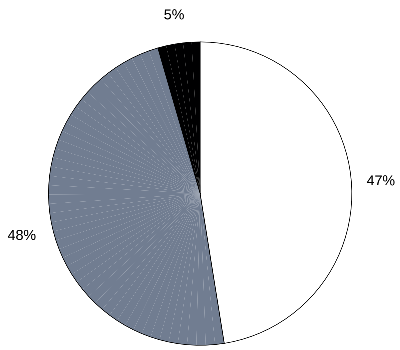

(a) 9-engine 500kg launch vehicle cost breakdown.

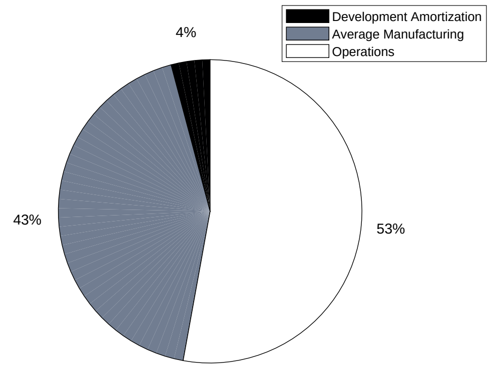

(b) 9-engine 100kg launch vehicle cost breakdown.

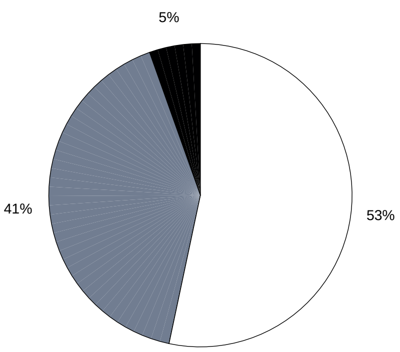

(c) 1-engine 500kg launch vehicle cost breakdown.

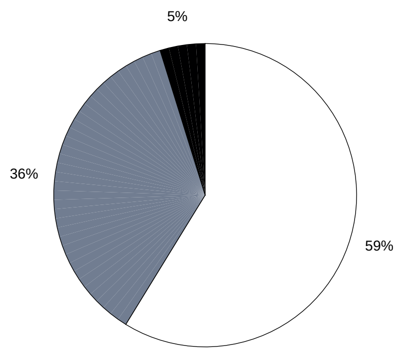

(d) 1-engine 100kg launch vehicle cost breakdown.

Figure 7.2: Graphical cost breakdown comparison between two different launch vehicles optimized for a 500kg and 100kg payload.

The results from the above study show that designing and optimizing a small, reusable launch vehicle with a payload of 100 kg is not a cost-effective solution to bring these systems to orbit. Thus, the remainder of the analysis excludes the 100 kg payload class.

The preliminary analysis conducted in this section serves to reduce the number of potential optimal designs. This reduction is summarized in Figure 7.3.

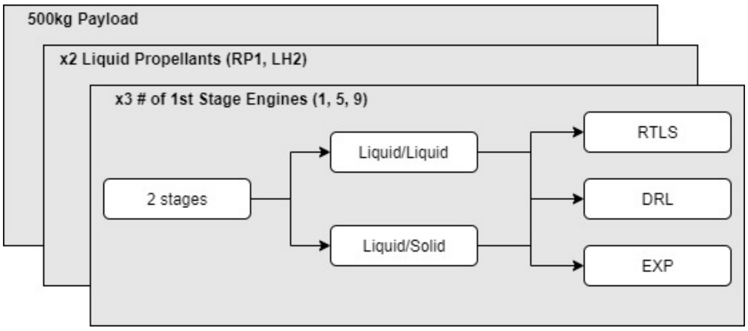

Figure 7.3: List of feasible configurations for a small, reusable launch vehicle.

The following section presents the results from the analysis of the remaining small, reusable launch vehicle options.

7.2. Feasible Design Selection

Now that the number of potential solutions is reduced, this section details the results for the remaining concepts. As the small, reusable launch vehicle can be designed for either return-to-launch-site or downrange landing reuse, the optimal designs are presented in the following subsections.

7.2.1. Return-to-Launch-Site Design

Two-stage reusable return-to-launch-site launch vehicles were first designed and optimized for a payload of 500 kg. As with the previous simulations, the initial conditions were a launch from Plesetsk Cosmodrome, with a target orbital altitude of 650 km, eccentricity below 0.1 and inclination of 98°. For this case, the reserved propellant for reuse was set to 17% of the total first stage propellant. Along with the aforementioned cost model constants presented in Section 5.1.4, the recovery cost was set to zero and the refurbishment cost was set to 50% of the average manufacturing cost. The former presents a lower estimate on recovery, while the latter presents an upper limit on refurbishment.

Several configurations were modelled in order to determine the optimal design for a return-to-launch-site vehicle. Using a population of 10 individuals evolved over 6000 generations, the price per flight and price per kilogram to orbit of six return-to-launch-site configurations are presented in Table 7.5.

Table 7.5: Price per flight comparison for six optimal return-to-launch-site reusable launch vehicles.

Propellant	Configuration	Price per flight [M$]	Price per kilogram [k$]
RP1	9-engine	9.10	18.19
	5-engine	8.92	17.86
	1-engine	8.63	17.25
LH2	9-engine	8.82	17.65
	5-engine	8.50	17.02
	1-engine	8.47	16.95

Table 7.5 presents interesting results, aside from the fact that all designs promise a cost-effective solution to orbit, being less than the $20.00k per kilogram benchmark set in Chapter 2. First, 9-engine configurations are more expensive than 1-engine configurations for both types of propellant, but the increase in price per flight is no more than 6.0% between these options. Furthermore, all configurations present a reduction in price per kilogram to orbit compared to the average reported $29.90k for expendable options on the market. Finally, LH2-propelled launch vehicles are always less expensive than their RP1-propelled counterpart, which is in line with the trends seen in a study conducted by Stappert [112]. To obtain more insight into these cost trends, the design parameters of the optimal configurations as well as key parameters for these launch vehicles are presented in Table 7.6 and Table 7.7, respectively.

Table 7.6: Optimal design parameters for six return-to-launch-site configurations.

	RP1			LH2		
Design Parameter	**9-engine**	**5-engine**	**1-engine**	**9-engine**	**5-engine**	**1-engine**
Stage 1						
P_c [bar]	199.3	198.3	192.4	198.2	145.3	145.7
P_e [bar]	0.6063	0.8212	0.3312	0.3200	0.5451	0.1614
D_s [m]	1.950	1.764	1.504	1.871	1.565	1.464
D_e [m]	0.440	0.521	1.504	0.418	0.454	1.463
t_b [s]	120.0	120.6	120.7	122.3	122.8	129.8
t_c [s]	5.438	5.364	5.323	5.473	5.405	5.429
OF [-]	2.503	2.594	2.505	6.500	6.500	6.416
Stage 2						
P_c [bar]	193.2	196.7	178.1	150.8	172.6	143.5
P_e [bar]	0.0102	0.0167	0.0156	0.0065	0.0056	0.0109
D_s [m]	1.950	1.764	1.504	1.871	1.565	1.464
D_e [m]	1.578	1.206	1.156	1.672	1.565	1.233
t_b [s]	433.8	451.8	424.3	445.2	495.6	455.2
t_c [s]	-	-	-	-	-	-
OF [-]	2.500	2.520	2.589	6.500	6.500	6.032

Table 7.7: Comparison of optimized return-to-launch-site configurations.

	RP1			LH2		
Parameter	**9-engine**	**5-engine**	**1-engine**	**9-engine**	**5-engine**	**1-engine**
Stage 1						
F_T [kN]	1397	1370	1125	755.6	697.9	561.1
M_{engine} [kg]	1792	1651	1270	1691	1312	865.5
M_p [kg]	51675	51753	40810	21933	21120	17014
L_{stage} [m]	22.14	26.38	29.10	26.63	35.36	33.85
M_{inert} [kg]	5349.5	5032.6	3951.4	4664.6	3916.0	2906.5
TFU [k$]	38183	33915	24442	37049	30429	21673
Stage 2						
F_T [kN]	74.56	65.73	55.82	54.00	42.45	45.35
M_{engine} [kg]	110.0	100.3	89.33	148.1	132.9	136.7
M_p [kg]	8785.5	8158.0	6523.7	5140.5	4466.5	4429.8
L_{stage} [m]	6.354	6.590	6.691	8.707	9.693	10.89
M_{inert} [kg]	585.67	496.01	387.84	698.07	558.51	552.79
TFU [k$]	3078.0	2768.0	2379.8	3786.4	3321.1	3339.6
Total						
$M_{fairing}$ [kg]	415.3	350.2	270.0	386.8	287.7	258.8
M_{inert} [kg]	7072.8	6592.1	5301.6	6480.8	5480.9	4424.6
GTOW [kg]	67753	66714	52825	33783	31284	26072
L [m]	34.28	38.26	40.44	40.91	49.85	49.29

Several conclusions can be made from the information in Table 7.6 and Table 7.7. The most important observation is that all six configurations present a cost-effective solution to orbit with a price per launch lower than $10.0M. Additionally, the 1-engine configuration is less expensive than the 5-engine and 9-engine counterparts due to the lower thrust from these engines, which in turn reduces the engine mass, propellant mass, and total inert mass of each stage. The smaller launch vehicle diameter of the 1-engine designs also reduces the mass of the fairing. Furthermore, there is a direct correlation between GTOW of the optimized launch vehicles and their price per flight when comparing designs using the same propellant. Due to the low density of LH2 compared to RP1, this results in a lower GTOW for LH2-propelled launch vehicles and in turn, a reduced price per flight when comparing similar engine configurations. The mass trends agree with the proprietary tool developed by the DLR for reusable launch vehicles [94, 102]. Moreover, the inert mass index, defined as the ratio of the launch vehicle's inert mass to its propellant mass, is higher for LH2-propelled designs than RP1-propelled designs, which also agrees with Stappert's model [102].

As the difference in price per flight between the six different launch vehicle configurations is minimal, a study of the reuse trajectory was done in order to determine the best option for reuse. This study yielded interesting results. First, the desired landing conditions for the LH2 9-engine and 5-engine designs could not be met with the given initial conditions. This can be visualized in Figure 7.4, where the altitude of the first stage is plotted as a function of the downrange distance. Here, the 9-engine configuration can thrust long enough to overcome the horizontal velocity but runs out of propellant during the re-entry burn, while the 5-engine configuration cannot overcome the horizontal velocity but can meet the landing requirements. This eliminates these two options from potential optimal designs within the scope of this study.

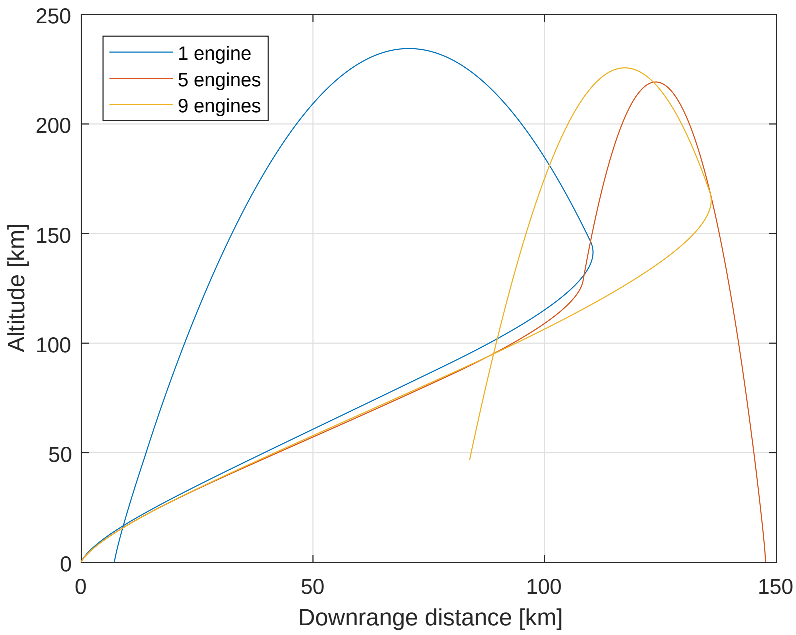

Figure 7.4: List of feasible configurations for a small, reusable launch vehicle.

Furthermore, the optimization process could not find a solution that met the requirements of the reuse trajectory for five of the six configurations. The dynamic pressure constraint that should not exceed 200 kPa could not be met for all except the RP1 9-engine launch vehicle. Figure 7.5 shows the dynamic pressure over time for the four remaining return-to-launch-site configurations. An investigation into the results of the optimization process for the reuse trajectory reveals key insights about this that is essential to the design of a small, reusable launch vehicle. As it can be seen in Table 7.8, the 1-engine re-entry burns are much shorter than the 5-engine and 9-engine designs. This is a result of the total thrust available for these manoeuvres. In this study, the maximum throttling for a single engine was set to 50.0%, which is the thrust used for each manoeuvre of the 1-engine designs. Conversely, the 5-engine and 9-engine configurations can use 20.0% and 11.1% of the total available first stage thrust by simply turning on a single engine instead of 5 and 9, respectively. This lowered thrust results in longer burn times, which is seen to reduce the dynamic pressure on the stage during re-entry, as per Figure 7.5. Although the 5-engine design approaches the 200 kPa limit, it is still not able to meet this requirement.

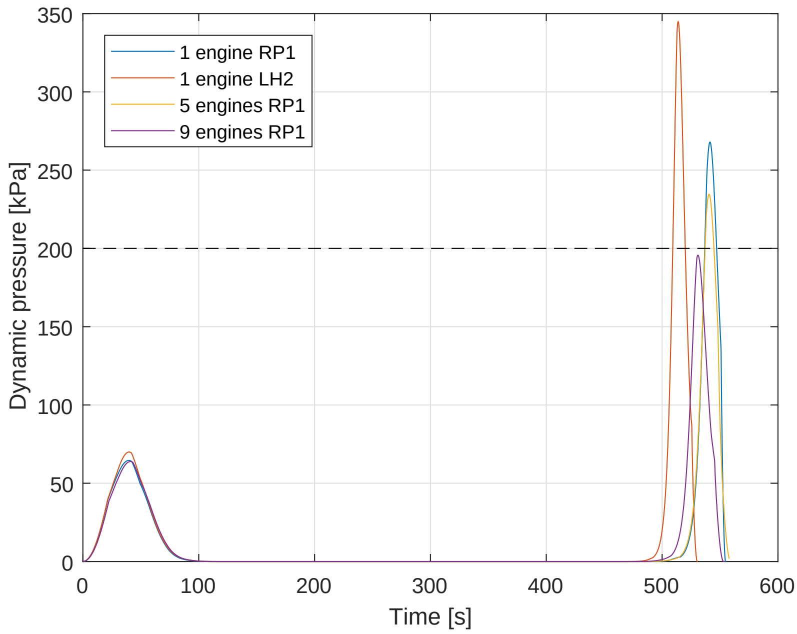

Figure 7.5: Dynamic pressure as a function of time for the first stage of the four remaining return-to-launch-site designs.

Table 7.8: Optimal reuse parameters for return-to-launch-site.

Parameter	**9-engine RP1**	**5-engine RP1**	**1-engine RP1**	**1-engine LH2**
Boostback time [s]	43.59	35.99	29.35	36.69
Re-entry Burn Initial Altitude [km]	65.89	72.89	50.76	50.33
Re-entry Burn Final Altitude [km]	38.96	41.00	36.83	45.72
Landing Burn Initial Altitude [km]	1.37	2.74	0.663	0.993

The above failures in the optimization process can potentially be mitigated by including additional constraints on the ascent trajectory in order to reduce the MECO velocity, or by reserving more than 17% of the first stage propellant to allow for longer burn times, which would in turn increase the price per flight of the launch vehicles. Furthermore, the inclusion of grid fins in the aerodynamic analysis would result in lower re-entry velocities and thus, dynamic pressures encountered by the stage [94]. This is left as a recommendation for further study.

This leaves a single feasible solution for the return-to-launch site reusable launch vehicle. The optimal launch vehicle design parameters can be seen in Table 7.6, while the final trajectory profile data is presented in Table 7.9, with three engines burning during the boostback burn and two engines burning during the re-entry and landing burns.

Table 7.9: Trajectory parameters for optimal return-to-launch-site launch vehicle.

Parameter	**Value**
Stage 1 Ascent	
MECO Time [s]	106.0
MECO Altitude [km]	79.63
MECO Downrange Distance [km]	59.33
MECO Velocity [m/s]	2507
Maximum Dynamic Pressure [kPa]	63.87
Stage 1 Descent	
Boostback time [s]	43.59
Re-entry Burn Initial Altitude [km]	65.89
Re-entry Burn Final Altitude [km]	38.96
Landing Burn Initial Altitude [km]	1.37
Yaw Angle [°]	9.25
Landing Altitude Error [m]	0.80
Landing Velocity [m/s]	1.67
Downrange Landing Distance [km]	4.16
Stage 2	
Final Altitude [km]	630.6
Final Eccentricity [-]	0.099
Final Inclination [°]	98.48

This section eliminated most potential designs for a return-to-launch-site, small, reusable launch vehicle. Nonetheless, a promising solution for reduction in price per flight was encountered in the form of the RP1-propelled, 9-engine design. The following section presents the results of the study for a downrange landing method.

7.2.2. Downrange Landing Design

A similar approach was taken to design and optimize a downrange landing launch vehicle. Using the same initial conditions and target orbit as the return-to-launch-site trajectory, 10 individuals were evolved for 6000 generations to optimize the price per launch of a downrange landing, small, reusable launch vehicle. For this case, the reserved propellant for reuse was set to 10% of the total first stage propellant. In addition, the recovery cost was set to 50% of the expendable operations cost and the refurbishment cost was set to 50% of the average manufacturing cost. These both represent upper limits on these values.

The six designs investigated in the return-to-launch-site study were again modelled for downrange landing. The price per flight and price per kilogram to orbit of the six optimal designs is presented in Table 7.10.

Table 7.10: Price per flight comparison for six optimal downrange landing reusable launch vehicles.

Propellant	**Configuration**	**Price per flight [M$]**	**Price per kilogram [k$]**
RP1	9-engine	11.41	22.82
	5-engine	11.06	22.11
	1-engine	11.05	22.11
LH2	9-engine	11.24	22.47
	5-engine	11.05	22.10
	1-engine	10.80	21.60

Comparing the results in Table 7.10 to Table 7.5, it can be concluded that the downrange landing option is more expensive to launch than the return-to-launch-site method under the preliminary assumptions of these models. While still presenting an advantage compared to the baseline $29.90k per kilogram to orbit, downrange landing systems do not achieve the $20.00k benchmark that has been set. Additionally, the optimal launch vehicles follow the same trends, becoming more expensive as more first stage engines are added and when comparing the RP1 to LH2 variants, which again agrees with the trends seen in a study conducted by Stappert [112]. The optimal design parameters and optimal downrange launch vehicle configurations are presented in Table 7.11 and Table 7.12, respectively.

Table 7.11: Optimal design parameters for six downrange landing configurations.

	RP1			LH2		
Design Parameter	**9-engine**	**5-engine**	**1-engine**	**9-engine**	**5-engine**	**1-engine**
Stage 1						
P_c [bar]	198.4	196.6	156.6	199.1	195.1	199.0
P_e [bar]	0.5615	0.6314	0.1799	0.4829	0.3517	0.1463
D_s [m]	1.718	1.574	1.591	1.506	1.493	1.273
D_e [m]	0.376	0.458	1.591	0.317	0.430	1.273
t_b [s]	128.0	120.0	126.1	122.7	161.7	134.0
t_c [s]	5.474	5.468	5.310	5.386	5.330	5.488
OF [-]	2.567	2.503	2.500	6.271	6.396	6.289
Stage 2						
P_c [bar]	159.7	186.5	196.7	200.0	175.9	173.1
P_e [bar]	0.0157	0.0059	0.0068	0.0082	0.0045	0.0076
D_s [m]	1.718	1.574	1.591	1.506	1.493	1.273
D_e [m]	1.071	1.428	1.337	1.302	1.492	1.128
t_b [s]	442.8	480.1	499.2	396.9	449.8	488.7
t_c [s]	-	-	-	-	-	-
OF [-]	2.598	2.599	2.592	6.500	6.500	6.500

Table 7.12: Comparison of optimized downrange landing configurations.

	RP1			LH2		
Parameter	**9-engine**	**5-engine**	**1-engine**	**9-engine**	**5-engine**	**1-engine**
Stage 1						
F_T [kN]	956.5	865.1	744.0	603.9	479.1	422.8
M_{engine} [kg]	1305	1094	849.1	1489	1018	660.4
M_p [kg]	37664	32063	27792	17794	18428	13002
L_{stage} [m]	20.62	21.03	19.18	32.70	34.11	34.17
M_{inert} [kg]	3834.7	3289.6	2738.8	3916.9	3105.9	2234.7
TFU [k$]	30819	25865	19720	33404	26398	18614
Stage 2						
F_T [kN]	46.73	38.40	38.28	41.60	32.15	28.48
M_{engine} [kg]	79.29	70.10	69.96	131.8	119.4	114.6
M_p [kg]	5713.1	4968.0	5156.7	3522.4	3054.7	2972.5
L_{stage} [m]	5.484	5.406	5.460	8.643	7.861	9.364
M_{inert} [kg]	409.4	340.2	346.3	504.6	456.1	403.1
TFU [k$]	2349.0	2072.1	2091.1	3136.9	2903.1	2728.7
Total						
$M_{fairing}$ [kg]	335.1	290.2	295.4	270.6	266.8	209.3
M_{inert} [kg]	5271.2	4599.3	4057.4	5396.4	4532.9	3531.2
GTOW [kg]	48838	41807	37181	26914	26217	19687
L [m]	31.27	31.25	29.50	46.00	46.59	47.66

The results in Table 7.11 and Table 7.12 reveal additional insights into important parameters of small, reusable launch vehicles. Trends similar to the return-to-launch-site designs can be seen when comparing the downrange landing 9-engine, 5-engine and 1-engine launch vehicles. As the number of engines decreases, the thrust force, engine mass and inert mass also decreases, which in turn results in a lower TFU cost. Additionally, the price per flight and price per kilogram to orbit decreases with lowered GTOW. The most interesting results of the downrange landing designs are that although the TFU cost of these are lower than the return-to-launch-site alternative, the price per flight is higher. To determine the reason for this, the cost breakdown of an RP1 9-engine RTLS vehicle is compared to that of an RP1 9-engine DRL vehicle, as seen in Figure 7.6.

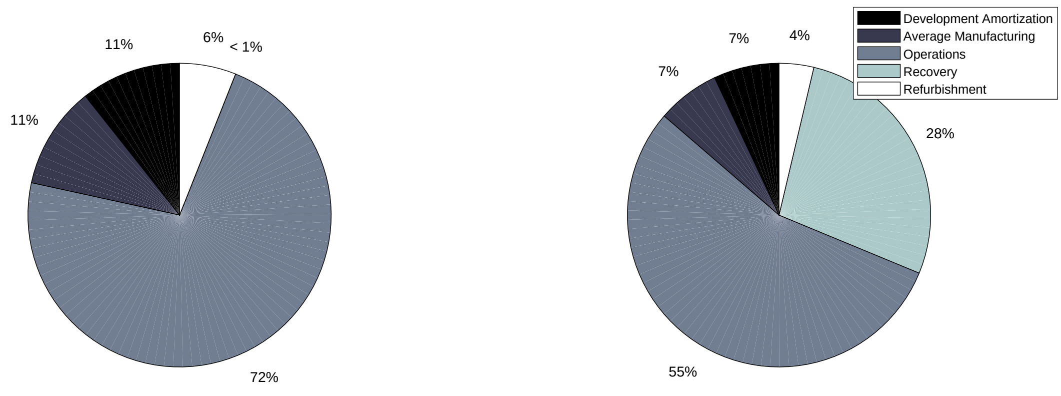

(a) RP1 9-engine RTLS launch vehicle cost breakdown.

(b) RP1 9-engine DRL launch vehicle cost breakdown.

Figure 7.6: Cost breakdown comparison between (a) return-to-launch-site and (b) downrange landing launch vehicle designs.

Figure 7.6 indicates that the development amortization and average manufacturing costs are similar for the return-to-launch-site and downrange landing launch vehicles. In fact, when comparing the TFU cost of the return-to-launch-site and downrange landing designs, these are always higher in the former than in the latter. However, the major difference arises when comparing the operations, recovery and refurbishment costs of the two optimal designs. For the RTLS option, the nominal operations costs dominate, with the recovery costs being non-existent and the refurbishment cost being equal to 50% of the average manufacturing cost. For the DRL option, the assumption that the recovery costs are equal to 50% of the operations costs account for a significant portion of the cost per flight of the launch vehicle. This makes the recovery cost a major cost driver.

As with the return-to-launch-site designs, the downrange landing reuse trajectory was heavily influenced by the 200 kPa dynamic pressure constraint. In fact, for this reuse method, no launch vehicle design was able to meet this constraint. Although the landing requirements from Section 2.6 could be met for all six configurations, the maximum dynamic pressure of 200 kPa was always exceeded by more than three times the allowable limit, as seen in Figure 7.7 for the three RP1 configurations.

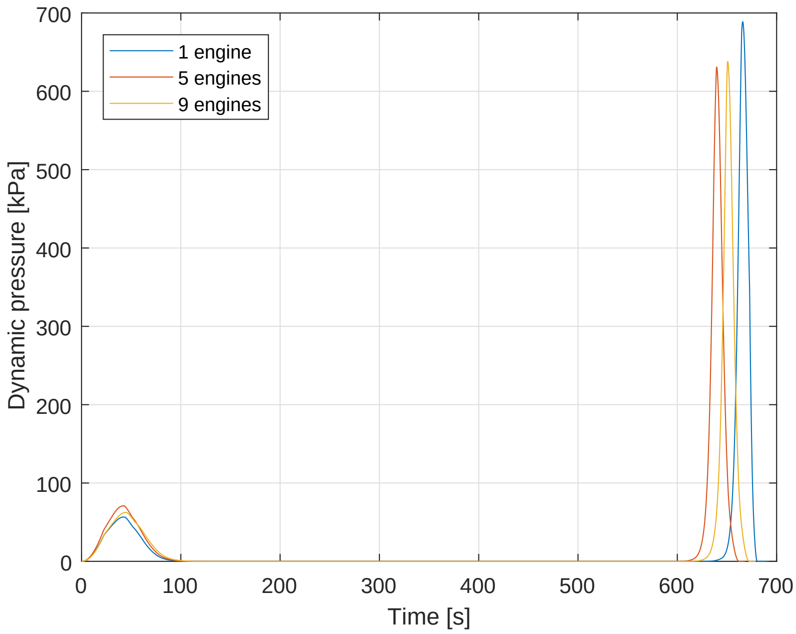

Figure 7.7: Dynamic pressure as a function of time for the first stage of the three RP1 downrange landing designs.

When comparing the dynamic pressure as a function of time for the LH2 downrange landing designs as seen in Figure 7.8, additional conclusions can be drawn about the reuse trajectory. For this case, the 5-engine configuration yields a lower maximum dynamic pressure than the 9-engine design. This is a result of the longer re-entry burn needed to achieve the desired landing conditions as seen in Table 7.13, which in turn reduces the maximum dynamic pressures, agreeing with the trends seen for the return-to-launch-site reuse trajectories. It is therefore imperative to minimize the re-entry burn final velocity in order to lower the maximum dynamic pressures.

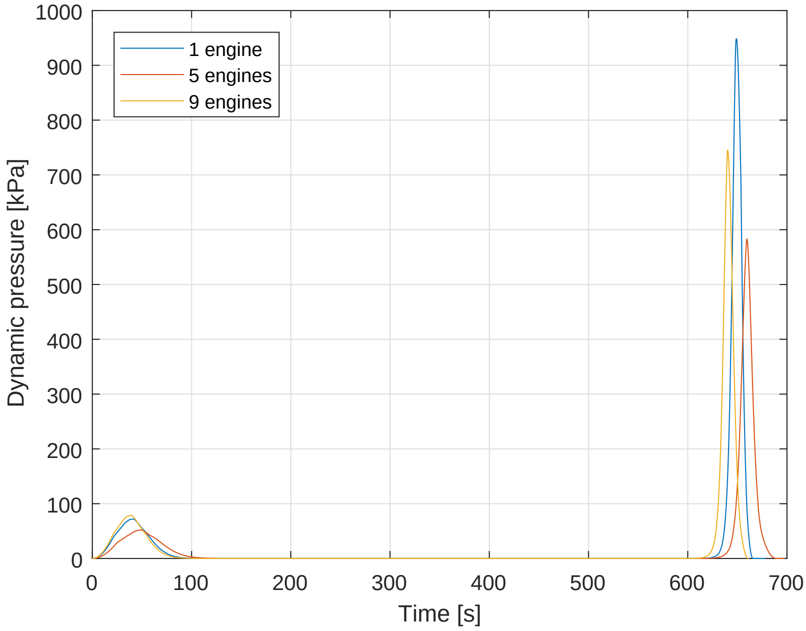

Figure 7.8: Dynamic pressure as a function of time for the first stage of the three LH2 downrange landing designs.

Table 7.13: Optimal reuse parameters for return-to-launch-site.

Parameter	9-engine LH2	5-engine LH2	1-engine LH2
Re-entry Burn Initial Altitude [km]	60.87	76.96	55.54
Re-entry Burn Final Altitude [km]	34.78	37.99	46.77
Landing Burn Initial Altitude [km]	16.28	9.805	4.565

The results from the downrange landing reuse trajectories suggest that more careful constraints should be placed on the ascent trajectory. The current constraint of limiting the downrange distance to be less than the altitude at MECO is not adequate for the reuse trajectory to meet the requirements of the mission. Constraints placed on the MECO cut-off velocity, as well as the inclusion of grid fins in the aerodynamic analysis as with the return-to-launch-site section, would reduce the maximum dynamic pressures encountered by the first stages [94]. Moreover, an additional burn at MECO similar to the boostback burn for return-to-launch-site trajectories could also help to reduce these high dynamic pressures by immediately reducing the stage velocity after separation. Within the scope of this study, no downrange landing design is feasible as a small, reusable launch vehicle solution.

7.2.3. Expendable Design Comparison

A study was conducted to compare the price per flight of an optimal expendable launch vehicle in order to determine if employing the return-to-launch-site reuse method is advantageous. Since the only feasible small, reusable launch vehicle is the 9-engine RP1 configuration, this design was compared to a wide range of expendable launch vehicles in order to determine its benefits on price per flight. For the same initial conditions and target orbit with a 500 kg payload, the price per flight of all the optimal expendable configurations are presented in Table 7.14, where LS signifies a liquid first stage and solid upper stage. The solid upper stages always include TVC as they are assumed to need precise orbit correction capabilities, despite these being out of the scope of this study.

Table 7.14: Price per flight comparison for multiple expendable launch vehicles configurations.

Propellant	**Configuration**	**Price per flight [M$]**	**Price per kilogram [k$]**
RP1	9-engine RTLS	9.10	18.19
	9-engine	11.89	23.78
	1-engine	10.26	20.51
	9-engine LS	13.01	26.03
	1-engine LS	11.53	23.07
LH2	9-engine	13.87	27.73
	1-engine	11.17	22.36
	9-engine LS	15.21	30.41
	1-engine LS	12.26	24.52
Solid	-	11.78	23.56

The results from Table 7.14 yield interesting results. A wide range of prices per kilogram are seen, with the lowest almost achieving the benchmark of $20.00k set for reusable systems at $20.51k, while the most expensive is slightly more than the baseline of $29.90k at $30.41k. Unlike the return-to-launch-site and downrange landing designs, the RP1-propelled launch vehicles have a lower price per flight than their LH2-propelled counterparts. Additionally, solid upper stages prove to be more expensive than all-liquid designs. To explain these trends, an investigation into the optimal design of each option is conducted. Omitting the optimal design parameters for the expendable launch vehicles for brevity purposes, conclusions can be made about these designs when comparing their general design, as shown in Table 7.15. First, it can be seen that there is no longer a correlation between GTOW and price per flight, as the LH2-propelled launch vehicles are still lighter than their RP1-propelled counterparts. However, when plotting the total inert mass of the optimized launch vehicle as a function of price per flight, there is a linear trend of increasing price per flight with increasing inert mass, as seen in Figure 7.9. As discussed in the literature study in Section 2.3, minimizing the design for minimum dry mass thus provides an alternative to minimizing for cost. A final remark should be made about the seemingly high price per flight of the fully-solid expendable launch vehicle. Although the solid stages have a lower inert mass compared to their liquid counterparts, the cost estimation relationship developed for these stages includes the mass of the propellant. For this reason, the TFU cost of solid stages is higher than liquid stages, driving the total price per flight higher. An interesting remark about the design of the RP1-propelled 1-engine expendable launcher is its first stage inert mass, which totals 1293.17 kg, is extremely similar to the 1290.00 kg first stage mass of the design from Snijders' study [11], suggesting that similar design choices were likely made by the NLR for the design of their proprietary small launch vehicle.

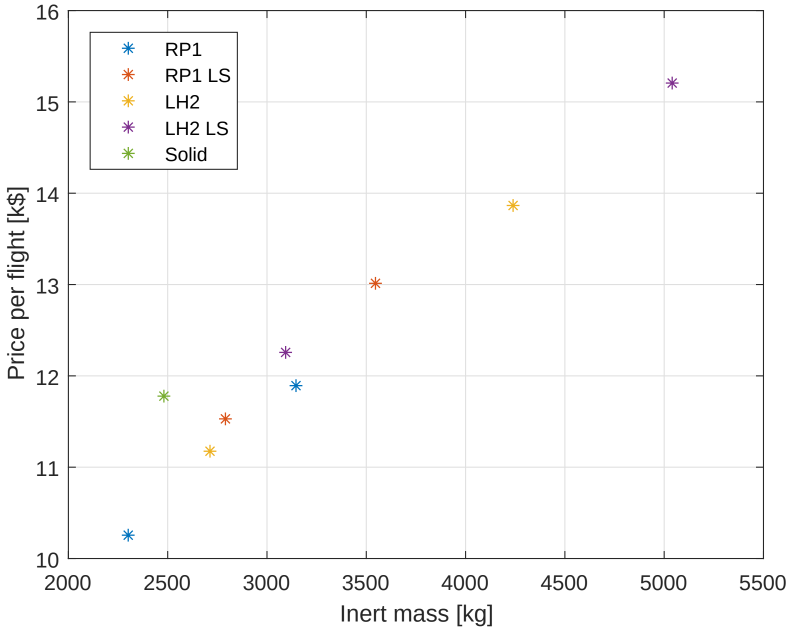

Figure 7.9: Price per flight as a function of inert mass for the investigated expendable options.

Table 7.15: Comparison of optimized expendable launch vehicle configurations.

	RP1					**LH2**				**Solid**
Parameter	**9-engine RTLS**	**9-engine**	**1-engine**	**9-engine LS**	**1-engine LS**	**9-engine**	**1-engine**	**9-engine LS**	**1-engine LS**	**-**
Stage 1										
F_T [kN]	1397	494.4	382.8	584.8	452.7	430.5	309.4	571.4	395.6	675.6
M_{engine} [kg]	1792	795.1	450.3	895.0	527.5	1260	497.4	1446	620.9	-
M_p [kg]	51675	22399	14457	29164	22687	13561	9864.0	20510	15953	30270
L_{stage} [m]	22.14	19.50	18.88	17.98	17.01	30.78	34.80	24.83	42.59	21.24
M_{inert} [kg]	5349.5	2017.9	1293.2	2411.2	1672.8	2852.5	1528.4	3678.3	2065.1	1492.6
TFU [k$]	38183	21864	13564	23921	15564	28911	15718	32663	18113	15836
Stage 2										
F_T [kN]	74.56	26.43	22.82	20.92	20.12	39.15	23.76	34.07	25.37	22.72
M_{engine} [kg]	110.0	56.88	52.90	-	-	128.6	108.4	-	-	-
M_p [kg]	8785.5	3458.9	2776.2	3001.1	2573.5	3546.5	2554.3	4025.5	2854.0	3012.9
L_{stage} [m]	6.354	4.980	5.150	2.236	3.690	10.38	10.69	3.313	3.360	3.923
M_{inert} [kg]	585.7	243.7	192.2	159.1	176.9	474.6	350.5	256.3	144.5	135.9
TFU [k$]	3078.0	1658.6	1457.1	3275.5	3077.1	3046.9	2526.7	3757.6	3177.8	3315.7
Total										
$M_{fairing}$ [kg]	415.3	228.1	176.0	305.9	277.8	225.7	165.5	391.6	199.9	160.1
M_{inert} [kg]	7072.8	3146.1	2301.3	3546.3	2790.7	4239.2	2713.0	5040.4	3093.8	2480.9
GTOW [kg]	67753	29158	19672	35879	28211	21531	15297	29787	22083	35954
L [m]	34.28	28.78	27.87	25.15	25.41	45.43	49.22	33.75	49.99	30.01

From the above analysis, it can be concluded that a return-to-launch-site, reusable launch vehicle is a cost-effective solution to bringing a 500 kg satellite to Sun-synchronous orbit when using the nominal launch parameters. Although reusable launch vehicles present higher TFU costs and thus, development costs, the reduction in production costs due to reusability outweigh the increased development costs, comparable to the results seen by Stappert [112].

A final case of interest is the price per flight of the expendable version of a reusable system. For expendable Falcon 9 launches, SpaceX uses the same launch vehicle as for reusable launches, but remove the landing legs and grid fins from the first stage. Therefore, for such analyses, all cost factors are assumed to be the same as for a reusable system, but the system flies without the 10% added structural mass and does not need to reserve extra propellant for re-entry and landing. Under these assumptions for the optimal return-to-launch-site vehicle, the price per flight is presented in Figure 7.10 as a function of number of launches per annum and number of first stage reuses assuming 100 total launches for the reusable cases.

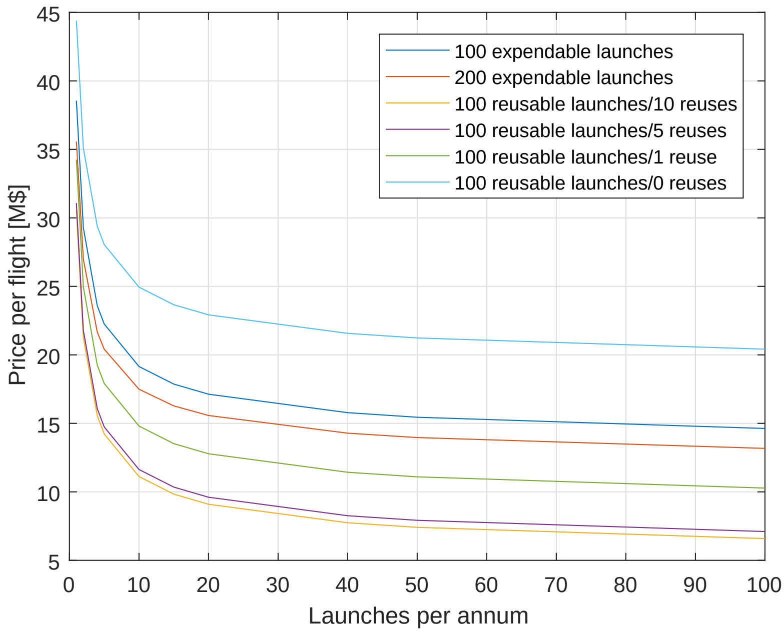

Figure 7.10: Price per flight as a function of number of launches per annum for expendable version of the optimal reusable system.

Important conclusions can be made from the results in Figure 7.10. First, as expected, if a reusable systems is flown as an expendable system with no reuses of the first stage, the price per flight of the former is always higher than the latter. However, as soon as the first stage is reused once, there is an advantage in price per flight for the reusable system, launch rates equal. In fact, when analyzing the percent decrease in price per flight when compared to the 100 expendable launches as seen in Figure 7.11, the target of 30% reduction is met after only 2 and 3 launches per annum for the 10 and 5 first stage reuses, respectively. For only one first stage reuse, this target reduction only occurs for an ambitious 100 launches per annum. Nonetheless, this analysis verifies the claims made by SpaceX officials for the comparison of two similarly-configured launch vehicles. One important final remark is that the payload was still fixed at 500 kg. The reduced first stage inert mass and propellant needed would certainly increase the payload capacity, in turn reducing the price per kilogram to orbit.

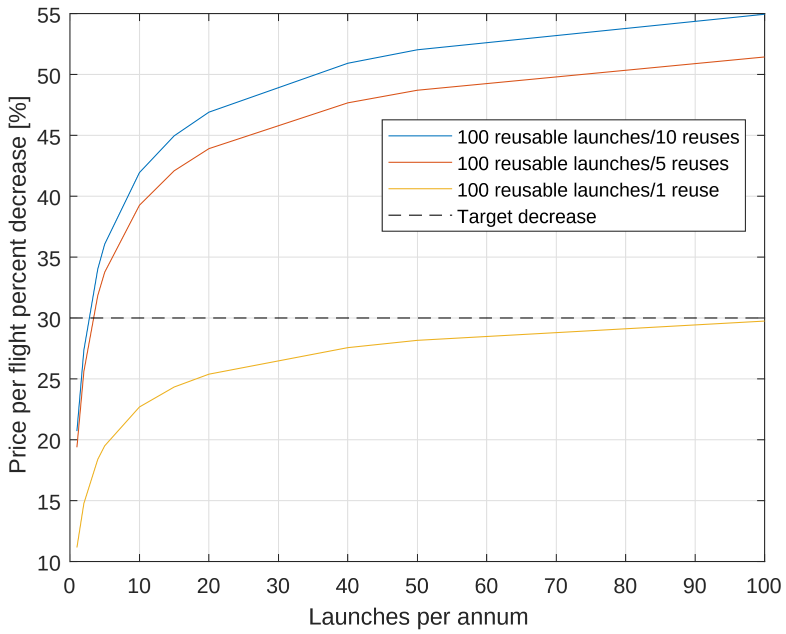

Figure 7.11: Price per flight reduction for reusable system compared to expendable version of same launch vehicle.

An investigation into the different cost drivers is presented in Section 7.4 to determine the point where a reusable launch vehicle may not be as cost-effective as an expendable system. Prior to this analysis, the effect of launch site and target orbit on the overall launch system and price per flight is investigated in the following section.

7.3. Effect of Launch Parameters on Optimal Design

A high-latitude launch to a Sun-synchronous orbit is a demanding requirement for a launch vehicle, as the velocity gained from the rotation of the Earth is less at a high latitude compared to an equatorial launch, and the launch vehicle must fly in the opposite direction of this rotation to get to its final orbit. As such, a return-to-launch-site RP1 9-engine reusable launch vehicle was optimized for different launch conditions to determine the effect of the launch vehicle itself and the price per flight.

Launching from Plesetsk as before, and Guiana Space Centre, the orbital launch site closest to the equator in the world, with a launch azimuth of 90° such that the launch vehicle's velocity is parallel to the rotation of the Earth, a population of 10 individuals were evolved over 6000 generations to determine the optimal price per launch of a return-to-launch-site reusable launch vehicle. In addition, the target orbital altitude was lowered to 500 km and the target inclination was unconstrained due to the launch azimuth constraint. The price per flight and price per kilogram to orbit of the nominal and new trajectories are presented in Table 7.16.

Table 7.16: Price per flight comparison for variation in launch site and target orbit of return-to-launch-site launch vehicle.

Propellant	**Configuration**	**Price per flight** [M$]	**Price per kilogram** [k$]
RP1	Nominal 9-engine RTLS	9.10	18.19
	Eastward 9-engine RTLS	8.24	16.49
	Kourou 9-engine RTLS	7.97	15.94

Table 7.16 shows that there is indeed a reduction in price per flight and price per kilogram for a launch to a different orbit and from Kourou compared to a launch from Plesetsk to Sun-synchronous orbit. To determine the reason for this, the key launch vehicle parameters are investigated, as shown in Table 7.17, with the expendable 9-engine design included for comparison purposes. It can be seen that the new RTLS launch vehicles, which meet all ascent and descent trajectory constraints, are smaller and lighter than their nominal, Plesetsk-launched, SSO orbit counterpart. In fact, an interesting remark can be made about the optimal

design of the new launch vehicles. As a result of the lowered target orbit and facilitated launch conditions, the new designs approach the configuration of an expendable launch vehicle. The required thrust of the first stage is reduced, in turn reducing the total engine mass, propellant mass and inert mass of the stage. This affects the second stage in the same manner. These results are in line with the results found by van Kesteren, where he showed that an increase in initial launch velocity resulted in a smaller, less expensive optimal launch vehicle [13]. Furthermore, a reduction in price per flight of 9.35% is seen when changing from an SSO Plesetsk launch to an eastward Plesetsk launch, compared to a 3.34% reduction when changing from an eastward Plesetsk launch to an eastward Kourou launch.

Table 7.17: Comparison of optimized return-to-launch-site configurations for two different launch sites and target orbits.

	RP1 9-engine			
Parameter	**Nominal RTLS**	**Eastward RTLS**	**Kourou RTLS**	**Nominal EXP**
Stage 1				
F_T [kN]	1397	881.0	797.3	494.4
M_{engine} [kg]	1792	1222	1130	795.1
M_p [kg]	51675	32509	29522	22399
L_{stage} [m]	22.14	18.48	19.32	19.50
M_{inert} [kg]	5349.5	3546.2	3226.5	2017.9
TFU [k$]	38183	29414	27735	21864
Stage 2				
F_T [kN]	74.56	55.86	47.51	26.43
M_{engine} [kg]	110.0	89.38	80.15	56.88
M_p [kg]	8785.5	7000.5	5320.2	3458.9
L_{stage} [m]	6.354	6.198	5.683	4.980
M_{inert} [kg]	585.7	439.6	366.2	243.7
TFU [k$]	3078.0	2520.8	2225.2	1658.6
Total				
$M_{fairing}$ [kg]	415.3	329.6	290.2	228.1
M_{inert} [kg]	7072.8	5002.4	4559.1	3146.1
GTOW [kg]	67753	44697	39574	29158
L [m]	34.28	29.81	29.82	28.78

The above results indicate that it is more important to design a launch vehicle for its target orbit rather than its intended launch site. The following section presents how sensitive the price per flight and price per kilogram are to cost design parameters.

7.4. Effect of Cost Parameters on Optimal Design

The nominal system has been designed for 20 launches per annum, with a total of 100 units produced and 10 reuses per first stage, with a learning curve factor of 0.90. This section presents the effects of deviations in these design parameters on the price per flight.

First, the number of first stage reuses was investigated. Holding the number of launches per annum fixed at 20, the number of reuses was varied when assuming a total of 50, 100 and 200 vehicles are launched. The results can be seen in Figure 7.12, where the price per flight for an RP1 1-engine expendable launch vehicle is plotted for comparison.

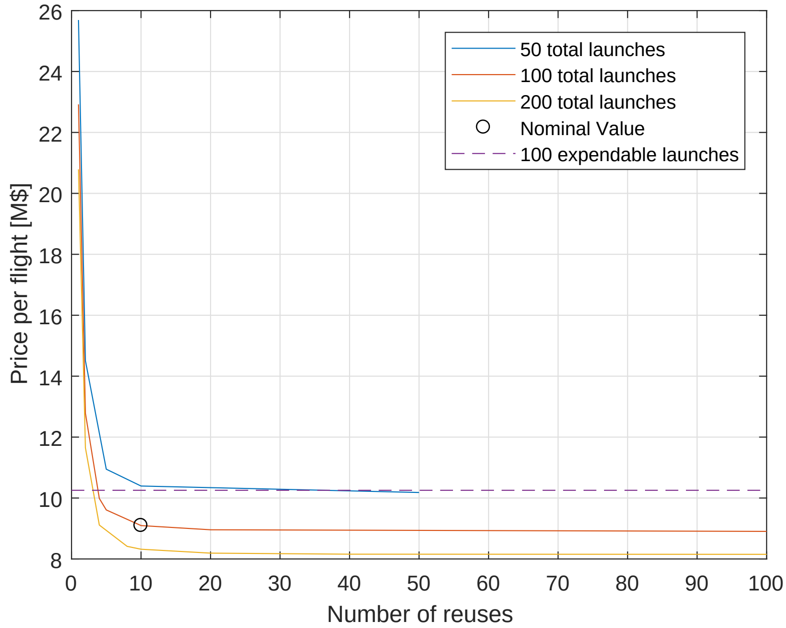

Figure 7.12: Price per flight as a function of number of first stage reuses.

Figure 7.12 shows that there is no significant reduction in price per flight when 50 total launches occur for a reusable launch vehicle. In fact, this situation is not entirely logical, as it would signify a launch program of only 2.5 years if there are 20 launches per annum. However, the reduction in price per flight is immediately seen if 100 total launches occur after only four first stage reuses, launch rates equal. Therefore, the added development, single-use manufacturing and operations costs are mitigated by the reusability if more than 100 second stages are launched, with first stages being reused more than four times. This is a feasible design, with SpaceX currently having reused a first stage three times. Interestingly, 4 reuses was also determined to be the decisive crossing point in a study conducted by Sowers from the United Launch Alliance [1, 113]. By simply estimating ratios of manufacturing costs between expendable and reusable launch vehicles, a reusable launch vehicle was deemed cost-effective after four reuses compared to an expendable counterpart. These results are confirmed if over 100 total launches occur, as seen in Figure 7.12.

Next, the sensitivity of the price per flight to launches per annum was investigated. The number of launches per annum is a variable that affects the price per launch of both expendable and reusable launch vehicles, thus it is important to compare these. The price per flight of the optimal return-to-launch-site vehicle was determined for both systems, where the number of reuses for the first stage was held constant at 10. The results are shown in Figure 7.13 for 50, 100 and 200 total launches. Figure 7.14 shows a close-up of the price per launch for up to 20 launches per annum, and yields interesting results. First, it can be seen that as the number of produced units increases, the number of launches per annum at which a reusable system becomes advantageous over an expendable system decreases. When 50 units are produced, over 13 launches per annum are necessary to see a benefit in a reusable system. However, when 200 units are produced, only 5 launches per annum are needed to see the benefits of a reusable system, and the benchmark of price per flight of $10.0M is met after 10 launches per annum. Therefore, it can be concluded that designing for a greater number of total launches is more cost-effective and allows for lower annual launch rates, giving the launch vehicle developers more room for error if the vehicle is designed for 20 launches per year but only achieves 10, which would not be the case for 50 total launches. From this specific study, the $10.0M price per flight benchmark is achieved if 11 launches per annum occur for 200 total launches, or if 16 launches per annum occur for 100 total launches.

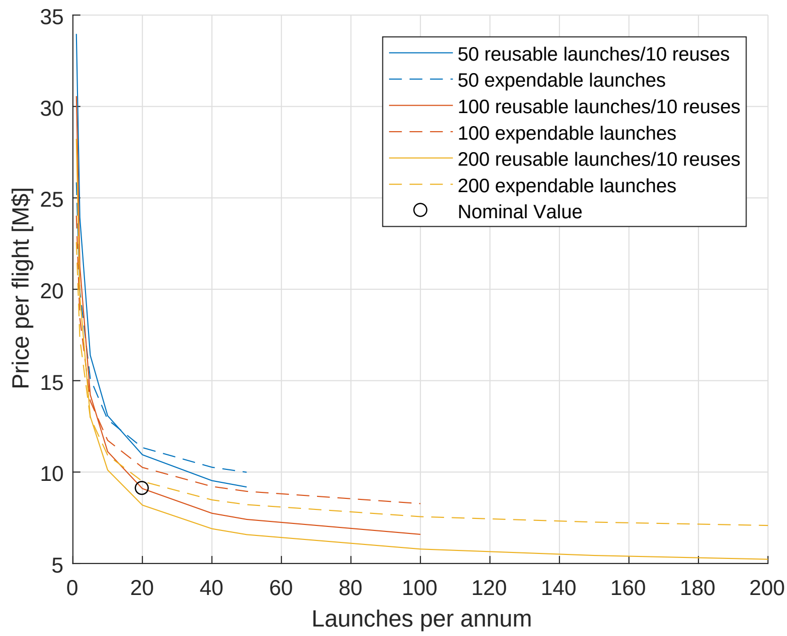

Figure 7.13: Price per flight as a function of launches per annum.

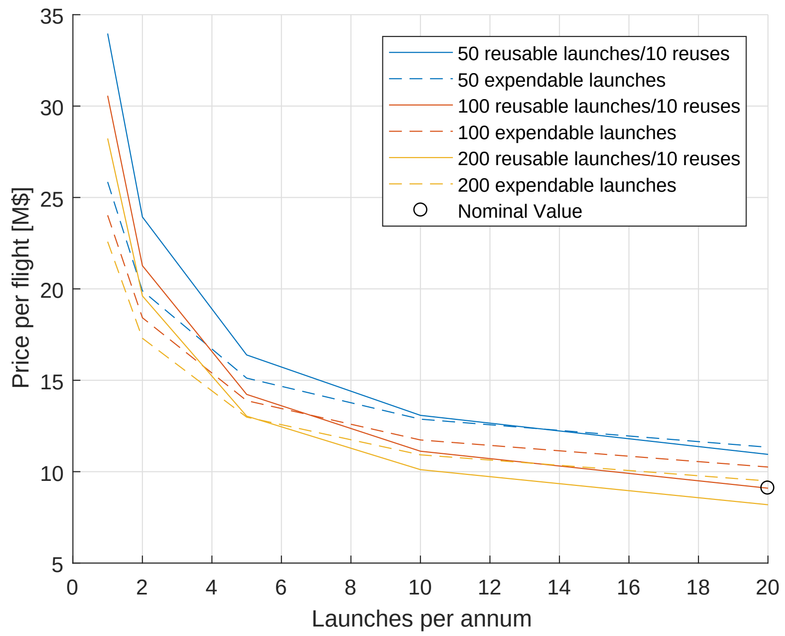

Figure 7.14: Price per flight as a function of number of launches per annum, with focus on 0 to 20 LpA.

Furthermore, the sensitivity to the learning curve production factor has been shown to have a significant effect of the price per launch of small launch vehicles [13]. Thus, its effects of the optimal configuration are also investigated. While in this study, a nominal value of 0.90 was chosen as the learning factor, this value has been shown to vary from 0.75 to 0.95. The effect of this variation on the nominal price per flight is shown in Figure 7.15. In this figure, it can be seen that an increase in the learning factor from 0.90 to 0.95 (5.56%) increases the price per flight by 10.0%, while a reduction in the learning factor from 0.90 to 0.85 decreases the price per flight by 7.91%. Properly estimating the learning curve production factor is thus essential to obtaining accurate price per flight estimates, yet, within the scope of this study, still shows that a reusable launch vehicle meets the target price per flight of $10.0M.

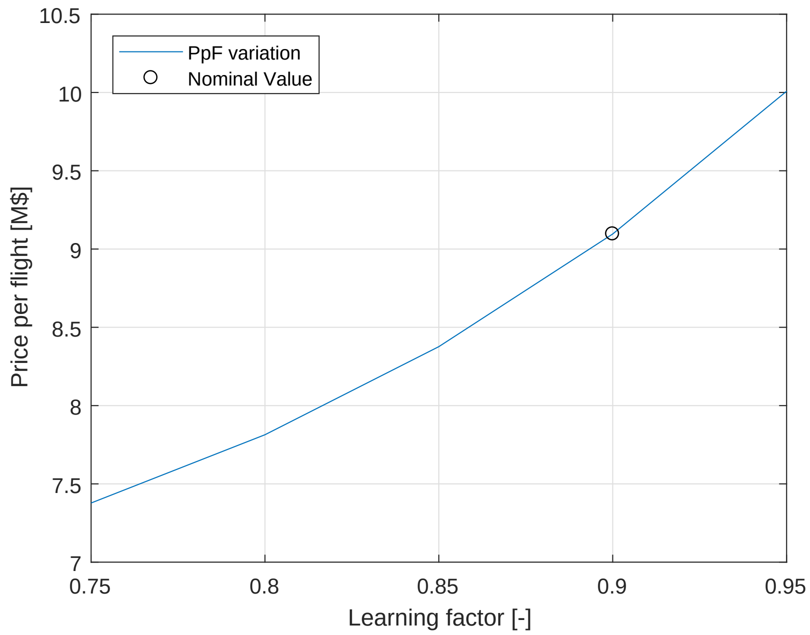

Figure 7.15: Price per flight as a function of learning curve factor.

Finally, the sensitivity of the price per flight to uncertainty in recovery and refurbishment costs is investigated. In this study, the former was estimated as a percentage of the total operations costs, while the latter was estimated as a percentage of the average manufacturing costs. The statement from Shotwell of the refurbishment costs being significantly less than half the cost of manufacturing a new first stage signifies that the nominal 50% value used in this study is an upper limit [105]. Koelle estimates this value to be near 30% of the average manufacturing cost [100], while Hermann varies this value between 1% and 20% of TFU costs [104]. It can be seen that the variations in this value do not have a large effect on the price per flight, where a reduction in refurbishment cost from 50% to an ideal 0% reduces the price per flight from $9.10M to $8.55M, a reduction in 6.02%.

However, a variation in recovery costs has a much more significant impact on the price per flight. Assumed to be an ideal 0% of operations cost for the return-to-launch-site design, changing the value to 50% of operations costs increases the price per flight to $12.39M, an increase of 36.2%. Wertz sets an upper limit of recovery costs to 20% and a lower limit to 10%, which implies an increase in 7.24% and 14.5% in price per flight, respectively [103]. These costs can also be calculated using a bottom-up approach, where each element needed in the recovery of a stage can be costed individually, as done by Stappert *et al.* [102], discussed in Section 5.1.4. The recovery costs using this method for a return-to-launch-site launch vehicle is estimated to be $243.73k, which is a mere 4.00% of the operations costs. This implies a price per flight increase to $9.34M, or by 2.67%, which is on the same order of magnitude as the refurbishment costs, still meeting the $10.0M benchmark set in Chapter 2.

As the realistic estimates of the refurbishment and recovery costs affect the price per flight by less than 10%, it can be concluded that the nominal values presented for price per flight of a return-to-launch-site launch vehicle are accurate and present an advantage compared to an expendable counterpart. Furthermore, as long as the recovery costs remain lower than 20% of the operations costs, the optimal configuration will have a price per kilogram to orbit of less than $20.00k, as desired. The variations on price per flight as a function of varying the refurbishment and recovery factors is plotted in Figure 7.16.

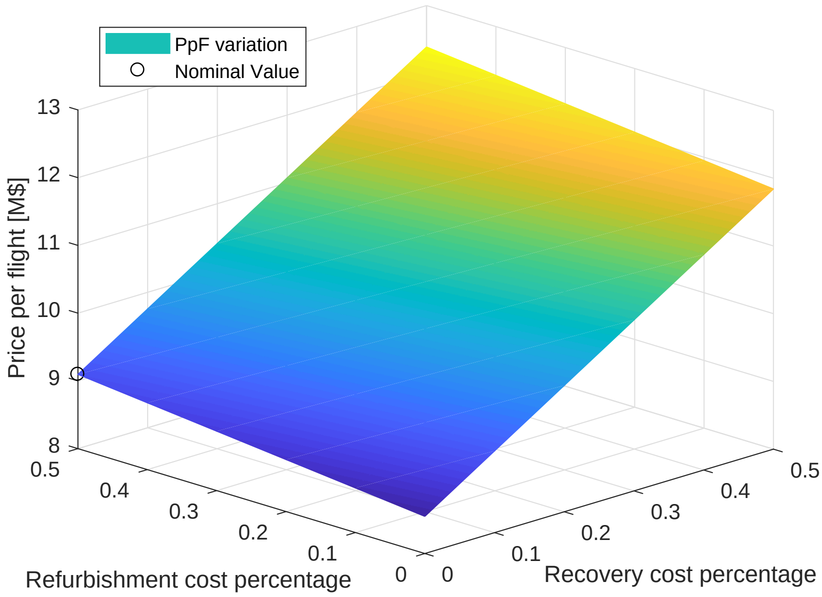

Figure 7.16: Price per flight as a function of number of recovery and refurbishment costs.

A final remark should be made about the price per flight's sensitivity on recovery costs. As mentioned, the downrange landing launch vehicle was assumed to have a refurbishment cost equal to 50% of the average manufacturing costs and a recovery cost equal to 50% of the operations costs. Above, it was deemed that 50% in recovery costs is an overestimation. The bottom-up approach conducted by Stappert *et al.* suggests the recovery costs of a DRL reusable launch vehicle totals $667.75k, which represents 11.48% of the operations cost of the optimal RP1-propelled 9-engine DRL launch vehicle. This yields a reduction in price per flight from $11.41M to $9.00M, a reduction in 21.2% and making this reuse method more cost-effective than a return-to-launch-site launch vehicle, and presenting an appealing $17.98k per kilogram to orbit. This price per launch and price per kilogram to orbit are now lower than the benchmark set in Chapter 2. With additional constraints placed on the trajectory such that this launch vehicle can meet the ascent and descent trajectory requirements, the downrange landing small, reusable launch vehicle presents more potential for cost benefits.

From this section, it can be concluded that at least 100 units should be launched over the life cycle of the launch vehicle, with more total launches further decreasing the price per flight, launch rates equal. To see the price per flight benefits compared to an optimal expendable counterpart, the reusable system should aim for at least 5 launches per annum, with more annual launches presenting further benefits. Careful consideration should be taken when designing for a certain learning factor, as this has an effect on price per flight by up to 10%. Nonetheless, the price per flight values still present a significant advantage for higher learning factors compared to the $29.90k per kilogram average reported price from Chapter 2. The uncertainty related to recovery and refurbishment costs should be reduced by a more in-depth bottom-up analysis of these expected costs, and by performing these activities for existing launch vehicles. Nonetheless, the optimal return-to-launch-site design offers a lower price per kilogram to orbit compared to the baseline $29.90k and optimized expendable counterparts, with the downrange landing designs presenting further advantages if additional or looser constraints are placed on the trajectory.

The following chapter presents the sensitivity of the design to uncertainty in model parameters.

8
Sensitivity Analysis

Although the respective models used to design and optimize the small, reusable launch vehicle have been verified and validated at each important step, it is important to determine the sensitivity of the optimal design to parameters that have uncertainty. This chapter deals with uncertainties in both launch vehicle parameters and cost model parameters for the return-to-launch-site RP1-propelled 9-engine design launching from Plesetsk to Sun-synchronous orbit. The effect of varying these parameters on the price per flight to orbit is investigated in two different ways, namely a one-at-a-time approach and a Monte Carlo analysis. Both of these methods have been used in launch vehicle sensitivity analyses in the past [13, 23].

8.1. One-At-A-Time Approach

The one-at-a-time sensitivity (OAT) analysis approach is a commonly used technique that allows a single parameter from a design to vary while the remaining variables are held constant [13]. As done by Castellini and van Kesteren, the parameters in Chapter 3 and Chapter 5 with an associated uncertainty are varied by the maximum potential error in these values [13, 23]. This section is separated into two subsections, where the effect of uncertainty in launch vehicle parameters is first evaluated before the uncertainty in cost model parameters is investigated.

8.1.1. Launch Vehicle Parameters Sensitivity

From the physical launch vehicle model, the uncertainty in vacuum thrust, specific impulse, the percentage of unused propellant K_u, the ullage volume, stage length and inert mass, and reusable structures inert mass are investigated. When varying these values for their maximum absolute error or maximum uncertainty, the effects on GTOW and price per flight are seen in Table 8.1 and Table 8.2 for positive and negative variations, respectively. An additional column is added to show how the variation in the parameter affects the price per flight. In other words, this value represents the percent variation in the parameter needed to achieve a 1% variation in price per flight. It is important to note that the uncertainty in these values are applied to both stages simultaneously.

Table 8.1: Results of the one-at-a-time approach for the optimal reuse launch vehicle when increasing the values of important physical parameters.

Parameter	**Variation**	**GTOW**		**PpF**		$\Delta_{par}/\Delta_{PpF}$
	[-]	[kg]	[%]	[M$]	[%]	[%/%]
Vacuum Thrust	+2.28%	67845.7	+0.14	9.12	+0.22	10.4
Vacuum Specific Impulse	+0.960%	67753.3	+0.00	9.10	+0.00	-
K_u	+50.0%	67857.4	+0.15	9.10	+0.024	2080
Ullage Volume	+10.0%	67761.8	+0.013	9.10	+0.034	294
Stage Length	+18.7%	67806.4	+0.078	9.13	+0.37	50.5
Stage Inert Mass	+20.26%	68955.8	+1.77	9.43	+3.67	5.52
Reuse Structure Mass	+10.0%	67802.0	+0.072	9.10	+0.051	196

Table 8.2: Results of the one-at-a-time approach for the optimal reuse launch vehicle when decreasing the values of important physical parameters.

Parameter	**Variation**	**GTOW**		**PpF**		$\Delta_{par}/\Delta_{PpF}$
	[-]	[kg]	[%]	[M$]	[%]	[%/%]
Vacuum Thrust	-2.28%	67661.0	-0.14	9.08	-0.22	10.4
Vacuum Specific Impulse	-0.960%	67753.3	-0.00	9.10	-0.00	-
K_u	-50.0%	67655.5	-0.14	9.09	-0.022	2270
Ullage Volume	-10.0%	67744.9	-0.012	9.09	-0.034	294
Stage Length	-18.7%	67700.3	-0.078	9.06	-0.37	50.5
Stage Inert Mass 1	-20.26%	66550.9	-1.77	8.75	-3.82	5.30
Reuse Structure Mass	-10.0%	67704.7	-0.072	9.09	-0.052	192

The results in Table 8.1 and Table 8.2 show that the optimal design is highly robust to changes in launch vehicle parameters. In fact, a variation in stage length by almost 20% will not change the GTOW or price per flight by more than 0.5%. The optimal design is most sensitive to uncertainty in the stage inert mass, yet variations of more than 20% affect the GTOW by less than 2% and the price per flight by less than 4%. The GTOW trends are comparable to those seen in van Kesteren's study [13]. As such, it can be concluded that the optimal design is not greatly affected by uncertainties in parameters that affect its performance and price per flight, but that most caution should be placed on uncertainty in the stage inert mass when refining the design, as the price per flight is most sensitive to variations in this value.

8.1.2. Cost Parameters Sensitivity

As presented in Table 5.3 of Chapter 5, each cost estimation relationship has an associated uncertainty, namely in the form of a standard error and relative standard error. As per the model of Drenthe [39], the errors in the CERs are not correlated and random, thus Equation 8.1 and Equation 8.2 can be used to determine the upper and lower bounds on the TFU cost estimates, respectively, where C in these equations is the nominal TFU cost.

$$C_{upp} = C \cdot e^{SE_{log}} \tag{8.1}$$

$$C_{low} = C / e^{SE_{log}} \tag{8.2}$$

Using the equations presented above, the upper and lower bounds on each element's TFU cost can be established, before summing these to get the upper and lower bounds on each stage's TFU cost. In Table 7.3 of Chapter 7, it was determined that the engine totals over 50% of the TFU cost for the optimal design. Therefore, instead of evaluating the uncertainty due to each CER individually, only the engine CER uncertainty is subject to a one-at-a-time analysis, before the uncertainty for all elements are taken into account all-at-once. The percentage change due to the uncertainty of the relationships is presented in Table 8.3, where the four stage rows show the bounds on the stage TFU cost, while the last row shows the bounds on the total launch vehicle TFU cost. From this analysis, it can be seen that the uncertainty in the engine cost estimation relationships can lower the stage TFU cost by up to 17.1% and raise it by up to 24.5%. When taking all of the uncertainties into account, the total launch vehicle TFU cost can vary from -23.9% to 32.8% of its nominal value. This wide range is similar to the results obtained by Drenthe when estimating the bounds on a liquid methane concept launch vehicle, which varied from -22.0% to 28.2% of the nominal value [39].

Table 8.3: Effect of uncertainty in cost estimation relationships on stage and launch vehicle TFU cost.

	C_{low}	C_{upp}
Stage 1 Engines	-17.1%	24.5%
Stage 2 Engines	-15.0%	21.2%
Stage 1	-23.9%	32.7%
Stage 2	-24.6%	33.4%
Total	-23.9%	32.8%

Important conclusions can be made about the uncertainty of the TFU cost estimation relationships. The method employed to estimate the TFU cost and their respective uncertainties is standard industry practice and is widely applied in many commercial cost engineering tools [39, 98]. Due to the limited public data, however, uncertainties in cost estimates are generally high, as seen in Table 8.3. This means that for future refinement of the method, caution must be taken when choosing the data used to develop the cost estimation relationships, especially for the engines as these are a main driver of total cost. Nonetheless, as confidentiality of data was not an issue during development, the model is as accurate as the data input by the developer [39].

Next, the development, manufacturing and operations cost factors in the cost model all have some inherent uncertainty associated to them as they are not determined analytically but empirically. Therefore, it is imperative to determine their effects on the cost model. The results of varying the cost factors on the price per flight are shown in Table 8.4.

Table 8.4: Results of the one-at-a-time approach for the optimal reuse launch vehicle when varying important cost model parameters.

Parameter	**Value**	**Variation**		**ΔPpF**		$\Delta_{par}/\Delta_{PpF}$
	[-]	[-]	[%]	[k$]	[%]	[%/%]
f_1	1.2	± 0.1	± 8.33	80.91	0.890	9.36
f_3	1.0	± 0.1	± 10.0	97.10	1.07	9.35
$f_{10,dev}$	0.8	± 0.05	± 6.25	60.69	0.667	93.7
$f_{10,man}$	0.8	± 0.05	± 6.25	96.25	1.06	5.90
$f_{11,man}$	0.55	± 0.05	± 9.09	140.0	1.54	5.90
f_c	0.7	+ 0.3	+ 42.9	321.2	3.53	12.2

The cost parameters in Table 8.4 have a linear effect on the price per flight of the small, reusable launch vehicle. These were varied within their uncertainty range and are shown to have a minimal effect on the price per flight, but highest sensitivity is observed from $f_{10,man}$ and $f_{11,man}$. Therefore, it is important to reduce the uncertainty in the manufacturing cost factors as much as possible when refining the design. From this analysis, it can be concluded that the sensitivity in price per flight to variations in these cost factors is smaller than the variation of the parameters themselves, again agreeing with the trends seen in van Kesteren's study [13]. Even with the large uncertainty associated with f_c, the launch vehicle processing type cost factor, the price per flight of the optimized design is only increased by 3.53% if the launch vehicle were to be vertically assembled on the launch pad, which still keeps the price per flight below the $10.0M benchmark.

8.2. Monte Carlo Analysis

In this section, a Monte Carlo analysis is conducted in order to determine the effect of varying multiple cost parameters at once, which allows the model to account for uncertainty in the various parameters simultaneously. This approach leads to realistic variations from the nominal case due to the combination of uncertainties, accounting for interactions [13].

As the physical launch vehicle parameters were shown to have a minimal effect on the GTOW and price per flight of the reusable launch vehicle in Section 8.1.1, these were not subject to a Monte Carlo analysis. The effect of randomly generating cost factors within the range presented in Table 8.4 on the price per flight of the optimal return-to-launch-site launch vehicle was investigated in the Monte Carlo analysis, keeping the remaining nominal values for number of units (100), number of reuses (10) and launches per annum (20). The price per flight for each iteration is presented in Figure 8.1. The orange line in this figure is the price per flight when the mean value of the uncertainty range is used for each variable, while the yellow line is the nominal price per flight. The only difference between the orange and yellow line is a change in f_c from 0.775 to 0.7.

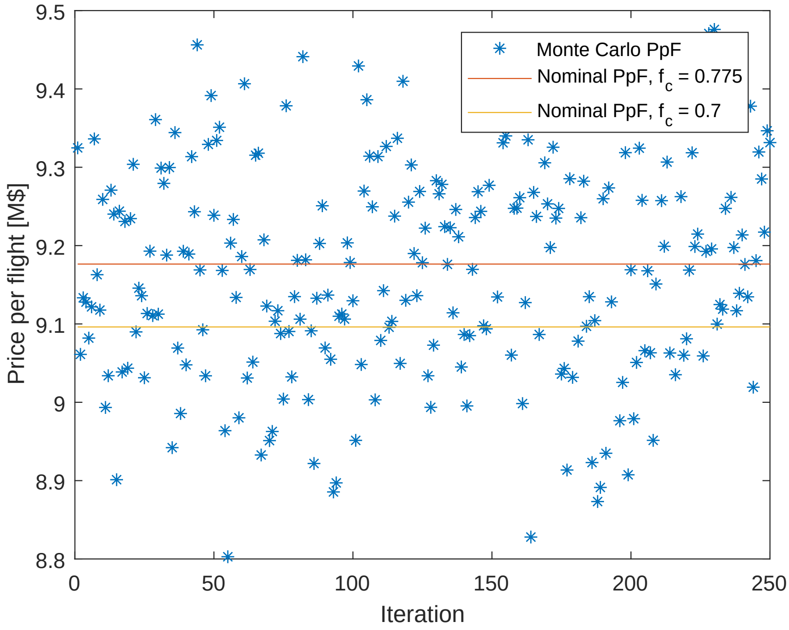

Figure 8.1: Price per flight for each Monte Carlo iteration.

Figure 8.1 shows a seemingly random spread of price per flight over 250 Monte Carlo iterations. To determine if this spread is indeed random, a normal probability density function of the difference in Monte Carlo price per flight and the nominal price per flight using an f_c of 0.775 is plotted in Figure 8.2. The symmetrical distribution centred around 0 signifies that the spread is random and that, over 250 Monte Carlo iterations, the price per flight is expected to average the nominal price per flight.

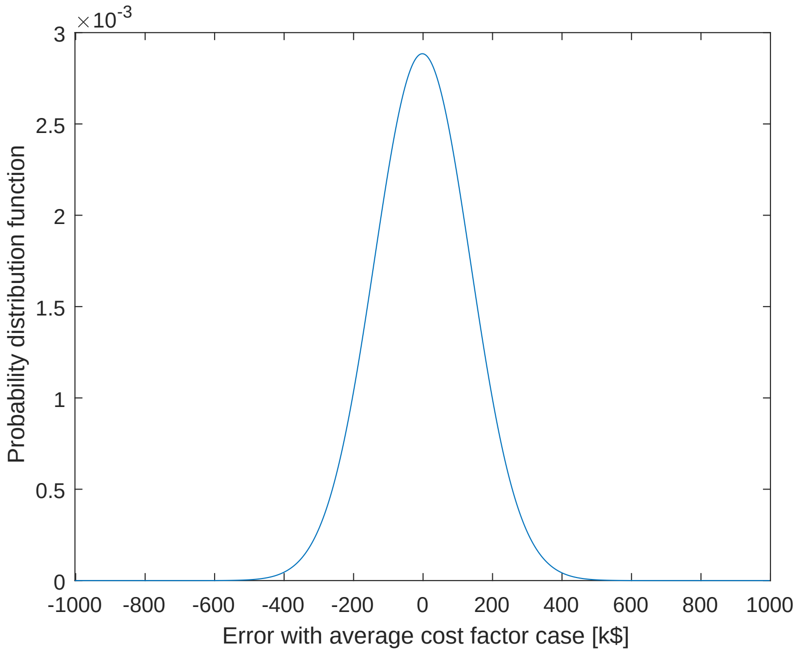

Figure 8.2: Probability distribution function of difference between Monte Carlo iterations and cost model using average cost factors.

The worst-case Monte Carlo run yielded a price per flight of $9.48M, while the best-case run yielded a price per flight of $8.80M, which represent a 4.18% increase and 3.22% decrease from the nominal, respectively. This is well within the requirements set by the tool for price per flight, and serves to validate the results.

These results also indicate that, even in the worst case, the optimal design meets the \$10.0M price per flight established in Chapter 2, thus one can confidently state that under the assumptions presented in this work, the system can definitively offer a 30% reduction in price per flight when compared to the reported average value.

9 Conclusions

This chapter presents the conclusions surrounding the research question and the work done during this thesis.

An investigation into combining reusability within a small launch vehicle presented a promising solution for a cost-effective way of bringing small satellites to orbit [1]. In this study, these systems were designed and optimized for cost to determine the cost benefit of a small, reusable launch vehicle compared to an expendable counterpart and to what currently exists on the market. The following research questions was addressed in this research.

Is a small, reusable launch vehicle a cost-effective solution to bringing small satellites into low-Earth orbit, and if so, under what conditions?

From the models developed and the analysis conducted in this research, it can be concluded that indeed, a small, reusable launch vehicle is a cost-effective solution to bringing small satellites into low-Earth orbit. This conclusion is expanded upon in the following paragraphs.

A small, vertically landing return-to-launch-site launch vehicle is a definitive improvement on an expendable counterpart when launching a 500 kg payload into low-Earth orbit. An optimized configuration of this launch vehicle yields a price per launch of $9.10M (2018), which totals $18.19k (2018) per kilogram to orbit. This is a 23.5% improvement compared to an optimized expendable vehicle with a similar engine configuration, which yields a price per launch of $11.90M (2018) and a price per kilogram of $23.78k (2018). Referring back to Shotwell's statement of a reduction in launch costs of "about 30%" for reusable launch vehicles, this study confirms that this is achievable for a total of 200 launches with 10 first stage reuses and 20 launches per annum, while the 50% launch cost reduction determined by Snijders for 10 first stage reuses and 10 launches per annum is optimistic under the assumptions made in this work. The best-case expendable design yields a price per launch of $10.25M (2018), or $20.51k (2018) per kilogram, which is still an 11.3% increase compared to the nominal reusable launch vehicle. Furthermore, the optimal solution is a 39.2% improvement on the average reported $29.90k (2018) per kilogram, further demonstrating its potential on the current market of small launch vehicles. Finally, assuming the optimal reusable system is flown as an expendable launch vehicle as with the Falcon 9, reductions in price per flight are seen after one first stage reuse, while the target reduction of 30% is seen after three launches per annum for five first stage reuses.

From the comparison of two-stage and three-stage launch vehicles, it can be concluded that two-stage configurations are more cost-effective solutions compared to three-stage designs. The additional cost associated with the third stage outweighs the reduction in first and second stage costs. The first stage costs of all optimal launch vehicles totals up to ten times the upper stage costs, thus a significant reduction in these is needed for three-stage designs to become more cost-effective than two-stage designs.

From the analysis of a 100 kg payload, it can be concluded that a small, reusable launch vehicle in this payload class is not a cost-effective solution to bringing these satellites into orbit under the assumptions made in this work. The reduction in optimal launch vehicle mass does not balance the fivefold reduction in payload mass when considering price per kilogram to orbit.

Although the price per flight of LH2-propelled reusable launch vehicles is slightly reduced compared to similarly configured RP1-propelled alternatives, the thrust-to-mass ratio of LH2-propelled launch vehicles is higher than the RP1-propelled alternative. This results in lower reuse burn times for the LH2-propelled launch vehicle, and in turn increases the velocity and dynamic pressure encountered by these stages. Thus, LH2-propelled launch vehicles are not feasible reusable designs within the scope of this study.

Building from the conclusion above, the analysis of return-to-launch-site and downrange landing reusability techniques revealed that the dynamic pressure re-entry constraint is a driving constraint to establishing feasible designs within the requirements set by the tool. To mitigate this constraint, the reusable trajectory optimizer should be updated to reduce the re-entry burn cut-off velocity, as shown in Section 7.2.2.

The choice of launch site and target orbit plays a significant role in the optimal design of a small, reusable launch vehicle. The nominal orbit of choice in this study was determined to be a resource-intensive launch, as a choice of lower target orbit with an eastward launch resulted in a 9.35% reduction in price per flight, with an additional reduction of 3.34% for a near-equatorial launch. It is concluded that it is more important to design a reusable launch vehicle for its target orbit than for its intended launch site. Nonetheless, a small, reusable launch vehicle is still a cost-effective solution as all target orbit and launch sites considered revealed a price per flight below $10.0M (2018).

The price per flight of the optimal launch vehicle is most sensitive to the total number of launches, the number of first stage reuses and the number of launches per annum. From the analysis conducted in this research, it can be concluded that at least 100 total units of a reusable launch vehicle should be launched. Over ten launches per annum and ten first stage reuses is determined to be the minimum target for significant cost benefits. Furthermore, the price per flight is significantly affected by the uncertainty in recovery and refurbishments costs, but the estimates used in this research are conservative compared to literature and show that even within the bounds of uncertainty, a small, reusable launch vehicle is cost-effective compared to an expendable counterpart.

The price per flight of the optimal launch vehicle design proved to be insignificantly sensitive (<5%) to launch vehicle and cost model parameters using a one-at-a-time approach and a Monte Carlo analysis.

The Multidisciplinary Design Analysis and Optimization tool meets all of the requirements set in Chapter 2, with the status of each requirement presented in Table 9.1. The only requirements that were not entirely successful were the stage inert mass and length predictions, however, these are due to ambiguities in reported values as mentioned in Section 3.5. Through extensive verification and validation at each step of the development process, it can be concluded that the optimal small, reusable launch vehicle is a feasible design within these requirements, achieving a price per flight below $10.0M (2018) for a 500 kg payload.

Table 9.1: Status of requirements set for the models and the tool developed in this work.

ID	Requirement	Status
REQ-LV-001	The tool shall be able to model the thrust of solid and liquid stages to within 10% accuracy.	Success
REQ-LV-002	The tool shall be able to model the specific impulse of solid and liquid stages to within 10% accuracy.	Success
REQ-LV-003	The tool shall be able to model the propellant mass of solid and liquid stages to within 10% accuracy.	Success
REQ-LV-004	The tool shall be able to model the inert mass of launch vehicle stages to within 10% accuracy.	Partial
REQ-LV-005	The tool shall be able to model the length of launch vehicle stages to within 10% accuracy.	Partial
REQ-LV-006	The tool shall be able to model the GTOW of launch vehicles to within 10% accuracy.	Success
REQ-TR-001	The tool shall be able to simulate the launch vehicle to within 3% of the desired altitude.	Success
REQ-TR-002	The tool shall be able to simulate the launch vehicle to an eccentricity less than 0.1.	Success
REQ-TR-003	The tool shall be able to simulate the launch vehicle to within 1° of the desired inclination	Success
REQ-TR-004	The tool shall be able to simulate the reuse landing altitude to within 1m of the desired value.	Success
REQ-TR-005	The tool shall be able to simulate the reuse landing velocity to less than 5m/s.	Success
REQ-TR-006	The tool shall be able to simulate the reuse desired downrange distance to within 5km.	Success
REQ-CT-001	The tool shall be able to model the price per flight of solid and liquid launch vehicles to within 20% accuracy.	Success
REQ-TL-001	The tool shall be developed in the Tudat environment, coded in C++.	Success
REQ-TL-002	The tool shall model and optimize return-to-launch-site and downrange landing reusable launch vehicles, as well as expendable launch vehicles to the accuracies shown in Table 2.2.	Success
REQ-TL-003	The tool shall be able to model a reusable launch vehicle in less than 0.5 seconds.	Success
REQ-TL-004	The tool shall be able to simulate the ascent and descent of a reusable launch vehicle in less than 1 second.	Success
REQ-TL-005	The tool shall be able to output the physical launch vehicle parameters necessary for analysis and comparison purposes.	Success
REQ-TL-006	The tool shall be able to output the full simulation time history of the ascent and descent trajectories in a text file.	Success
REG-TL-007	The tool shall output the optimal objective function and optimal design parameters in a text file.	Success
REQ-TL-008	The inputs of the tool shall be read from user-modifiable text files.	Success

10
Recommendations

In this section, recommendations regarding potential improvements to the models and to the tool are given, followed by general recommendations for future research into small, reusable launch vehicles.

10.1. Model Recommendations

Although validated at each step of development, certain recommendations can be made about improvements to the models that have been developed. These are listed in this section.

- Reliability has not been studied in this research. In future iterations, accounting for reliability is recommended to determine how this affects the design and cost of the launch vehicle. For the latter, it can be implemented in the cost model by accounting for additional costs necessary for re-ignition of the liquid engines, reuse of hardware, and recovery and reuse operations as a fraction compared to an expendable design as suggested by Pepermans [10].
- The re-entry trajectory model was the deciding factor when determining the feasibility of a small, reusable launch vehicle. Additional constraints should be placed on the first stage cut-off altitude, velocity and downrange distance, or on the maximum dynamic pressure encountered by the launch vehicle during ascent, in order to achieve a larger set of feasible designs. It is expected that, as with the validation performed with the Falcon 9 trajectory, a lower and slower first-stage cut-off will result in a larger set of feasible designs. Furthermore, allowing the engines to throttle deeper than 50% of their maximum thrust and variable throttling during flight may also achieve similar results.
- As seen with previous Falcon 9 missions [93], the addition of a boostback burn for downrange landing vehicles, not to alter the direction of flight as with the return-to-launch-site method but to immediately reduce the stage velocity, would result in a lower maximum dynamic pressure as well. This should be investigated in future models.
- The Multidisciplinary Design Analysis and Optimization environment developed from this studies decouples the optimal launch vehicle and ascent trajectory from the reuse trajectory. In future iterations, it is recommended to couple these in order to obtain an optimal solution that can also meet the re-entry trajectory constraints.
- As the Missile DATCOM database does not currently allow for the inclusion of grid fins, it would be beneficial to add their contribution to the aerodynamic forces in future models, perhaps as an added drag coefficient sub-module. Their inclusion will likely result in re-entry and landing burns closer to those of Falcon 9 missions, as they are highly effective for reducing velocity at supersonic speeds and for control at subsonic speeds [114]. Furthermore, they will reduce the dynamic pressure encountered by the first stage upon re-entry, potentially allowing a larger set of feasible designs. The aerodynamic effects of the stowed landing legs should also be investigated in future iterations.
- Further studying the geometry and mass effects of the reusable hardware including landing legs, grid fins and cold gas thrusters will lead to more accurate mass and aerodynamic estimations of the reusable launch vehicle, which in turn will lead to better estimations on the re-entry conditions.
- The addition of wind into the atmospheric and aerodynamic models will especially affect the behaviour of the first stage upon re-entry and landing. Wind should thus be taken into consideration in future iterations of the model to better represent realistic missions and to derive attitude control requirements.

- Following from the above recommendation, a full aerodynamic and structural study of the reusable first stage with its surrounding environment is highly recommended before constructing such a stage to obtain critical insight into the aerothermal loads encountered during flight.
- The tool developed in this study could not find a cost-effective solution for 100 kg payloads. However, as many small launch vehicle developers are aiming to put payloads of this mass into orbit, it would be interesting to determine the effects of innovative manufacturing techniques on the total mass and price per flight of a small, reusable launch vehicle to establish the feasibility of these designs. For example, the engine mass of the Merlin 1D is overestimated by 70% in Section 3.5, and these were shown to be a major cost driver. Thus, the potential for further reducing the price per flight does exist and should be investigated, as small launch vehicle developers mentioned in the Introduction are advertising even lower launch prices than the optimal design established in this study.
- Using the same liquid engine on the upper stage as the first stage could potentially reduce development and manufacturing costs, as well as the total price per flight. Modelling the full reusable launch vehicle with one engine could results in an even more cost-effective solution as shown by the high engine costs and the reduction in price per flight due to the learning factor.
- Although the modelled descent trajectory is verified and validated, further investigation into the actual attitude control of the first stage, as well as using a varied boostback burn pitch or re-entry angles of attack could lead to results that are more in line with current Falcon 9 missions, and can provide better estimates about the needed attitude control systems needed within the optimal first stage designs.

10.2. Tool Recommendations

The recommendations associated with the tool that has been developed are given in this section.

- The tool developed in this work has been modified to be compatible with the new Tudat environment. It is recommended to expand upon this tool to account for additional reusability techniques such as mid-air retrieval or with aerodynamic decelerators.
- Making Tudat compatible with a numerical programming environment such as MATLAB would make the interface much more user-friendly and would allow for quicker data visualization and analysis, a task that is time consuming in the current Tudat environment.
- The sensitivity analysis is currently a manual operation, where the sensitivity to each parameter must be input into the code individually. Making the tool more versatile to changes in various parameters would make such analyses easier and less time-consuming.

10.3. General Recommendations

Additional recommendations for future studies are given in this section.

- Any student interested in further developing the models in the Tudat environment is strongly encouraged to take *AE4868 - Numerical Astrodynamics* and *AE4866 - Propagation and Optimization in Astrodynamics* offered by TU Delft to obtain a necessary foundation in C++ and familiarity with the programming environment.
- Further insight into reusable launch vehicle recovery and refurbishment costs are only going to be made available with the development and testing of these systems. Sub-scale models or prototypes should be developed by private companies and educational institutions alike to be able to better quantify these highly ambiguous cost drivers.
- Small satellite launch service provider Rocket Lab has recently announced the development of a reusable first stage using mid-air retrieval techniques [115]. The addition of this method, as well as other reusability techniques within the tool could provide further insight into potential cost reduction of small launch vehicles.

Bibliography

[1] S. Contant, “Small, Reusable Launch Vehicles: A Literature Study on the Feasibility of Small Launch Vehicles with Reusable First Stages.” Unpublished. Available upon request, 2019.

[2] N. Crisp, K. Smith, and P. Hollingsworth, “Small satellite launch to LEO: a review of current and future launch systems,” *Transactions of the Japan Society for Aeronautical and Space Sciences, Aerospace Technology Japan*, vol. 12, no. ISTS29, pp. 39–47, 2014.

[3] C. Niederstrasser, “Small Launch Vehicles – A 2018 State of the Industry Survey,” in *Proceedings of the AIAA/USU Conference on Small Satellites*, 2018.

[4] M. Baylor, “With Block 5, SpaceX to increase launch cadence and lower prices,” May 2018. Available: `https://www.nasaspaceflight.com/2018/05/block-5-spacex-increase-launch-cadence-lower-prices/` (Accessed on 07/12/2018).

[5] L. A. Davis, “First stage recovery,” *Engineering*, vol. 2, no. 2, pp. 152–153, 2016.

[6] N. Bray, “Space Shuttle and International Space Station,” 2017. Available: `https://www.nasa.gov/centers/kennedy/about/information/shuttle_faq.html#10` (Accessed on 09/01/2019).

[7] N. Chetram, “Why did the Space Shuttle cost so much? Wasn’t it a reusable vehicle?,” 2017. Available: `https://www.quora.com/Why-did-the-Space-Shuttle-cost-so-much-Wasnt-it-a-reusable-vehicle` (Accessed on 09/01/2019).

[8] M. Sheetz, “Elon Musk says the new SpaceX Falcon Heavy rocket crushes its competition on cost,” February 2018. Available: `https://www.cnbc.com/2018/02/12/elon-musk-spacex-falcon-heavy-costs-150-million-at-most.html` (Accessed on 09/01/2019).

[9] L. Grush, “SpaceX successfully landed its Falcon 9 rocket after launching it to space,” December 2015. Available: `https://www.theverge.com/2015/12/21/10640306/spacex-elon-musk-rocket-landing-success` (Accessed on 07/12/2018).

[10] L. Pepermans, “Reusable Rocket Upper Stage: Development of a Multidisciplinary Design Optimization Tool to Determine the Feasibility of Upper Stage Reusability,” Master’s thesis, Delft University of Technology, 2019.

[11] M. Snijders, “Cost effectiveness of the first stage recovery of a small satellite launcher,” Master’s thesis, Delft University of Technology, 2017.

[12] J. M. Vandamme, “Assisted-launch performance analysis: Using trajectory and vehicle optimization,” Master’s thesis, Delft University of Technology, 2012.

[13] M. W. van Kesteren, “Air Launch versus Ground Launch: a Multidisciplinary Design Optimization Study of Expendable Launch Vehicles on Cost and Performance,” Master’s thesis, Delft University of Technology, 2013.

[14] F. Miranda, “Design Optimization of Ground and Air-Launched Hybrid Rockets,” Master’s thesis, Delft University of Technology, 2015.

[15] Earth Observation Portal, “Satellite Missions Database,” 2018. Available: `https://directory.eoportal.org/web/eoportal/satellite-missions` (Accessed on 29/11/2018).

[16] E. Dumont, S. Stappert, T. Ecker, J. Wilken, S. Karl, S. Krummen, and M. Sippel, "Evaluation of future ariane reusable vtol booster stages," in *Proceedings of the International Astronautical Congress, IAC*, 2017.

[17] W. Graham, "SpaceX conducts historic Falcon 9 re-flight with SES-10 – Lands booster again," March 2017. Available: `https://www.nasaspaceflight.com/2017/03/spacex-historic-falcon-9-re-flight-ses-10/` (Accessed on 02/12/2018).

[18] Space Exploration Technologies, "Falcon User's Guide," January 2019.

[19] Space Exploration Technologies, "Gallery," 2017. Available: `https://www.spacex.com/galleries` (Accessed on 04/08/2019).

[20] B. Zandbergen, "AE1222-II: Aerospace Design & Systems Engineering Elements I." Unpublished. Delft University of Technology, 2017.

[21] F. M. Villanueva, H. Linshu, and X. Dajun, "Small Solid Propellant Launch Vehicle Mixed Design Optimization Approach," *Journal of Aerospace Technology and Management*, vol. 6, no. 3, pp. 291–300, 2014.

[22] F. M. Villanueva, H. Linshu, and X. Dajun, "Kick solid rocket motor multidisciplinary design optimization using genetic algorithm," *Journal of Aerospace Technology and Management*, vol. 5, no. 3, pp. 293–304, 2013.

[23] F. Castellini, *Multidisciplinary design optimization for expendable launch vehicles.* PhD thesis, Politecnico Di Milano, 2012.

[24] J. Jodei, M. Ebrahimi, and J. Roshanian, "Multidisciplinary design optimization of a small solid propellant launch vehicle using system sensitivity analysis," *Structural and Multidisciplinary Optimization*, vol. 38, no. 1, pp. 93–100, 2009.

[25] A. Saqlain and L.-s. He, "Optimization and sizing for propulsion system of liquid rocket using genetic algorithm," *Chinese Journal of Aeronautics*, vol. 20, no. 1, pp. 40–46, 2007.

[26] M. Balesdent, N. Berend, P. Depince, and A. Chriette, "A survey of multidisciplinary design optimization methods in launch vehicle design," *Structural and Multidisciplinary Optimization*, vol. 45, no. 5, pp. 619–642, 2012.

[27] D. G. Maringer, *Portfolio management with heuristic optimization*, vol. 8. Springer Science & Business Media, 2006.

[28] D. H. Wolpert and W. G. Macready, "Coevolutionary free lunches," *IEEE Transactions on Evolutionary Computation*, vol. 9, no. 6, pp. 721–735, 2005.

[29] E. Zitzler, K. Deb, and L. Thiele, "Comparison of multiobjective evolutionary algorithms: Empirical results," *Evolutionary computation*, vol. 8, no. 2, pp. 173–195, 2000.

[30] D. J. Bayley, R. J. Hartfield, J. E. Burkhalter, and R. M. Jenkins, "Design optimization of a space launch vehicle using a genetic algorithm," *Journal of Spacecraft and Rockets*, vol. 45, no. 4, pp. 733–740, 2008.

[31] M. Balesdent, *Multidisciplinary Design Optimization of Launch Vehicles.* PhD thesis, École Doctorale Sciences Pour l'Ingénieur, Géosciences et Architecture, Nantes, France, 2011.

[32] G. Cai, H. Zhu, D. Rao, and H. Tian, "Optimal design of hybrid rocket motor powered vehicle for suborbital flight," *Aerospace Science and Technology*, vol. 25, no. 1, pp. 114–124, 2013.

[33] K. S. G. Anglim, Z. Zhang, and Q. Gao, "Minimum-Fuel Optimal Trajectory for Reusable First-Stage Rocket Landing Using Particle Swarm Optimization," *International Journal of Mechanical and Mechatronics Engineering*, vol. 11, no. 5, pp. 981–990, 2017.

[34] A. Pagano and E. Mooij, "Global launcher trajectory optimization for lunar base settlement," in *AIAA/AAS Astrodynamics Specialist Conference*, 2010.

[35] M.-u.-D. Qazi, H. Linshu, and T. Elhabian, “Rapid trajectory optimization using computational intelligence for guidance and conceptual design of multistage space launch vehicles,” in *AIAA guidance, navigation, and control conference and exhibit*, 2005.

[36] European Space Agency, “PAGMO & PYGMO,” 2018. Available: `https://esa.github.io/pagmo2/`.

[37] Delft University of Technology, “TU Delft Astrodynamic Toolbox,” 2018. Available: `http://tudat.tudelft.nl/index.html`.

[38] D. Woodward, “Space Launch Vehicle Design: Conceptual design of rocket powered, vertical takeoff, fully expendable and first stage boostback space launch vehicles,” Master’s thesis, University of Texas at Arlington, 2017.

[39] N. Drenthe, “SOLSTICE: Small Orbital Launch Systems, a Tentative Initial Cost Estimate,” Master’s thesis, Delft University of Technology, 2016.

[40] N. Drenthe, B. Zandbergen, R. Curran, and M. Van Pelt, “Cost estimating of commercial smallsat launch vehicles,” *Acta Astronautica*, vol. 155, pp. 160–169, 2019.

[41] B. Zandbergen, “AE4S01 - Thermal Rocket Propulsion (Version 2.06).” Unpublished. Delft University of Technology, 2017.

[42] B. McBride and G. Sanford, “NASA Chemical Equilibrium with Applications (CEA),” *NASA Chemical Equilibrium with Applications (CEA)*, 2017.

[43] G. P. Sutton and O. Biblarz, *Rocket propulsion elements*. John Wiley & Sons, 2016.

[44] J. Whitehead, “Single stage to orbit mass budgets derived from propellant density and specific impulse,” in *32nd Joint Propulsion Conference and Exhibit*, 1996.

[45] B. T. C. Zandbergen, “Simple mass and size estimation relationships of pump fed rocket engines for launch vehicle conceptual design,” in *6th European Conference for Aeronautics and Space Sciences (EUCASS)*, 2015.

[46] P. Simplicio, A. Marcos, and S. Bennani, “A Reusable Launcher Benchmark with Advanced Recovery Guidance,” in *The 5th CEAS EuroGNC Conference*, 2019.

[47] E. Ralph, “SpaceX tests Falcon 9 Block 5’s landing leg retraction and preps for first reuse,” July 2018. Available: `https://www.teslarati.com/spacex-falcon-9-block-5-landing-leg-retraction-reuse/` (Accessed on 12/07/2019).

[48] P. V. Tartabini, J. R. Beaty, R. A. Lepsch, and M. G. Gilbert, “Payload Performance Analysis for a Reusable Two-Stage-to-Orbit Vehicle,” 2015. National Aeronautics and Space Administration Technical Memorandum.

[49] P. Blau, “Falcon 9 v1.1 & F9R Launch Vehicle Overview,” 2015. Available: `http://www.spaceflight101.net/falcon-9-v11.html` (Accessed on 06/06/2019).

[50] H. W. Price, R. D. Braun, R. Manning, and E. Sklyanski, “A high-heritage blunt-body entry, descent, and landing concept for human mars exploration,” in *54th AIAA Aerospace Sciences Meeting*, pp. 1–16, 2016.

[51] W. J. Larson, *Applied Space Systems Engineering*. McGraw-Hill Learning Solutions, 2009.

[52] Northrop Grumman, “Propulsion Products Catalog,” June 2018.

[53] SNECMA, “HM7B,” 2010.

[54] P. Blau, “Ariane 5 ECA,” 2019. Available: `http://spaceflight101.com/spacerockets/ariane-5-eca/` (Accessed on 21/05/2019).

[55] M. Wade, “LE-5B Engine,” 2019. Available: `http://www.astronautix.com/l/le-5bengine.html` (Accessed on 20/05/2019).

[56] P. Blau, “H-IIB Launch Vehicle,” 2019. Available: http://spaceflight101.com/spacerockets/h-iib/ (Accessed on 21/05/2019).

[57] M. Wade, “LE-7A,” 2019. Available: http://www.astronautix.com/l/le-7a.html (Accessed on 20/05/2019).

[58] Mitsubishi Heavy Industries, “MHI LAUNCH SERVICES: Launch Vehicles,” 2019. Available: https://www.mhi.com/products/space/launch_srv_lineup.html (Accessed on 21/05/2019).

[59] Pratt & Whitney, “RL10B-2,” 2009.

[60] P. Blau, “Delta IV Medium+ (4,2),” 2019. Available: http://spaceflight101.com/spacerockets/delta-iv-medium-42/ (Accessed on 21/05/2019).

[61] Aerojet Rocketdyne, “RL10 Propulsion System,” 2019.

[62] Wikipedia, “Atlas V,” 2019. Available: https://en.wikipedia.org/wiki/Atlas_V (Accessed on 21/05/2019).

[63] EADS Astrium, “Vinci Thrust Chamber Cryogenic Upper Stage,” 2006.

[64] ArianeGroup, “140 Successful Tests and Several “Firsts” for Vinci, the Engine for Ariane 6,” 2018. Available: https://www.safran-group.com/media/140-successful-tests-and-several-firsts-vinci-engine-ariane-6-20180215 (Accessed on 20/05/2019).

[65] EADS Astrium, “Vulcain Rocket Engine - Thrust Chamber,” 2012. Available: http://cs.astrium.eads.net/sp/launcher-propulsion/rocket-engines/vulcain-rocket-engine.html (Accessed on 19/05/2019.

[66] Wikipedia, “Ariane 5,” 2019. Available: https://en.wikipedia.org/wiki/Ariane_5 (Accessed on 21/05/2019).

[67] P. Blau, “Angara 1.2,” 2019. Available: http://spaceflight101.com/spacerockets/angara-1-2/ (Accessed on 06/05/2019).

[68] Wikipedia, “RD-191,” 2019. Available: https://en.wikipedia.org/wiki/RD-191 (Accessed on 20/05/2019).

[69] M. Wade, “YF-100,” 2019. Available: http://www.astronautix.com/y/yf-100.html (Accessed on 20/05/2019).

[70] Wikipedia, “YF-100,” 2019. Available: https://en.wikipedia.org/wiki/YF-100 (Accessed on 20/05/2019).

[71] “Evolution of the SpaceX Merlin-1 Engine,” 2019. Available: http://www.b14643.de/Spacerockets_2/United_States_1/Falcon-9/Merlin/ (Accessed on 22/05/2019).

[72] NPO Energomash, “RD-120 Description,” 2016. Available: http://engine.space/dejatelnost/engines/rd-120/ (Accessed on 21/05/2019).

[73] Wikipedia, “RD-120,” 2019. Available: https://en.wikipedia.org/wiki/RD-120 (Accessed on 21/05/2019).

[74] Ecoruspace, “Propulsion system: 11D58M,” 2016. Available: http://ecoruspace.me/11%25D0%259458%25D0%259C.html (Accessed on 23/05/2019).

[75] Wikipedia, “Zenit (rocket family),” 2019. Available: https://en.wikipedia.org/wiki/Zenit_(rocket_family) (Accessed on 22/05/2019).

[76] Wikipedia, “Merlin (rocket engine family),” 2019. Available: https://en.wikipedia.org/wiki/Merlin_(rocket_engine_family) (Accessed on 22/05/2019).

[77] Wikipedia, “RD-58,” 2019. Available: https://en.wikipedia.org/wiki/RD-58 (Accessed on 22/05/2019).

[78] Arianespace, “Ariane 5 User’s Manual,” October 2016.

[79] Japan Aerospace Exploration Agency, “H-IIB Launch Vehicle,” 2003. Available: https://global.jaxa.jp/projects/rockets/h2b/index.html (Accessed on 22/05/2019).

[80] P. Blau, “H-IIA 202 Launch Vehicle,” 2019. Available: http://spaceflight101.com/spacerockets/h-iia-202/ (Accessed on 22/05/2019).

[81] P. Blau, “Long March 7 Launch Vehicle,” 2019. Available: http://spaceflight101.com/spacerockets/long-march-7/ (Accessed on 22/05/2019).

[82] P. Blau, “Zenit-3SL – Launch Vehicle,” 2019. Available: http://spaceflight101.com/spacerockets/zenit-3sl/ (Accessed on 22/05/2019).

[83] P. Blau, “Long March 6 Launch Vehicle,” 2019. Available: http://spaceflight101.com/spacerockets/long-march-6/ (Accessed on 22/05/2019).

[84] B. Zhang, “China’s new generation of liquid oxygen kerosene engine 3: YF100/115 main characteristics,” 2014. Available: https://web.archive.org/web/20160304055915/http://www.shenkong.net/Explore/1410/ZGXYDYYMYFDJ3-YF100-115ZYTX26045110.htm (Accessed on 24/05/2019).

[85] Space Exploration Technologies, “Falcon 1 Launch Vehicle Payload User’s Guide,” 2008.

[86] P. Blau, “Falcon 9 FT (Falcon 9 v1.2),” 2019. Available: http://spaceflight101.com/spacerockets/falcon-9-ft/ (Accessed on 22/05/2019).

[87] K. F. Wakker, *Fundamentals of Astrodynamics*. Delft University of Technology Institutional Repository Library, 2015.

[88] M. Interbartolo, “Earth Parking Orbit and Translunar Injection,” 2009. National Aeronautics and Space Administration Technical Memorandum.

[89] T. J. Kreiter, “Comparison of direct and indirect ascent modes for the 1966-1967 mars opportunity with an atlas-centaur launch vehicle,” 1965. National Aeronautics and Space Administration Technical Memorandum.

[90] C. D. Brown, “Spacecraft Mission Design – Second Edition,” *American Institute of Aeronautics and Astronautics*, 1998.

[91] P. Lu, K. Horneman, D. Neal, J. Schierman, and S. Su, “Pitch-over maneuver and guidance for rocket-back boosters,” in *AIAA Guidance, Navigation, and Control Conference*, pp. 1–18, 2011.

[92] E. Brendel, B. Hérissé, and E. Bourgeois, “Optimal guidance for toss back concepts of reusable launch vehicles,” in *8th European Conference for Aeronautics and Space Sciences (EUCASS)*, 2019.

[93] D. Murphy, “Flight Club: The Orbital Launch Simulator and Trajectory Visualisation Software.” Available: https://www2.flightclub.io/, 2019.

[94] J. Wilken, S. Stappert, L. Bussler, M. Sippel, and E. Dumont, “Future European Reusable Booster Stages: Evaluation of VTHL and VTVL Return Methods,” *IAC-2018 D*, vol. 2, 2018.

[95] M. Sippel, S. Stappert, L. Bussler, and E. Dumont, “Systematic assessment of reusable first-stage return options,” in *Proceedings of the International Astronautical Congress, IAC*, no. D2. 4.4, 2017.

[96] Space Exploration Technologies, “CRS-10 Dragon Resupply Mission Press Kit,” 2017.

[97] National Aeronautics and Space Administration, “SpaceX CRS-10 Mission Overview,” 2017.

[98] O. Trivailo, M. Sippel, and Y. A. Şekercioğlu, "Review of hardware cost estimation methods, models and tools applied to early phases of space mission planning," *Progress in Aerospace Sciences*, vol. 53, pp. 1–17, 2012.

[99] Science Applications International Corporation, *NASA and Air Force Cost Model, NAFCOM 96 Manual.*

[100] D. E. Koelle, *Handbook of Cost Engineering and Design of Space Transportation Systems: With TransCost 8.2 Model Description; Statistical-analystical Model for Cost Estimation and Economic Optimization of Launch Vehicles.* TCS, 2012.

[101] J. R. Wertz, "Responsive launch vehicle cost model," in *AIAA Paper RS2-2004-2004, Presented at the 2nd AIAA Responsive Space Conference, Los Angeles, CA*, Citeseer, 2004.

[102] S. Stappert, J. Wilken, L. Bussler, and M. Sippel, "A Systematic Comparison of Reusable First Stage Return Options," in *8th European Conference for Aeronautics and Space Sciences (EUCASS)*, 2019.

[103] J. R. Wertz, "Economic model of reusable vs. expendable launch vehicles," in *IAF, International Astronautical Congress, 51 st, Rio de Janeiro, Brazil*, 2000.

[104] T. Herrmann and D. Akin, "A critical parameter optimization of launch vehicle costs," in *Space 2005*, 2005.

[105] H. Jones, "The Recent Large Reduction in Space Launch Cost," 48th International Conference on Environmental Systems, 2018.

[106] C. D. Hunt, "2018 NASA New Start Inflation Index." Available: `https://www.nasa.gov/sites/default/files/atoms/files/2018_nasa_new_start_inflation_index_for_fy19_use_final_dist.xlsx`, 2019.

[107] National Aeronautics and Space Administration, "Commercial Market Assessment for Crew and Cargo Systems." Available: `https://www.nasa.gov/sites/default/files/files/Section403(b)CommercialMarketAssessmentReportFinal.pdf`, 2011.

[108] E. C. Coşkun, *Multistage launch vehicle design with thrust profile and trajectory optimization.* PhD thesis, Department of Mechanical Engineering, Middle East Technical University, 2014.

[109] C. Peraza, F. Valdez, and O. Castillo, "A harmony search algorithm comparison with genetic algorithms," in *Fuzzy Logic Augmentation of Nature-Inspired Optimization Metaheuristics*, pp. 105–123, Springer, 2015.

[110] European Space Agency, "Improved Harmony Search (IHS)," 2018. Available: `https://esa.github.io/pagmo2/docs/cpp/algorithms/ihs.html` (Accessed on 11/08/2019).

[111] M. Mahdavi, M. Fesanghary, and E. Damangir, "An improved harmony search algorithm for solving optimization problems," *Applied mathematics and computation*, vol. 188, no. 2, pp. 1567–1579, 2007.

[112] S. Stappert, J. Wilken, and M. Sippel, "Cost Estimations for Preliminary Design Stage of Reusable Booster Stages." ESA Space Cost Engineering Conference, 2019.

[113] G. Sowers, "Reuse Business Case," 2015.

[114] E. Fleeman, *Missile Design and System Engineering.* American Institute of Aeronautics and Astronautics, Inc., 2012.

[115] Rocket Lab Ltd., "Rocket Lab Announces Reusability Plans For Electron Rocket." Available: `https://www.rocketlabusa.com/news/updates/rocket-lab-announces-reusability-plans-for-electron-rocket/`, 2019.

[116] P. Blau, "Electron," 2019. Available: `http://spaceflight101.com/spacerockets/electron/` (Accessed on 06/05/2019).

[117] P. Blau, "Minotaur I," 2019. Available: `http://spaceflight101.com/spacerockets/minotaur-i/` (Accessed on 06/05/2019).

[118] P. Blau, "Minotaur IV," 2019. Available: http://spaceflight101.com/spacerockets/minotaur-iv/ (Accessed on 06/05/2019).

[119] P. Blau, "Minotaur C," 2019. Available: http://spaceflight101.com/spacerockets/minotaur-c/ (Accessed on 06/05/2019).

[120] P. Blau, "Minotaur V," 2019. Available: http://spaceflight101.com/spacerockets/minotaur-v/ (Accessed on 06/05/2019).

[121] P. Blau, "Atlas V 401," 2019. Available: http://spaceflight101.com/spacerockets/atlas-v-401/ (Accessed on 06/05/2019).

[122] P. Blau, "Atlas V 421," 2019. Available: http://spaceflight101.com/spacerockets/atlas-v-421/ (Accessed on 06/05/2019).

[123] P. Blau, "Atlas V 501," 2019. Available: http://spaceflight101.com/spacerockets/atlas-v-501/ (Accessed on 06/05/2019).

[124] P. Blau, "Delta II 7320," 2019. Available: http://spaceflight101.com/spacerockets/delta-ii-7320/ (Accessed on 06/05/2019).

[125] P. Blau, "Angara A3," 2019. Available: http://spaceflight101.com/spacerockets/angara-a3/ (Accessed on 06/05/2019).

[126] P. Blau, "Vega," 2019. Available: http://spaceflight101.com/spacerockets/vega/ (Accessed on 06/05/2019).

[127] P. Blau, "Epsilon," 2019. Available: http://spaceflight101.com/spacerockets/epsilon/ (Accessed on 06/05/2019).

[128] P. Blau, "Long March 3A," 2019. Available: http://spaceflight101.com/spacerockets/long-march-3a/ (Accessed on 06/05/2019).

[129] P. Blau, "PSLV Launch Vehicle," 2019. Available: http://spaceflight101.com/spacerockets/pslv/ (Accessed on 06/05/2019).

A
Fairing Estimation Relationship Data

The data used to develop the length and mass estimation relationship for the payload fairing are presented in Table A.1. Additionally, these data points are plotted along with the lines of best fit in Figure A.1 and Figure A.2 for the length and mass relationships, respectively.

Table A.1: Data used to derive fairing estimation relationships.

Launch Vehicle	Fairing Diameter [m]	Fairing Length [m]	Fairing Mass [kg]
Falcon 9 FT [86]	5.2	13.1	1750
Electron [116]	1.2	2.50	50
Minotaur I [117]	1.27	3.78	300
Minotaur IV [118]	2.34	6.40	450
Minotaur C [119]	1.33	3.93	300
Minotaur V [120]	2.34	5.71	450
Atlas V 401 [121]	4.2	12.0	2127
Atlas V 421 [122]	4.2	12.9	2305
Atlas V 421 [122]	4.2	13.8	2487
Atlas V 501 [123]	5.4	20.7	3524
Atlas V 501 [123]	5.4	23.4	4003
Delta II 7320 [124]	2.9	8.49	880
Delta IV Medium (4,2) [60]	4.0	11.75	2800
Angara 1.2 [67]	2.56	7.80	500
Angara 1.2 [67]	3.0	9.88	810
Angara A3 [125]	4.35	15.84	1600
Ariane 5 ECA [54]	5.4	17.0	2500
Vega [126]	2.6	7.88	540
H-IIB [56]	5.1	15.0	3200
Epsilon [127]	2.5	9.19	700
H-IIA 202 [80]	4.07	12.0	1400
Long March 3 [128]	4.0	9.56	1500
PSLV [129]	3.2	8.30	1150

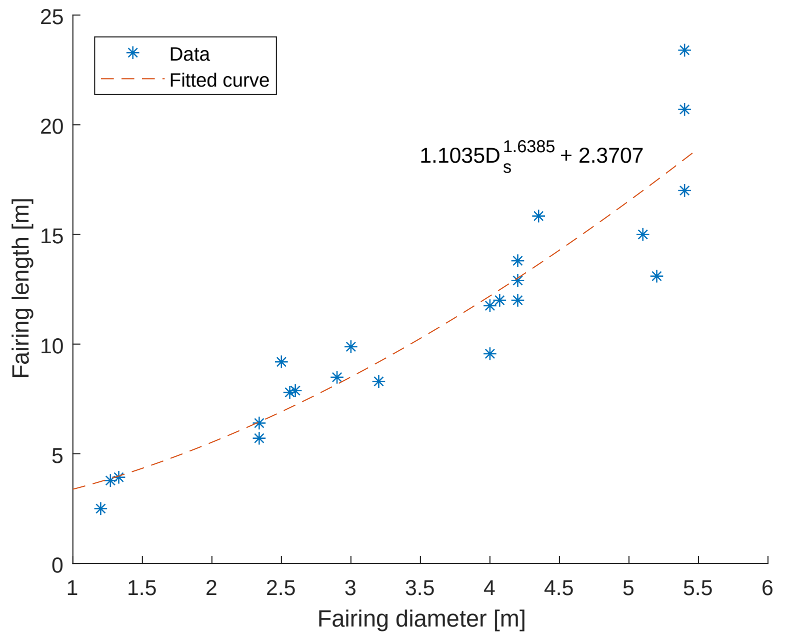

Figure A.1: Data and fitness for the payload fairing length estimation relationship.

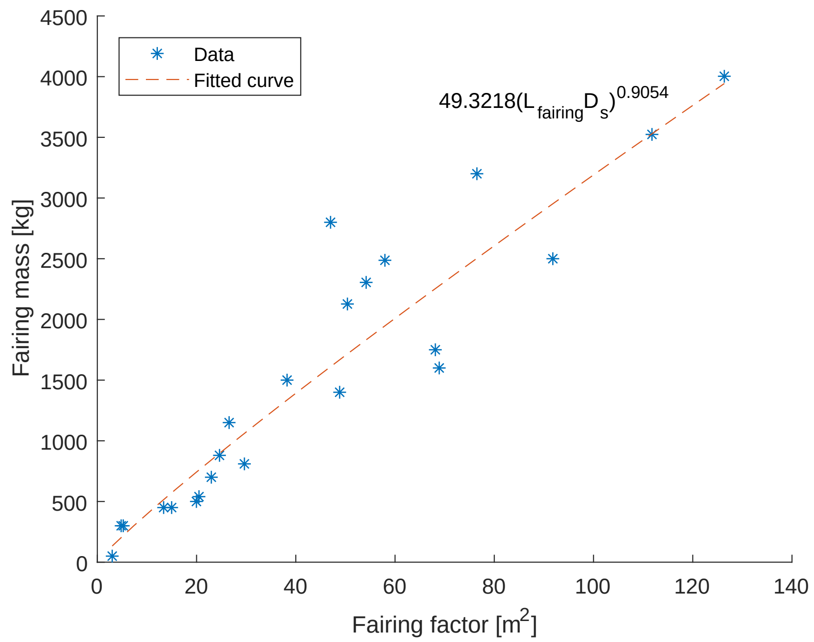

Figure A.2: Data and fitness for the payload fairing mass estimation relationship.

B
Launch Vehicle Validation Data

This section includes additional data used to validate the launch vehicle propulsion, geometry and mass models. Table B.1 shows the design parameters used as inputs to the model. Table B.2 shows the key outputs of each stage with the actual values also reported for comparison, while Table B.3 shows the key outputs of the launch vehicles as a whole. Finally, Table B.4 and Table B.5 show the relative errors between the modelled and actual values for the stages and launch vehicles, respectively.

Table B.1: Zenit, Falcon 9 v1.1 and Falcon 9 FT design parameters used for validation.

	Design Parameter						
Launch Vehicle (Stage #)	P_c [bar]	P_e [bar]	D_s [m]	D_e [m]	t_b [s]	OF [-]	Prop.
Zenit (1)	245.2	0.70214	3.900	2.950	130.0	2.63	RP1
Zenit (2)	178.1	0.12962	3.900	1.954	315.0	2.60	RP1
Zenit (3)	79.0	0.02073	3.700	1.400	650.0	2.82	RP1
Falcon 9 v1.1 (1)	97.2	0.5285	3.700	1.070	180.0	2.34	RP1
Falcon 9 v1.1 (2)	97.2	0.06617	3.700	2.498	375.0	2.36	RP1
Falcon 9 FT (1)	108.0	0.8520	3.660	0.9987	162.0	2.38	RP1
Falcon 9 FT (2)	108.0	0.04875	3.660	2.970	397.0	2.38	RP1

Table B.2: Zenit, Falcon 9 v1.1 and Falcon 9 FT stage validation data.

	Actual Values					**Model Values**				
Launch Vehicle (Stage #)	I_{sp} [s]	F_T [kN]	M_p [kg]	L_s [m]	$M_{s,inert}$ [kg]	I_{sp} [s]	F_T [kN]	M_p [kg]	L_s [m]	$M_{s,inert}$ [kg]
Zenit (1)	337.0	8064.0	326786	32.90	27564.0	332.0	8174.3	327306	37.37	26594.2
Zenit (2)	350.0	912.0	82487	10.40	9017.0	349.8	885.5	81538	13.3	4746.3
Zenit (3)	361.0	85.00	15850	5.600	3861.0	357.9	85.95	15962	6.112	2149.8
Falcon 9 v1.1 (1)	320.0	742.4	395700	45.70	23100.0	318.4	708.1	368410	42.72	22609.8
Falcon 9 v1.1 (2)	347.0	805.1	92670	13.80	3900.0	346.7	768.4	84997	14.25	4301.0
Falcon 9 FT (1)	314.3	7607.0	411000	47.00	22200.0	313.2	8104.1	428682	49.81	27619.9
Falcon 9 FT (2)	348.0	934.0	107500	12.60	4000.0	351.8	867.4	100093	16.04	4691.5

Table B.3: Zenit, Falcon 9 v1.1 and Falcon 9 FT launch vehicle validation data.

	Actual Values				**Model Values**			
Launch Vehicle	$M_{fairing}$ [kg]	$GTOW$ [kg]	L_{tot} [m]	M_{inert} [kg]	$M_{fairing}$ [kg]	$GTOW$ [kg]	L_{tot} [m]	M_{inert} [kg]
Zenit	-	465800	58.7	40667.0	1414.6	469744	69.7	44221.1
Falcon 9 v1.1	1750.0	505846	68.4	-	1414.6	491389	68.7	37325.9
Falcon 9 FT	1750.0	549054	70.0	-	1383.1	572194	77.4	42729.4

Table B.4: Zenit, Falcon 9 v1.1 and Falcon 9 FT stage validation data relative errors.

	Error [%]				
Launch Vehicle (Stage #)	I_{sp}	F_T	M_p	L_s	$M_{s,inert}$
Zenit (1)	-1.48	1.37	1.59	13.6	-3.52
Zenit (2)	-0.04	-2.90	-1.15	27.6	-47.4
Zenit (3)	-0.85	1.12	0.71	9.14	-44.3
Falcon 9 v1.1 (1)	-0.50	-4.63	-6.90	-6.52	-2.12
Falcon 9 v1.1 (2)	-0.09	-4.57	-8.28	3.26	10.3
Falcon 9 FT (1)	-0.35	6.54	4.30	5.99	24.4
Falcon 9 FT (2)	1.10	-7.13	-6.89	27.3	17.3

Table B.5: Zenit, Falcon 9 v1.1 and Falcon 9 FT launch vehicle validation data relative errors.

	Error [%]			
Launch Vehicle	$M_{fairing}$	$GTOW$	L_{tot}	M_{inert}
Zenit	-	0.85	18.8	8.74
Falcon 9 v1.1	-19.2	-2.86	0.47	-
Falcon 9 FT	-20.1	4.22	10.6	-

C
Detailed Development Cost Breakdown

This section presents the additional equations needed to convert the Theoretical First Unit cost into the cost and price per flight, specifically detailing the development cost breakdown. To determine the cost of the First Flight Model, $FM1$, the percentage of Manufacturing & Product Assurance costs is subtracted from the Theoretical First Unit cost, as in Equation C.1.

$$FM1 = TFU - M/PA\% \tag{C.1}$$

The total Management & Product Assurance M/PA and Engineering ENG costs make up the Project Office PO costs, as seen in Equation C.2.

$$PO = ENG + MP/A \tag{C.2}$$

The Engineering costs are described in Equation C.3, where it is given as a function of the Design and Development DD FM1. In this study, DD is fixed to 3 as an estimate on the scope of the design effort needed [39].

$$ENG = DD \cdot FM1 \tag{C.3}$$

The Management & Product Assurance cost is given in Equation C.4, where $MAIT$ represents the Manufacturing, Assembly, Integration and Test costs.

$$MP/A = (MAIT + ENG) \cdot M/PA\% \tag{C.4}$$

The MAIT costs are calculated as in Equation C.5. Below, STH represents the system test hardware fixed at 3.1, and L_d represents the learning curve associated with the development of the total number of hardware units needed per stage, $\#HW$, fixed at 1 for all hardware except for the engines when necessary.

$$MAIT = FM1 \cdot (STH + L_d \cdot \#HW) \tag{C.5}$$

For further insight into the above equations, the reader is referred to the work of Drenthe [39, 40].

D
Historical EUR/USD Exchange Rates

This section presents the historical exchange rates between the European euro and the American dollar, used for conversion throughout the cost model developed in this research.

Table D.1: Historical EUR/USD exchange rates [39].

Year	Exchange Rate
2015	1.1101
2014	1.3285
2013	1.3281
2012	1.2858
2011	1.3923
2010	1.3272
2009	1.3943
2008	1.4707
2007	1.3708
2006	1.2562
2005	1.2445

E
USD Inflation Table

This section presents a portion of the NASA New Start inflation table used for normalizing historical costs [106].

Table E.1: NASA FY2018 inflation table [106].

Year	2005	2006	2007	2008	2009	2010	2011	2012	2013	2014	2015	2016	2017	2018
2005	1.000	1.042	1.079	1.110	1.125	1.151	1.175	1.186	1.208	1.233	1.252	1.268	1.296	1.330
2006		1.000	1.036	1.066	1.080	1.105	1.127	1.138	1.159	1.184	1.201	1.216	1.243	1.277
2007			1.000	1.029	1.042	1.066	1.088	1.099	1.119	1.143	1.159	1.174	1.200	1.232
2008				1.000	1.013	1.037	1.058	1.068	1.088	1.111	1.127	1.141	1.167	1.198
2009					1.000	1.023	1.044	1.054	1.074	1.096	1.112	1.127	1.152	1.182
2010						1.000	1.020	1.030	1.050	1.071	1.087	1.101	1.125	1.156
2011							1.000	1.010	1.029	1.050	1.065	1.079	1.103	1.133
2012								1.000	1.018	1.040	1.055	1.069	1.092	1.121
2013									1.000	1.021	1.036	1.049	1.072	1.101
2014										1.000	1.015	1.028	1.050	1.079
2015											1.000	1.013	1.035	1.063
2016												1.000	1.022	1.050
2017													1.000	1.027
2018														1.000

F
Overview of Tool Outputs

This section presents the time history of all of the dependent variables from the tool. In this specific case, the time history of the optimal RP1-propelled, 9-engine return-to-launch-site launch vehicle is simulated.

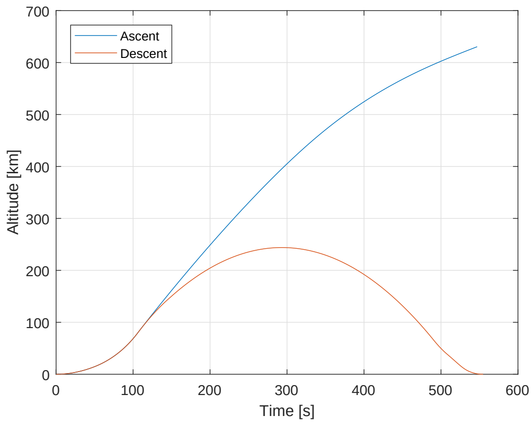

(a) Altitude time history.

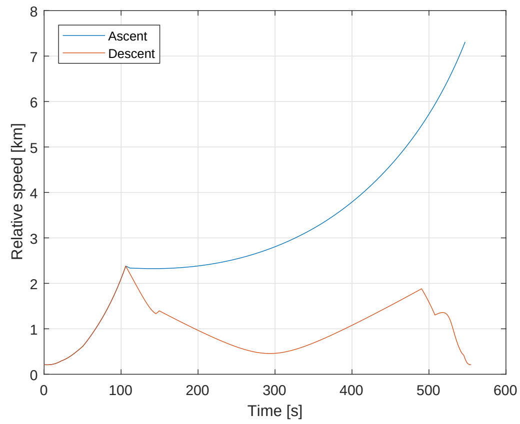

(b) Relative speed time history.

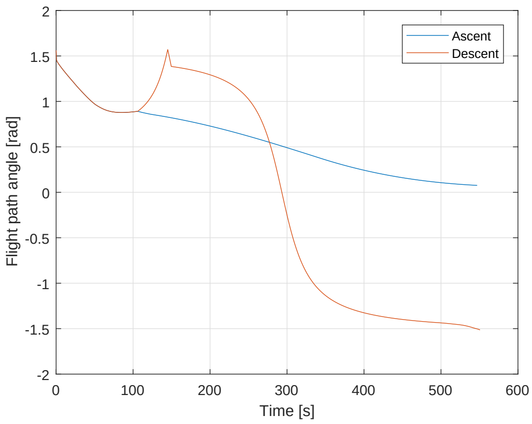

(c) Flight path angle time history.

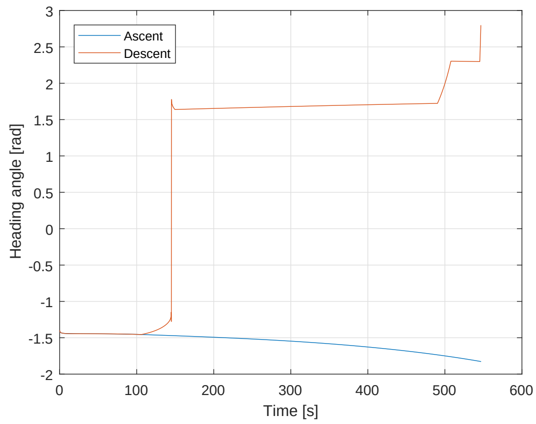

(d) Heading angle time history.

Figure F.1: Time history of first four dependent variables output by the tool.

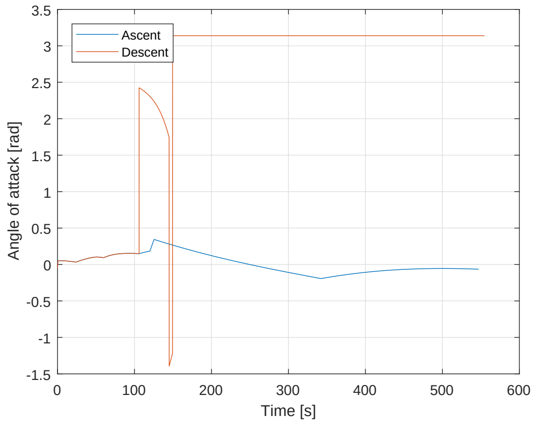

(a) Angle of attack time history.

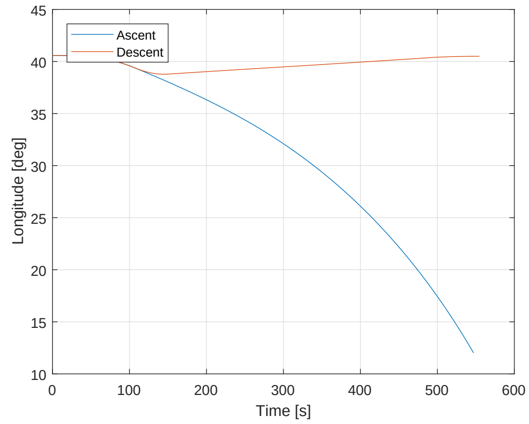

(b) Longitude time history.

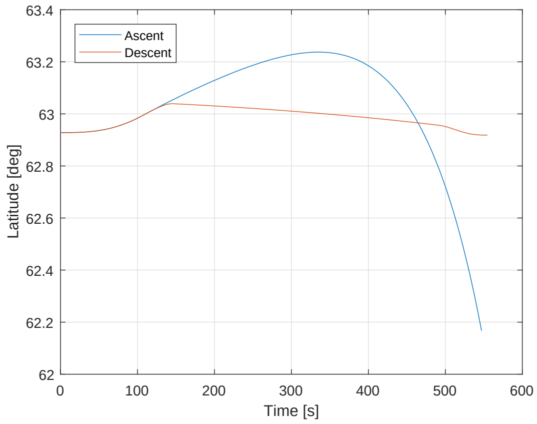

(c) Latitude time history.

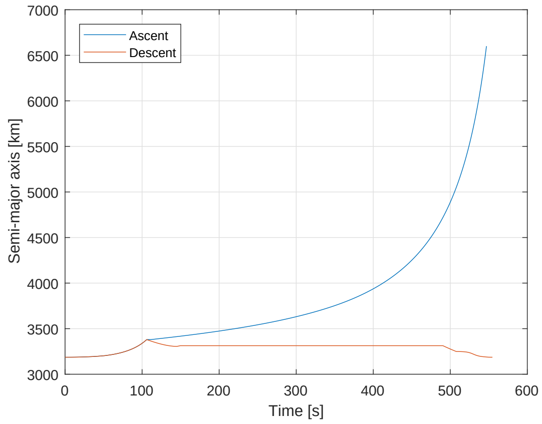

(d) Semi-major axis time history.

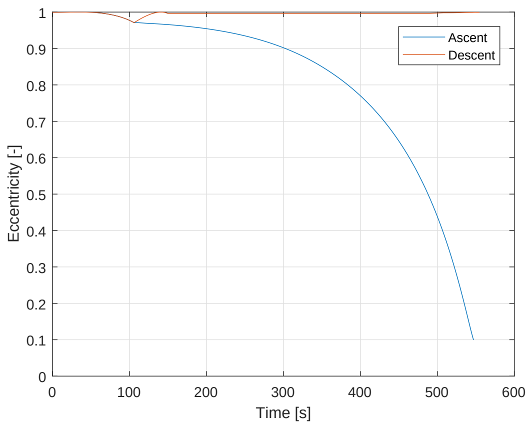

(e) Eccentricity time history.

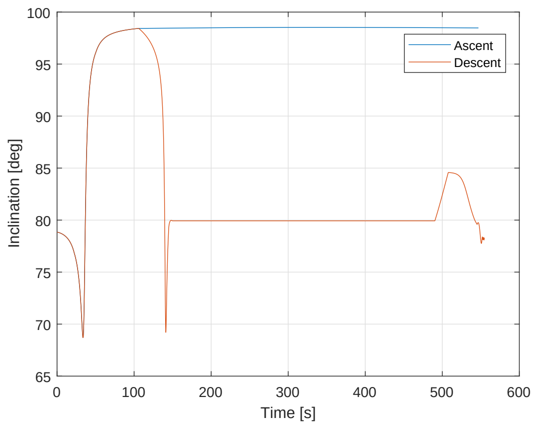

(f) Inclination time history.

Figure F.2: Time history of following six dependent variables output by the tool.

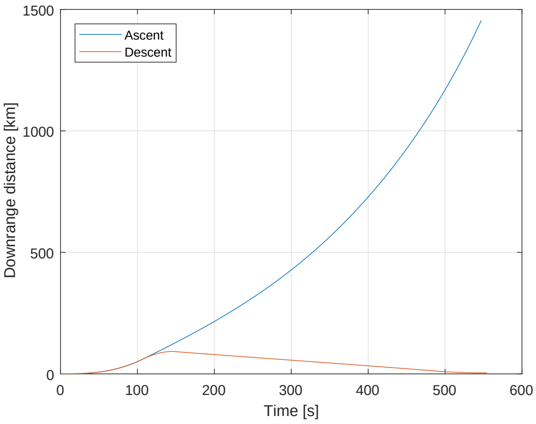

(a) Downrange distance time history.

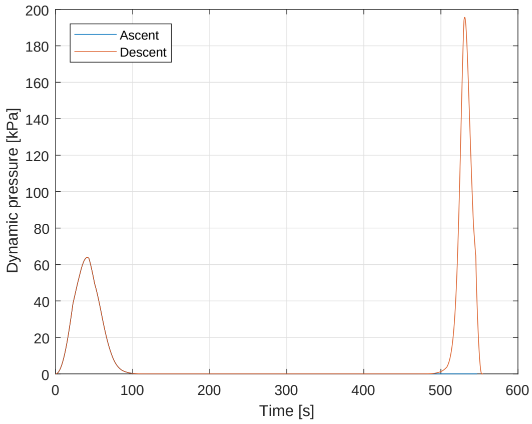

(b) Dynamic pressure time history.

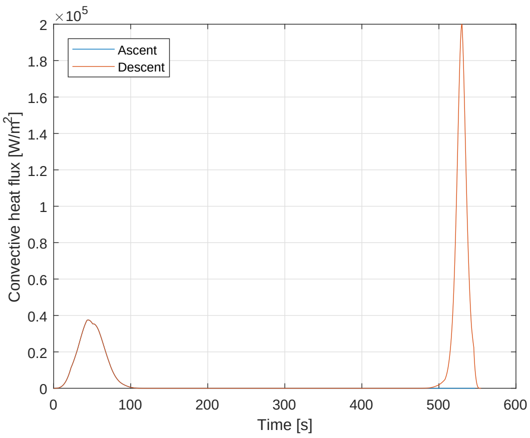

(c) Heat flux time history.

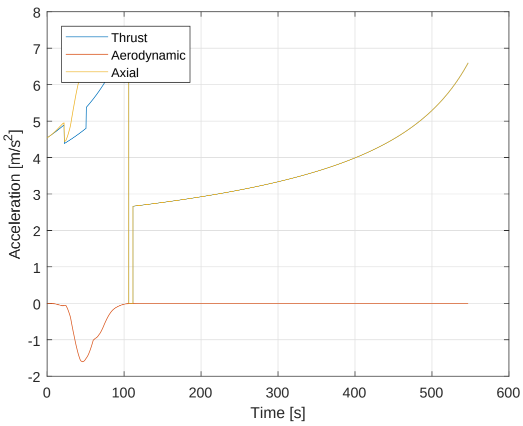

(d) Ascent trajectory load history.

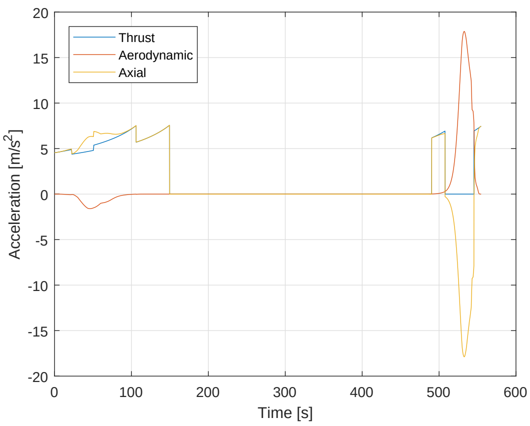

(e) Descent trajectory load history.

Figure F.3: Time history of final five dependent variables output by the tool.

G
Aerospace Europe Conference 2020 Abstract

This section presents the abstract that has been submitted to the Aerospace Europe Conference 2020, located in Bordeaux, France. The author is expected to receive an update about the potential publication on November 16, 2019.

G.1. Introduction

The rapid rise in production of small satellites in recent years has created a need for dedicated launch systems to bring these into orbit. Small launch vehicles capable of bringing payloads below 1000 kg into orbit have seen an increase in development over the last decade, as these systems promise lower launch prices per kilogram compared to ride-share and cluster launch alternatives and allow for flexible target orbits [3]. In parallel, reusability of launch vehicles has become a topic of interest as of late due to its potential to reduce overall launch prices, especially when considering first stage vertical landing techniques as employed by SpaceX [5]. The added benefit of reduction in material consumption and debris may make small, reusable launch vehicles a green, cost-effective solution to the small satellite launch needs. The proposed research summarizes the development of an open-source tool capable of designing and optimizing such a system for cost, while also contesting claims made by small launch vehicle developers.

G.2. Discussion

A complex multidisciplinary design analysis and optimization environment has been adopted to model a small, reusable launch vehicle, which allows a set of design parameters to vary and evolve towards an optimal solution based on an objective function that minimizes cost [26]. The propulsion of solid and liquid stages is first modelled from the set of design parameters. Using key outputs from this module such as thrust and specific impulse, the geometry and mass of the launch vehicle is estimated using validated size and mass estimation relationships. Once the launch vehicle has been constructed, a validated parametric cost model estimates the launch price of the system. Subsequently, the launch vehicle is simulated to a target 650km Sun-synchronous orbit using force and aerodynamic analyses in a direct ascent trajectory model. Upon separation of the first stage, the model simulates the re-entry of this system for two specific reuse cases, namely a downrange landing and a return-to-launch-site landing.

G.3. Conclusion

The results of this study will provide a set of conceptual small, reusable launch vehicles that are optimized for launch price based on different engine and propellant configurations. In addition, the study will provide insight into key reusable launch vehicle cost drivers such as number of reuses, launch rate, target orbit and payload mass, and addresses sources of uncertainty through a sensitivity analysis. The launch rate can be used to assess the positive environmental impact of a reusable system when compared to launching the same number of expendable launch vehicles.